

UCSF

UC San Francisco Electronic Theses and Dissertations

Title

Organelle Size and Quality Control in Chlamydomonas Reinhardtii

Permalink

<https://escholarship.org/uc/item/1jg3874h>

Author

Perlaza, Karina

Publication Date

2021

Supplemental Material

<https://escholarship.org/uc/item/1jg3874h#supplemental>

Peer reviewed|Thesis/dissertation

Organelle Size and Quality Control in Chlamydomonas reinhardtii

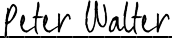
by
Karina Perlaza

DISSERTATION
Submitted in partial satisfaction of the requirements for degree of
DOCTOR OF PHILOSOPHY

in
Biochemistry and Molecular Biology

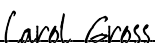
in the
GRADUATE DIVISION
of the
UNIVERSITY OF CALIFORNIA, SAN FRANCISCO

Approved:

DocuSigned by:

Peter Walter
9C44B4D1D50740D... Chair

DocuSigned by:

Wallace Marshall

DocuSigned by:

Carol Gross
7AFBE9046E0744C...

Committee Members

Copyright 2021

by

Karina Perlaza

Acknowledgements

Doing a PhD is such a privilege and I am so grateful to all the factors and people in my life that helped get me here.

My first shout-out goes to my pedagogical upbringing: the NYC Public School System and the City University of New York (CUNY) system. In my elementary schooling, I pushed myself to be strong academically because there were teachers that believed in me- Ms. Carrafiglio, Ms. Gaffney, Ms. Allen, I can go on and on. They encouraged asking questions and promoted good work values which I think helped me out in the long run. While at Hunter College (CUNY), I balanced part-time jobs and kept my grades up. This focus helped me get into the Minority Access to Research Careers (MARC) program. The MARC program was the catalyst that helped me get into UCSF. I am extremely grateful and thankful to my undergraduate mentors Dr. Thomas Schmidt- Gleneweinkel, Marlon Jansen and Dr. Shirley Raps. They helped introduce me to the world of academia. Thank you Dr. Thomas Schmidt-Gleneweinkel for letting me join the lab without any previous experience. Thank you to Marlon, my amazing daily mentor, helping me dip my toes into the world of bench-work research. At Hunter College, I had the opportunity to connect with the chair of the Department, Dr. Shirley Raps. Her gravitas, calm yet no B.S very NYC demeanor, all combined with her passion for uplifting talented, historically marginalized students will always be such an inspiration to me. Thank you Dr. Raps.

In graduate school, I was fortunate to find a faculty mentor that parallels Dr. Raps in many ways, Carol Gross. I am forever indebted to her for all the emotional help and actionable steps she took to improve my experience at UCSF. Thank you Carol Gross!

Thank you to my graduate school cohort, starting class of 2014, you are all so amazing, talented, and fun! I cannot imagine a set of people more nerdy, encouraging and supportive of one another.

In my final stretch at UCSF, I grew a stronger connection with the Society of Advancement of Chicanos and Native-Americans Society (SACNAS) community. It was refreshing to engage with a group of scientists that worked collectively and tirelessly to increase representation and accessibility to help gain equity in STEM careers. The behind-the-scenes work they do doesn't get nearly as much credit as it merits.

Thank you to my siblings: Chris, Tatin and Xiomy. I am so grateful to have such a goofy, fun, and outgoing group of siblings that love and support me so much. Thank you to my family at large, tios and tias, cousins in Colombia and NYC, y mis abuelitos for all the love and encouragement they gave me. Thank you to my lovely family here in the Bay Area: Adrianita, Brian, Doña Adriana y Don Fernando. It was so nice to escape lab craziness and relax in a family atmosphere.

I would like to give a wholehearted thank you to the two scientists that advised this work: Peter Walter and Wallace Marshall. Peter- thank you for welcoming me to your lab while I was an undergraduate student and exposing me to the fascinating field of protein quality control. I try my best to emulate your fearlessness when exploring scientific questions. It was amazing to work with you and all of the talented and creative scientists in your lab. In particular, a special thank you to Margaret who was my daily mentor during my two summer internships in Peter's lab while I was an undergraduate. Margaret was such a great role model to me, besides being kind and patient, our interactions made me believe that I had a shot at being a scientist. I would also like to extend my deepest gratitude to Han. We got close in the Walter lab and I am so thankful for her incredible

insight, wisdom, and advice during graduate school. Wallace- I don't know how to begin to express my gratitude for your mentorship. Every scientific conversation we had inspired me, motivating me to learn something new in my project. Because of you, I learned tons about flagellar biology and how to think about systems biology using quantitative approaches! I am so grateful for all of the amazing scientists in your lab and the wonderful atmosphere they create. A special shout-out to my classmate and lab mate, Athena, she was so fun to work with- I strive to be as selfless and thoughtful as her. Also, thank you to Mary, her gentle guidance, expertise, and enthusiasm helped keep me motivated and focused during the second half of my thesis work.

No se que haría sin el amor y el apoyo que me dieron mis papás, Nelly y Julio, durante la escuela de posgrado y en general. Mis papás me aconsejaron y me dieron la confianza que necesitaba en las decisiones más difíciles en mi carrera en el posgrado. Se que no fue fácil estar tan alejados pero ojalá reconozcan que siempre los tengo en mi corazón y en mi voluntad. Los quiero muchísimo y gracias por lograr este doctorado conmigo Ma y Pa.

Last, but definitely not least, I would like to thank Fernando, my partner, grad-school sweetheart, and confidant. One of the best outcomes from graduate school was that my awesome rotation in Dave T's lab led to us getting to know each other. You have taught me so much about myself, my own limits, on how to be kind to myself, and to trust in my abilities. I don't know where I would be without your patience, kindness, and sweet gestures throughout graduate school.

PUBLISHED WORK

Chapter 1 is a reprint of:

Perlaza, K., Toutkoushian H., Boone M., Lam M., Iwai M., Jonikas M.C., Walter P., Ramundo S. (2019). The Mars1 kinase confers photoprotection through signaling in the chloroplast unfolded protein response. *eLife* 8 (October). DOI: <https://doi.org/10.7554/eLife.49577>.

UNPUBLISHED WORK

Chapter 2 is a manuscript in-progress:

Perlaza, K., Mirvis M., Ishikawa H., Marshall W. Late stages of flagellar assembly require the TOG-domain array protein, Crescerin/SHF1.

ABSTRACT

ORGANELLE SIZE AND QUALITY CONTROL IN *CHLAMYDOMONAS*

REINHARDTII

Karina Perlaza

Organelles represent dynamic entities within the cell that undergo differential protein quality control regulation and size control changes depending on fluctuations in cellular conditions, environmental cues, and cell stage. In both halves of my study I used the unicellular algae, *Chlamydomonas reinhardtii*, to study these two facets of biology using two of its organelles: the chloroplast and the flagellum. In the first half of this study, I investigated a signaling pathway known as the chloroplast Unfolded Protein Response (cpUPR). In response to proteotoxic stress, chloroplasts communicate with the nuclear gene expression system through a chloroplast unfolded protein response (cpUPR). We isolated mutants that disrupt cpUPR signaling and identified a gene encoding a previously uncharacterized cytoplasmic protein kinase, termed Mars1—for mutant affected in chloroplast-to-nucleus retrograde signaling—as the first known component in cpUPR signal transmission. Lack of cpUPR induction in MARS1 mutant cells impaired their ability to cope with chloroplast stress, including exposure to excessive light. In the second half, I studied organelle size control using regenerating flagella. We discovered a loss-of-function mutation in a gene that leads to shortened flagella. This gene, which encodes a *Chlamydomonas* ortholog of Crescerin, corresponds to the previously unknown short flagella gene SHF1. Crescerin/SHF1 has been identified as a cilia-specific TOG-domain array protein that binds to tubulin. In this mutant, we found that flagellar regeneration occurs with the same initial kinetics as wild-type cells, but plateaus at a shorter length. We place this finding in the larger context of tubulin dynamics by

suggesting that this TOG-domain array protein is necessary to efficiently and preemptively increase tubulin levels to offset decreasing IFT cargo at the tip as flagellar assembly progresses.

Table of Contents

CHAPTER 1

The Mars1 kinase confers photoprotection through signaling in the chloroplast unfolded protein response.....1

1.1 ABSTRACT.....3

1.2 INTRODUCTION.....4

1.3 RESULTS AND DISCUSSION.....6

1.4 CONCLUSION.....15

1.4 AUTHOR CONTRIBUTIONS.....16

1.5 ACKNOWLEDGEMENTS.....17

1.6 MATERIALS AND METHODS.....18

1.7 REFERENCES.....50

Chapter 2

Late stages of flagellar assembly require the TOG-domain array protein,

Crescerin/SHF1.....	110
2.1 ABSTRACT.....	112
2.2 INTRODUCTION.....	114
2.3 RESULTS	118
2.4 DISCUSSION.....	129
2.5 AUTHOR CONTRIBUTIONS.....	136
2.6 ACKNOWLEDGEMENTS.....	137
2.7 MATERIALS AND METHODS.....	138
2.8 REFERENCES.....	154

LIST OF FIGURES

CHAPTER 1

Figure 1-1	Reporter strain for high-throughput screening for cpUPR mutants.....	59
Figure 1-2	Genetic screen identifying <i>mars1-1</i> and <i>mars1-2</i>	60
Figure 1-3	Characterization of Mars1.....	62
Figure 1-4	<i>mars1</i> cells are hypersensitive to photooxidative stress.....	64
Figure 1-5	<i>mars1</i> cells do not activate the cpUPR transcriptional program.....	65
Figure 1-6	Basal induction of the cpUPR renders cells more resistant to chloroplast stress....	67
Figure 1-1S1	Design of a reporter strain for high-throughput detection of the cpUPR signaling in <i>C. reinhardtii</i>	69
Figure 1-2S1	The genetic screen yields two cpUPR silencing mutants: <i>mars1-1</i> and <i>mars1-2</i> ...	71
Figure1-2S2	Genetic analysis of <i>mars1-1</i>	73
Figure 1-2S3	Genetic analysis of <i>mars1-2</i>	75
Figure 1-2S4	Genetic analysis of <i>mars1-3</i> and <i>mars1-4</i>	76
Figure 1-3S1	A catalytic active Mars1 kinase is required for signaling during the cpUPR.....	79
Figure 1-3S2	Specific immunodetection of the Mars1 Flag protein.....	81

Figure 1-4S1	Mars1 confers protection against photooxidative stress.....	83
Figure 1-4S2	<i>mars1</i> cells can cope with ER stress.....	85
Figure 1-5S1	<i>mars1</i> cells do not induce the cpUPR transcriptional program.....	87
Figure 1-5S2	MARS1 gene expression pattern.....	89
Figure 1-5S3	<i>mars1</i> cells do not activate autophagy and sulfur starvation genes during cpUPR inducing conditions.....	91
Figure 1-5S4	<i>mars1</i> cells activate sulfur starvation genes and survive in sulfur-limiting conditions.....	93
Figure 1-5S5	Regulation of photosynthesis-associated genes is not affected in <i>mars1</i> cells.....	95
Figure 1-6S1	The MARS1-E transgene causes mild induction of cpUPR signaling.....	96
CHAPTER 2		
Figure 2-1	Discovery of gene lesion resulting in short-flagellar phenotype.....	169
Figure 2-2	Cre06.g278219 encodes a conserved TOG-domain array protein.....	170
Figure 2-3	Expression of Crescerin transgene leads to rescue of short-flagellar phenotype...	171
Figure 2-4	The previously identified SHF1 gene is encoded by Crescerin/Cre06.g278219...	172
Figure 2-5	The <i>shf-B</i> mutant regenerates with similar early kinetics as W.T and has a precursor pool size similar to W.T.....	173

Figure 2-6	Localization of HA-Crescerin/SHF1 and tubulin within flagella during regeneration.....	174
Figure 2-7	Two hypothesized mechanisms for how Crescerin/SHF1 could regulate flagellar length.....	175
Figure 2-8	The modeling simulations of regeneration kinetics in W.T and the <i>shf-1</i> mutant fit best with Model B: Tubulin-IFT loading.....	177
Figure 2-9	Crescerin/SHF1 is important for growth from longer lengths.....	178
Figure 2-1S1	Discovery of gene lesion resulting in short-flagellar phenotype (related to Figure (1)).....	179
Figure 2-4S1	The previously identified SHF1 gene is encoded by Crescerin/Cre06.g278219 (related to Figure (4)).....	180
Figure 2-5S1	The <i>shf-B</i> and <i>shf-1</i> mutant regenerate with similar early kinetics as W.T and have precursor pool sizes similar to W.T (related to Figure (5)).....	181
Figure 2-6S1	Localization of HA-Crescerin/SHF1 and tubulin within flagella during regeneration (related to Figure (6)).....	183
Figure 2-9S1	Crescerin/SHF1 is important for growth from longer lengths (related to Figure (9)).....	184

LIST OF TABLES

CHAPTER 1

Table 1-1	Strain Positions for Screening Table.....	22
Table 1-2	Strain Table.....	97
Table 1-3	Plasmids table.....	103
Table 1-4	Primers table.....	105

CHAPTER 1

**The Mars1 kinase confers photoprotection through signaling in the chloroplast
unfolded protein response**

**The Mars1 kinase confers photoprotection through signaling in the chloroplast
unfolded protein response**

Karina Perlaza^{1,2}, Hannah Toutkoushian^{1,2}, Morgane Boone^{1,2}, Mable Lam^{1,2}, Masakazu Iwai³,
Martin C Jonikas⁴, Peter Walter^{1,2*}, Silvia Ramundo^{1,2*}

¹Howard Hughes Medical Institute, University of California, San Francisco, San Francisco,
U.S.A

²Department of Biochemistry and Biophysics, University of California, San Francisco, San
Francisco, U.S.A

³Molecular Biophysics and Integrated Bioimaging Division, Lawrence Berkeley National
Laboratory, Berkeley, U.S.A

⁴Department of Molecular Biology, Princeton University, Princeton, U.S.A

This work was originally published in eLife 2019;8:e49577 and is reproduced under a Creative
Commons Attribution 4.0 International license (CC BY 4.0)

ABSTRACT

In response to proteotoxic stress, chloroplasts communicate with the nuclear gene expression system through a chloroplast unfolded protein response (cpUPR). We isolated *Chlamydomonas reinhardtii* mutants that disrupt cpUPR signaling and identified a gene encoding a previously uncharacterized cytoplasmic protein kinase, termed Mars1—for mutant affected in chloroplast-to-nucleus retrograde signaling—as the first known component in cpUPR signal transmission. Lack of cpUPR induction in MARS1 mutant cells impaired their ability to cope with chloroplast stress, including exposure to excessive light. Conversely, transgenic activation of cpUPR signaling conferred an advantage to cells undergoing photooxidative stress. Our results indicate that the cpUPR mitigates chloroplast photodamage and that manipulation of this pathway is a potential avenue for engineering photosynthetic organisms with increased tolerance to chloroplast stress.

INTRODUCTION

In photosynthetic eukaryotes chloroplasts fulfill many essential functions such as photosynthetic conversion of light into chemical energy, synthesis of essential amino acids, fatty acids and other secondary metabolites. Moreover, they act as signaling platforms during plant development and stress adaptation, as they can alter the expression of thousands of nuclear genes and influence many cellular activities that are key to plant performance (Chan et al., 2016). Selective impairment of protein homeostasis in chloroplasts triggers the chloroplast unfolded protein response (cpUPR), a conserved organelle quality control pathway (Ramundo et al., 2014; Llamas et al., 2017). Akin to unfolded protein responses operating from the endoplasmic reticulum (ER) and mitochondria (Walter and Ron, 2011; Shpilka and Haynes, 2018), the cpUPR invokes comprehensive transcriptional changes thought to mitigate an increased burden of proteotoxicity in the organelle. As such, the cpUPR comprises the selective up-regulation of nuclear encoded chloroplast-localized small heat shock proteins, chaperones, proteases, and proteins involved in chloroplast membrane biogenesis. Furthermore, other pathways, such as autophagy and sulfur uptake are activated to mitigate general cellular stress caused by chloroplast metabolic dysfunctions (Ramundo et al., 2014).

In the single-celled alga *Chlamydomonas reinhardtii*, the cpUPR is induced after either inactivation of the Clp protease, which degrades misfolded chloroplast proteins in the organelle's stroma (Figure 1A), or exposure to higher than normal light intensity (high light 'HL'), which causes protein damage through the production of reactive oxygen species in the chloroplast (Ramundo et al., 2014). Similarly, in higher plants, mutants with constitutively reduced levels of the Clp and FtsH proteases selectively upregulate the expression of chloroplast chaperones, such as Cpn60, Hsp70, Hsp90, Hsp100 (Llamas et al., 2017; Zybaïlov et al., 2009; Sjögren et al., 2004;

Rudella et al., 2006; Dogra et al., 2019). However, the mechanism by which chloroplast proteotoxic stress is monitored and how the signal is transmitted from the organelle to the nucleus has remained unknown.

RESULTS AND DISCUSSION

To identify molecular components that mediate cpUPR signaling, we carried out a forward genetic screen in *C. reinhardtii*. To this end, we developed a high-throughput plate-based imaging assay to detect transcriptional activation of cpUPR target genes. In brief, we engineered a reporter strain, in which a truncated promoter and 5' untranslated region of VIPP2 (Nordhues et al., 2012), an early responsive and highly selective cpUPR target gene (Ramundo et al., 2014), was fused to the coding sequence of yellow fluorescent protein (YFP) (Figure 1A). The reporter cells also contained a vitamin-toggled chimeric promoter/riboswitch that allowed efficient shut-down of ClpP1 expression upon addition of two vitamins (Vit), thiamine and vitamin B12, to the medium (Ramundo et al., 2014; Croft et al., 2007; Helliwell et al., 2014). ClpP1 is an essential chloroplast-encoded subunit of the Clp protease (Kuroda and Maliga, 2003; Huang et al., 1994). Such design allowed us to trigger the cpUPR by replica plating onto media containing Vit, yielding a quantitative readout of cpUPR activation (Figure 1B–C, Figure 1—figure supplement 1A–B). Immunoblotting confirmed that the reporter strain induced YFP with comparable kinetics to those of the Vipp2 protein induction upon ClpP1 repression (Figure 1C). As expected, HL, representing a more physiological stress, similarly induced expression of YFP (Figure 1—figure supplement 1C).

For mutagenesis, we randomly integrated a cassette expressing paromomycin resistance into the reporter cells. We isolated colonies and re-arrayed them robotically in 384-well agar plates and then replicated them onto plates without Vit (ClpP1-permissive) or with Vit (ClpP1-nonpermissive). We screened 10,709 insertional mutants for YFP intensity and colony size at 2 and 6 days after replica plating (Figure 2A–B, Figure 2—source data 1). We next scored mutants carrying cpUPR-silencing mutations by their lack of YFP fluorescence in the ClpP1-

nonpermissive condition (+Vit) and those carrying cpUPR-activating mutations by their constitutive YFP fluorescence even in the ClpP1-permissive condition (-Vit) (Figure 2A).

We focused on the cpUPR-silencing mutants that exhibited YFP levels at least three standard deviations lower-than-average YFP fluorescence of all mutants subjected to ClpP1 repression (Figure 2A). This non-saturating screen yielded 68 mutants, of which 51 gave rise to colonies larger than those of the parental cpUPR reporter strain on ClpP1-nonpermissive plates (Figure 2B), suggesting that they impaired ClpP1 repression (e.g., Figure 2—figure supplement 1A–C). Of the remaining 17 mutants, we excluded 15 based on immunoblot analyses that suggested that these mutants contain an insertion affecting only the YFP reporter (e.g., false positive shown in Figure 2—figure supplement 1D). The two remaining mutants exhibited a complete defect in the induction of the cpUPR target genes upon ClpP1 repression, demonstrated by their lack of Vipp2 and Hsp22E/F, another strongly induced protein during the cpUPR (Ramundo et al., 2014; Rutgers et al., 2017; Figure 2C). Vipp2 and Hsp22E/F induction was also impaired during HL, further underscoring the two mutants' cpUPR-silencing phenotype (Figure 2C). As we show below, the two mutants are allelic, both bearing disruptions in Cre16.g692228 (Figure 2D). We henceforth refer to this gene as MARS1 (for mutants affecting retrograde signaling) and the mutants as *mars1-1* and *mars1-2*.

MARS1 is a previously uncharacterized nuclear gene located at the end of chromosome XVI (Figure 2D). It encodes a large protein with no known motifs but a predicted serine/threonine kinase domain toward its C-terminus.

In the case of *mars1-1*, the gene was disrupted by insertion of the mutagenic cassette in intron 21 (Figure 2D). Both tetrad and random spore analyses of WT x *mars1-1* backcrosses

confirmed that the insertion of the cassette in MARS1 (conferring paromomycin resistance) co-segregated with the cpUPR-silencing phenotype (Figure 2E, Figure 2—figure supplement 2A–D). By contrast, in *mars1-2*, the mutagenic cassette mapped to an intergenic of chromosome seven and tetrad analysis of WT x *mars1-2* backcrosses (showing perfect 2:2 segregation) revealed that the causative mutation was unlinked from the cassette insertion (Figure 2E, Figure 2—figure supplement 3A–C) yet due to a single Mendelian mutation (Figure 2—figure supplement 3A–C). Whole genome sequencing of pooled progeny revealed a 13 kb deletion at the end of chromosome XVI, encompassing MARS1 along with two adjacent genes (Figure 2D, Figure 2—figure supplement 3D–E), indicating that the cpUPR-silencing phenotype in *mars1-2* also arose from a mutation in MARS1. To corroborate this conclusion, we picked two additional MARS1 loss-of-function alleles from a *C. reinhardtii* mutant library (Li et al., 2019). As predicted, these mutants—*mars1-3* and *mars1-4*, carrying insertions in MARS1 intron 19 and exon 18, respectively (Figure 2D)—were defective in inducing Vipp2 upon exposure to HL (Figure 2F). Tetrad analyses confirmed that the insertional cassette used to generate this library co-segregated with the cpUPR silencing phenotype in *mars1-3* and *mars1-4* (Figure 2—figure supplement 4A–C).

Moreover, other conditions that disrupt chloroplast protein homeostasis—namely chloroplast translation inhibition by spectinomycin treatment and oxidative stress by hydrogen peroxide exposure (Erickson et al., 2015; Bobik and Burch-Smith, 2015; Blaby et al., 2015)—likewise failed to trigger the cpUPR in these MARS1 mutants (Figure 2—figure supplement 4D), further supporting a causative link between mutations in MARS1 and the cpUPR-silencing phenotype.

Reverse transcriptase PCR (RT-PCR) analyses further validated that the MARS1 mutants were defective in the expression of MARS1 mRNA. As expected, MARS1 mRNA was absent in

mars1-2, *mars1-3* and *mars1-4* (Figure 2—figure supplement 3D–E, Figure 2—figure supplement 4E). By contrast, we detected residual MARS1 mRNA levels in *mars1-1* cells, suggesting that a strong reduction in MARS1 gene expression is sufficient to impair activation of the cpUPR (Figure 2—figure supplement 4E).

The Phytozome-annotated (URL: <https://phytozome.jgi.doe.gov/pz/portal.html>) MARS1 gene model specifies an unusually long 5' untranslated region (5' UTR) that spans the first five exons of MARS1 and predicts that the start site of the MARS1 open reading frame is in the middle of exon 5 (Figure 3A, ATG(ii)). However, in the same gene model, an alternative in-frame translation start-site can be found in exon 1 (Figure 3A, ATG(i)). Interestingly, the coding sequence starting from ATG(ii) would give rise to a Mars1 protein with a potential N-terminal chloroplast target peptide, while the 138aa N-terminal extension translated from the alternative start codon ATG(i) predicts a Mars1 protein with a cytosolic localization. For complementation analyses, we generated two epitope tagged MARS1 transgenes (MARS1-A and MARS1-D). These two transgenes include the endogenous promoter, 5'UTR and 3'UTR, but the 3x-Flag epitope is in different positions (Figure 3A). In MARS1-A, we placed the 3x-Flag far downstream of the two putative translation start sites, yet upstream of the putative kinase domain. In MARS1-D, we placed the 3x-Flag epitope directly after ATG(ii), at the beginning of the putative N-terminal chloroplast target peptide that might be translated from this potential start site. Immunoblot and qPCR analyses of *Vipp2* and *Hsp22E/F* confirmed that expression of either transgene could rescue the cpUPR-silencing phenotype of the MARS1 mutants (Figure 3A, Figure 3—figure supplement 1A–E and Figure 4D). Moreover, the Mars1 protein could be detected by Flag immunoblot analysis not only in the case of MARS1-A but also when the MARS1-D transgene was used (Figure 3A and Figure 4D). Since the N-terminus of chloroplast stromal proteins is cleaved and

promptly degraded upon organellar import, this result suggested that Mars1 was translated from ATG(i) and, therefore, would likely be localized in the cytosol. To support this notion, we performed biochemical fractionation and dual immunofluorescence microscopy using the internally tagged MARS1 transgene (MARS1-A) (Figure 3C–D, Figure 3—figure supplement 2A–B). These orthogonal methods confirmed that Mars1 was enriched in the cytosol while depleted from the chloroplast, nuclear and mitochondrial compartments (Figure 3C–D).

To explore whether the predicted kinase activity of Mars1 would be involved in cpUPR signaling, we introduced a point mutation, which disrupts the conserved catalytic triad of the kinase (D1871A) in both MARS1-A and MARS1-D transgenes and tested the ability of these Flag-tagged MARS1-KD constructs (KD for kinase-dead) to rescue *mars1* cells. In contrast to MARS1, expression of either MARS1-A KD or MARS1-D KD transgene failed to restore cpUPR signaling, as demonstrated by its lack of VIPP2 and other cpUPR target gene induction upon Clp repression and HL stress (Figure 3B and Figure 3—figure supplement 1A–D). These results strongly suggest that an enzymatically active kinase domain in Mars1 is required for cpUPR signaling.

The discovery of a critical player in the cpUPR gave us a unique opportunity to examine the physiological role of the cpUPR during conditions of chloroplast proteotoxicity. To this end, we compared the sensitivity of WT and *mars1* cells to HL stress. Upon prolonged exposure to HL, *mars1* cells exhibited accelerated photobleaching and slower growth recovery relative to WT cells (Figure 4A–B, Figure 4—figure supplement 1A, Figure 4—figure supplement 1—source data 1). Notably, both phenotypes were rescued by expression of wild-type MARS1 but not by MARS1-KD (Figure 4A–B, Figure 4—figure supplement 1A, Figure 4—figure supplement 1—source data 1).

We next tested the sensitivity of MARS1 mutants towards metronidazole, a drug that selectively generates hydrogen peroxide in chloroplasts when cells engage in photosynthesis upon light exposure (Schmidt et al., 1977; Dent et al., 2015). *mars1* cells proved remarkably more sensitive than WT to metronidazole in photoheterotrophic and in phototrophic conditions, while their growth was not affected when grown in the dark (Figure 4C, Figure 4—figure supplement 1B–F). By contrast, WT and *mars1* cells were equally sensitive to tunicamycin, a chemical inducer of proteotoxic stress in the ER (Figure 4—figure supplement 2A–C) (Yamaoka et al., 2018). Moreover, as we observed for other conditions inducing the cpUPR, the metronidazole mediated activation of cpUPR target genes, such as VIPP2 and HSP22E/F, was dependent on Mars1 and its kinase activity (Figure 4D). Notably, by performing Flag affinity purification followed by mass spectrometry using Mars1-D and Mars1-D KD subjected to metronidazole treatment, we identified three serine residues (S69, S280 and S1888) that were selectively phosphorylated in Mars1-D but not in Mars1-D KD (Supplementary file 1). Furthermore, we detected peptide spectra derived from the first 138 aa of Mars1. Thus, taken together, our results strongly suggest that Mars1 is a cytosolic kinase that is required for the tolerance of chloroplast proteotoxic stress.

To characterize more comprehensively the function of Mars1 in transcriptional activation of cpUPR target genes, we compared the transcriptome of WT versus *mars1-1* cells by RNA sequencing following Clp repression and HL exposure (Figure 5A–D, Figure 5—figure supplement 1A). Given the previously reported complexity of cell stress responses in algae and higher plants (Chan et al., 2016; Erickson et al., 2015; Bobik and Burch-Smith, 2015), we aimed to identify a core set of MARS1-responsive genes under both cpUPR-inductive conditions (Figure 5A–B). Seven of the eight genes annotated as most highly co-expressed with VIPP2 in the Phytozome database were up-regulated only in wild-type but not in *mars1* cells, including those

encoding chloroplast small heat shock proteins (Figure 5—figure supplement 1B, Figure 5—figure supplement 2—source data 1). Similarly, the transcriptional activation of CLPB3, DEG11 and stromal APX, which are evolutionarily conserved genes involved in chloroplast protein quality control and detoxification of reactive oxygen species, was impaired in *mars1* cells (Figure 5A). The MARS1-dependent transcriptome also comprised gene clusters involved in RNA metabolism, autophagy, and sulfur uptake (Figure 5—figure supplement 1C, Figure 5—figure supplement 3A–B). Importantly, *mars1* cells did not show reduced growth when subjected to sulfur deprivation, a different stress condition in which activation of autophagy and sulfur starvation genes are essential for cell survival (Figure 5—figure supplement 4A–E) (Kajikawa et al., 2019; Zhang et al., 2004). Thus, Mars1 selectively responds to chloroplast proteotoxic stress (Ramundo and Rochaix, 2014; Heredia-Martínez et al., 2018). Intriguingly, although *mars1* cells displayed a growth defect under HL conditions, several HL controlled genes encoding components of the photosynthesis machinery did not require MARS1 (Figure 5C–D, Figure 5—figure supplement 5). Likewise, the activation of genes that function in non-photochemical quenching (NPQ), a pathway that contributes to HL tolerance by dissipating excess energy as heat, was not impaired in *mars1* cells (Erickson et al., 2015; Correa-Galvis et al., 2016) (Figure 5C–D, Figure 5—figure supplement 5). Thus, the cpUPR entails a unique transcriptional response that is likely to act in concert with other known HL tolerance mechanisms.

The publicly available transcriptomics data on *Chlamydomonas* circadian cell cycle show that MARS1 belongs to a gene cluster that exhibits its expression peak at dawn and its expression trough at night (Figure 5—figure supplement 2A). The steady increase in MARS1 mRNA level immediately preceding exposure to light supports the notion that the Mars1 kinase may be important for responding to light fluctuations. Indeed, in our transcriptomics dataset, MARS1

mRNA was expressed roughly 10-fold and 2-fold more upon HL exposure and ClpP1 repression, respectively (Figure 5—figure supplement 1B, Figure 5—figure supplement 2B). However, in the hypomorphic *mars1-1* mutant allele, where residual amounts of MARS1 transcript were detected, (Figure 5—figure supplement 1B, Figure 5—figure supplement 2B), the stress-dependent MARS1 upregulation was lost. It is therefore possible that the activation of a mild chloroplast UPR may be part of the physiological circadian cycle and that MARS1 gene expression may be regulated through a positive feedback loop.

Finally, we took advantage of the serendipitous finding that expression of the MARS1-E transgene (Figure 6A), bearing a 6x-Flag tag insertion after Leu402 of Mars1, upregulated both Vipp2 and Hsp22E/F even in the absence of stress (Figure 6B–C). The dominant activating phenotype of MARS1-E was not observed in wild-type cells expressing other Flag-tagged alleles of MARS1 (Figure 6—figure supplement 1A), and was dependent on Mars1’s enzymatic function, as it was blocked by the D1871A kinase inactivating mutation (Figure 6B–C, Figure 6—figure supplement 1B). We consider it likely that the constitutive cpUPR phenotype results from a fortuitous activation of Mars1, perhaps by inactivation of an auto-repressive feature of the enzyme or by modification of a protein-protein or a protein-metabolite interface. MARS1-E was sufficient to trigger activation of the canonical cpUPR, as confirmed by qPCR analysis of MARS1-dependent transcripts, such as those in the VIPP2 co-expression cluster (Figure 6C). Conversely, MARS1-independent transcripts such as those involved in NPQ were unaffected by expression of MARS1-E (Figure 6C). These results suggest that Mars1 is an integral component directly involved in cpUPR signaling since its activation is not only required but can also be sufficient to induce the cpUPR transcriptional program. Notably, cells expressing MARS1-E exhibited a higher

resistance to metronidazole and to HL stress (Figure 6D–E), indicating that induction of the cpUPR can confer a growth advantage in the presence of chloroplast proteotoxicity.

CONCLUSION

In summary, our results suggest that, upon onset of chloroplast proteotoxic stress, a signal transduction pathway, originating in the chloroplast, leads to activation of the cytosolic kinase Mars1, which in turn orchestrates the cpUPR transcriptional program. Activation of cpUPR through Mars1 mitigates photooxidative stress and delays photobleaching. However, loss of Mars1 does not impair expression of genes involved in non-photochemical quenching. Thus, the exact mechanism by which the cpUPR pathway confers photoprotection remains to be deciphered. Input conditions that activate the cpUPR, as well as cpUPR target genes identified to date, are phylogenetically conserved from *C. reinhardtii* to *A. thaliana* (Llamas et al., 2017; Zybailov et al., 2009; D'Andrea et al., 2018). Thus, despite not yet having identified a functional ortholog of MARS1 in higher plants, it is reasonable to assume that the cpUPR's previously unknown role in protecting cells against photooxidative stress would likewise be conserved. This notion is particularly appealing in light of the observation that basal induction of the cpUPR conferred a protective effect in response to stress and that, conversely, loss of Mars1 activity profoundly sensitized cells towards HL and other chloroplast stressors. Hence, engineering plants with constitutive cpUPR activation may be a promising strategy to enhance their tolerance to environmental stresses.

AUTHOR CONTRIBUTIONS

Karina Perlaza: Conceptualization, Investigation, Methodology, Validation, Formal analysis, Data Curation, Visualization, Writing – original draft preparation, Writing – review and editing

Hannah Toutkoushian: Investigation, Methodology, Validation, Data Curation, Visualization

Morgane Boone, Mable Lam, and Masakazu Iwai: Software, Validation, Formal analysis, Resources, Data Curation, Visualization

Martin C Jonikas: Methodology, Resources, Funding acquisition

Peter Walter: Conceptualization, Resources, Writing – original draft preparation, Writing – review and editing, Supervision, Project administration, Funding acquisition

Silvia Ramundo: Conceptualization, Investigation, Methodology, Validation, Resources, Data Curation, Writing – original draft preparation, Writing – review and editing, Visualization, Supervision, Project administration

ACKNOWLEDGEMENTS

We thank Jean David Rochaix for his generous donation of key reagents and critical feedback on this work, Olivier Vallon, Michael Schroda and Arthur Grossman for providing the ClpP1, Hsp22E/F and Sultr2 antibodies, respectively. We thank Fran Sanchez for preparing growth media for maintenance of our strains, Luke Mackinder, Nina Ivanova, Julia Wei for help with the genetic screen, and Lorenzo Costantino, Susan Dutcher, Stephane Gabilly, Ursula Goodenough, Robert Jinkerson, Yuval Kaye, Elif Karagoz, Xiaobo Li, Daniel Neusius, Jorg Nickelsen, Masayuki Onishi, Leif Palessen, Weronika Patena, Jirka Peschek, Shai Saroussi, Setsuko Wakao, Lan Wang and Tyler Wittkopp for invaluable advice in various aspects of this project. We thank Ryan Leib and Kratika Singhal who curated Mass-Spec analysis for this work and all Walter and Jonikas lab members for insightful discussions on this project.

MATERIALS AND METHODS

General maintenance of *C. reinhardtii* strains

All *C. reinhardtii* strains were maintained on Tris-Acetate-Phosphate (TAP) solid media (1.6% agar, USP grade, Thermo Fisher Scientific) with revised Hutner's trace elements (Kropat et al., 2011) at 22°C in low light ($\sim 10\text{--}20 \mu\text{mol photons m}^{-2} \text{ s}^{-1}$). Lines harboring the ClpP1 repressible gene were maintained in the media supplemented with 100 $\mu\text{g/ml}$ spectinomycin (Sigma). Lines harboring a mutagenic cassette disrupting the MARS1 gene were maintained in the media supplemented with 20 $\mu\text{g/ml}$ paromomycin (Sigma). Lines harboring a MARS1 transgene construct were maintained in the same conditions with solid media supplemented with 20 $\mu\text{g/ml}$ hygromycin (Thermo Fisher Scientific). Sulfur-depleted TAP liquid and agar plates were prepared as previously described (Davies et al., 1994). Generally, during liquid growth, no antibiotic was supplemented. For the experiments shown in Figure 4—figure supplement 2A–C, TAP liquid cultures and agar plates were supplemented with 5 mg/ml or 0.2 mg/ml tunicamycin (EMD Millipore), respectively. All strains used in this study are listed in Table 1.

Generation of the cpUPR reporter strain

The cpUPR reporter strain (CrPW1) was generated by nuclear transformation of the *C. reinhardtii* ClpP1 repressible strain (DCH16; Ramundo et al., 2014), using 300 ng of Nde1-linearized pPW3217 plasmid (Table 2 for plasmids used in this study). Nde1 and all the other restriction enzymes described in this publication were purchased from NEB. The nuclear transformation was carried out via electroporation as described below (section on 'Insertional mutagenesis'). Transformants isolated on TAP agar plates containing 20 $\mu\text{g/ml}$ hygromycin and tested by Flag immunoblot analysis upon ClpP1 repression and exposure to HL. As previously observed (Ramundo et al., 2014; Ramundo et al., 2013), during random insertion of a construct with

regulatory regions in its promoter, less than 10% of the hygromycin resistant transformants preserved the correct gene expression pattern of the downstream coding sequence. Among them, we selected CrPW1 for further studies. The pPW3217 plasmid, containing a minimum region of the VIPP2 gene promoter, its 5' untranslated region and its exon and intron, the yellow fluorescent protein coding sequence (YFP CDS), C-terminally appended to a triple Flag epitope the 3' untranslated region of the RBCS2 gene, was generated by In-Fusion cloning (Clontech). The VIPP2 genomic fragment was amplified from genomic DNA with primers SR510 and SR502 (see Table 3 for primers used in this study). The YFP CDS fused to a 3x-Flag epitope was amplified from pLM005 (Chlamydomonas Resource Center) with primers SR503 and SR504. The 3' untranslated region of the RBCS2 gene was amplified from pHyg3 (Berthold et al., 2002) with primers SR505 and SR506. All PCRs were performed using Phusion Hotstart II polymerase (Thermo Fisher Scientific). PCR products were gel-extracted using NucleoSpin Gel and PCR Clean-Up Kit (Takara) according to manufacturer's instructions, and they were further purified by ultrapure phenol:chloroform:isoamyl alcohol (25:24:1, v/v/v) (Life Technologies) extraction and ice-cold ethanol (Sigma) precipitation. These three purified DNA fragments were then mixed with a purified and linearized pHyg3 vector, previously digested by PciI and EcoRV, and incubated with the In-Fusion reagents (Takara) as per manufacturer's instructions. The In-Fusion product was transformed into Stellar competent cells (Takara) according to manufacturer's instructions and putative positive clones were selected in LB solid media (1.7% agar) supplemented with ampicillin after overnight incubation. The resulting plasmid, pPW3217, was purified using the Kit PureYield Plasmid Miniprep System (Promega) and verified by analytical digestion and sequencing. All constructs made by In-Fusion cloning for this publication follow this same protocol from transformation through plasmid isolation.

Preparation of the paromomycin cassette for insertional mutagenesis

The mutagenic DNA cassette was isolated by restriction enzyme digestion of pMJ016c (provided by the Jonikas laboratory), which contains the HSP70-RBCS2 chimeric promoter, the paromomycin resistance gene AphVIII, and the PSAD and RPL12 chimeric terminator (Mackinder et al., 2016). Using the MlyI enzyme, a blunt fragment of 2204 bp (containing the mutagenic DNA cassette) was isolated and extracted from a 1% agarose gel through the NucleoSpin Gel and PCR Clean-Up Kit (Takara) per the manufacturer's instructions. To further remove possibly contaminating DNA, the mutagenic DNA cassette was electrophoresed on a 1% agarose gel, extracted and repurified as explained above.

Insertional mutagenesis and maintenance of mutant library prior to the screen

A 1-liter liquid culture of cpUPR reporter strain (CrPW1) was grown in TAP medium in low light ($\sim 30 \mu\text{mol photons m}^{-2} \text{s}^{-1}$) to a density of about $2\text{--}4 \times 10^6$ cells ml⁻¹. Cells were collected at room temperature (RT) by centrifugation at $3000 \times g$ for 5 min and gently resuspended in TAP supplemented with 40 mM sucrose at 2×10^8 cells ml⁻¹. Multiple aliquots of 250 mL of cell suspension were then transferred into Gene Pulser electroporation cuvettes (0.4 cm gap, Bio-Rad) and incubated at 16°C for 5–30 min. In each cuvette, about 20 ng of mutagenic DNA cassette was added to the cell suspension and quickly mixed by pipetting. Electroporation was performed immediately using a Gene Pulser II electroporation system (Bio-Rad) with the following parameters: capacitance = 25 mF and voltage = 800 V. Electroporated cells from each cuvette were then diluted into 8 ml TAP supplemented with 40 mM sucrose and allowed to recover overnight by gentle agitation in very dim light ($5\text{--}10 \mu\text{mol photons m}^{-2} \text{s}^{-1}$). The next day, cells were collected by centrifugation at $1000 \times g$ for 5 min, resuspended in 1 ml of TAP medium, plated on TAP agar

plates containing 20 µg/ml paromomycin and incubated in darkness for about three weeks before picking colonies.

Approximately 55,000 total mutants were picked and re-arrayed in a 384-colony format on rectangular agar plates (Singer Instruments) using a Norgren CP7200 colony-picking robot. In each 384-mutant array plate, the last two rows were kept empty to include internal positive and negative controls for the next stage of the screen (for details, read section ‘Execution of YFP mutant screen on agar plates’). This library of mutants (of approximately 150 agar plates) was grown in complete darkness at 22°C and propagated every 3–4 weeks by robotically passaging the mutant arrays to fresh 1.5% agar solidified TAP medium containing 100 µg/ml spectinomycin using a Singer RoToR robot (Singer Instruments). Unfortunately, numerous mutants were lost during propagation due to a wide-spread contamination event.

Execution of YFP mutant screen on agar plates

To screen for YFP silencing or activating mutants, rectangular agar plates, each containing 97 ml of TAP medium $-/+$ Vit (400 mM thiamine-HCl (Sigma) and 80 ng ml⁻¹ of vitamin B12 (Sigma)), were prepared. In each agar plate ($-/+$ Vit), 12 colonies of the cpUPR reporter strain (CrPW1), 12 colonies of the parental ClpP1 repressible strain (DCH16) and 12 colonies of 2 different positive YFP expressor strains (CrPW2 and CrPW3) were robotically spotted in the last two rows of the 384-colony array to be used as internal positive and negative controls during the YFP screen (see scheme in section ‘Semi-automated identification of YFP mutants through Image-J macroscripts’). Next, insertional mutants (freshly propagated) were spotted onto these same plates. Plates were incubated in dim light (20–30 µmol photons m⁻² s⁻¹) at 25°C and were imaged after 2 and 6 days using a Typhoon TRIO fluorescence scanner (GE Healthcare). For each round, 12 plates of insertional mutants (six without and six with Vit) were simultaneously scanned with the settings

described below. Chlorophyll Autofluorescence: Excitation 633 nm, Emission filter 670/30 nm, PMT 300, Sensitivity Normal, Pixel size 500 nm. YFP Fluorescence: Excitation 532 nm, Emission filter 555/20 nm, PMT 800, Sensitivity Normal, Pixel size 500 nm. The focal plane parameter was set at 'plus 3 mm' to focus the optics 3 mm higher than the glass plate. This last detail and the thickness of the agar plate (97 ml of liquid agar) were critical parameters to successfully detect the YFP signal.

Semi-automated identification of YFP mutants through Image-J macroscripts

We used macroscripts in ImageJ64 software (Schneider et al., 2012) to quantify the intensity values of colonies in the mutant library (for details, please refer to Source code 1). Each plate was imaged in the YFP and in the chlorophyll channel. To orient each image, the bottom two rows of each plate were spotted with characterized positive and negative YFP strains (CrPW1, DCH16, CrPW2, and CrPW3) in the specific order outlined in the scheme below, where (-) denotes lack of YFP signal and (+) denotes presence of YFP signal. The ordering of these colonies conferred a reproducible fluorescent pattern in the YFP channel, which was used to identify the bottom two rows of each image.

Table 1-1: Strain Positions for Screening

Plate without vitamins																								
position	1	2	3	4	5	6	7	8	9	10	11	12	13	14	15	16	17	18	19	20	21	22	23	24
Cell line	DCH16		CrPW1		DCH16		CrPW2		CrPW3		CrPW1		CrPW3		CrPW1		CrPW2		DCH16		CrPW2		CrPW3	
YFP signal	-	-	-	-	-	-	+	+	+	+	-	-	+	+	-	-	+	+	-	-	+	+	+	+
Plate with vitamins																								
position	1	2	3	4	5	6	7	8	9	10	11	12	13	14	15	16	17	18	19	20	21	22	23	24
Cell line	DCH16		CrPW1		DCH16		CrPW2		CrPW3		CrPW1		CrPW3		CrPW1		CrPW2		DCH16		CrPW2		CrPW3	
YFP signal	-	-	+	+	-	-	+	+	+	+	+	+	+	+	+	+	+	+	-	-	+	+	+	+

To quantify the YFP intensity of each mutant, a 16 × 24 array containing 384 Regions-Of-Interest (ROIs) was constructed for each image in the chlorophyll channel, where all living colonies exhibited signal. The same grid was applied to the corresponding image in the YFP channel. From each ROI on autothresholded images, the maximum intensity in the YFP channel was measured. To account for variability in the magnitude of the YFP response on different plates (due to slight variations in agar thickness), it was necessary to normalize the YFP intensity of each mutant colony to the YFP intensity of its parental strain (CrPW1) from the same plate (average of n = 12). Colonies exhibiting YFP fluorescence higher than three standard deviations from the average of all colonies were labeled as potential activators, while colonies with YFP intensities below three standard deviations from the average were labeled as potential silencers. Of the potential cpUPR silencers, we observed that many of these mutants grew to a larger colony size than the parental CrPW1 strain after 6 days. Their robust growth suggested suppression of vitamin-induced ClpP1 inactivation. To exclude these suppressor mutants, we analyzed the area of all the colonies at 2 and 6 days by measuring the particle area of autothresholded images in the chlorophyll channel. The average colony size increase was 1.38-fold for the 10000-plus colonies analyzed. Candidate colonies that increased 2-fold in colony area (more than one standard deviation away from the average) were regarded as suppressors. Of the remaining silencing candidates, *mars1-1* exhibited the most attenuated YFP response in the presence of Vit.

We indicate *mars1-2* with an asterisk (*) in Figure 2A because this mutant was identified in a secondary screen but its position in the original mutant library was lost due to contamination of the plate. To evaluate the YFP response and colony size of *mars1-2* in the context of the entire mutant library, we re-spotted *mars1-2* on a fresh agar plate containing the characterized cpUPR reporter strain and the other positive and control strains in the bottom two rows as described above.

The normalized YFP intensity of *mars1-2* in the absence and presence of Vit was then mapped onto the quantification of the original mutant colonies.

Genomic DNA extraction

With the single exception of the DNA samples submitted for whole genome sequencing, all the other genomic DNA (gDNA) extractions were performed as described below. A 6 ml aliquot of a liquid TAP culture in mid-log phase were spun down, and the media was decanted. The pellet was resuspended in 400 μ l of water and then 1 vol of 2x DNA lysis buffer was added (200 mM Tris HCl pH 8.0, 6% Sodium Dodecyl Sulfate (SDS), 2 mM EthyleneDiamineTetraAcetic acid (EDTA). To digest proteins, 5 μ l of 20 mg/ml proteinase K (Life Technologies) was added and allowed to incubate at Room Temperature (RT) for 15 min. 200 μ l of 5M NaCl was then added and mixed gently. Next, to selectively precipitate nucleic acids, 160 μ l of 10% cetyltrimethyl ammonium bromide (CTAB) (EMD Millipore) in 0.7 M NaCl was added and allowed to sit for 10 min at 65°C with gentle agitation. Two or more consecutive rounds of DNA extraction using ultrapure phenol:chloroform:isoamyl alcohol (25:24:1, v/v/v) were performed to achieve a clean interphase. Then, the upper aqueous phase was retained and mixed with 1 vol of 2-propanol (Sigma). This was mixed gently for 15 min at RT. Then it was spun down for half an hour at 21,000 x g at 4°C. The supernatant was removed and 1 vol of ice-cold 70% ethanol was added and mixed with the pellet. This mixture was spun down for 15 min at 21,000 x g. The supernatant was removed and the DNA precipitate was dried in a speed-vac for about 10–25 min and resuspended in 40 μ l of nuclease-free water (Ambion). To ensure complete removal of any potential RNA contamination, in most cases, the gDNA prep was then subjected to in-solution ribonuclease treatment using Rnase A/Rnase T1 mix (Thermo Fisher Scientific) according to manufacturer's instructions. Finally, the gDNA was quickly repurified through an additional round of DNA

extraction using ultrapure phenol:chloroform:isoamyl alcohol (25:24:1, v/v/v) and 2-propanol precipitation as described above.

The purity of the gDNA prep was assessed by Nanodrop (Thermo Fisher Scientific), ensuring absorbance ratios at 260/280 nm and 260/230 nm to be ~1.8 and ~2.0, respectively, prior to using the gDNA preparation for most of the follow-up applications. For the pooled (whole genome sequencing) DNA samples, the genomic DNA extraction was performed with the following protocol adapted from the Qiagen, DNeasy Plant Mini Kit using its proprietary buffers (Buffer P3, AW1, AW2, AE). A 25 ml culture of each progeny was grown for ~2 days to about 3×10^6 cells/ml. Cells were then pelleted and resuspended in 0.5 ml of SDS-EB lysis buffer (50 mM Tris-HCl, 200 mM NaCl, 20 mM EDTA, nuclease-free H₂O, 2% SDS, 1% Polyvinylpyrrolidone average molecular weight = 40,000-, 1 mg/ml of proteinase K) and allowed to incubate for ~10 min. One volume of phenol:chloroform:isoamyl alcohol (25:24:1, v/v) was added and mixed vigorously. The mixture was spun at 13,500 x g for 5 min at RT. The upper phase was transferred into new Eppendorf tubes and 5 ml of 100 mg/ml of RNase A, was added and incubated at RT for 30 min. The lysate was mixed with 130 μ l aliquot of Buffer P3 and incubated on ice for 5 min. This mixture was spun at 18,400 x g for 5 min at RT. The lysate was transferred to the QIAshredder Mini column and spun for 18,500 x g for 2 min. The flow-through fraction was transferred into a new tube and 1.5 volumes of Buffer AW1 was added to the cleared lysate and mixed well. This mixture was then transferred to a DNeasy Mini column and spun at 7600 x g for 1 min. The flow-through fraction was discarded and this step was repeated for any remaining mixture. The DNeasy Mini column was transferred to a new collection tube and 500 μ l of Buffer AW2 was added, centrifuged at 7600 x g for 1 min and the flow-through discarded. Another 500 μ l of Buffer AW2 was added and centrifuged at 18,400 x g to dry the membrane. The column was then transferred to

a new Eppendorf tube. 90 ml of Buffer AE was added onto the DNeasy membrane and incubated for 5 min at RT. The DNA was eluted by centrifugation at 7600 x g for 1 min. This step was repeated again, using the 90 ml of Buffer AE collected after the first centrifugation. The quality of the DNA samples was assessed by Nanodrop as described above. The DNA samples were then stored in 20°C until use.

Single-colony LEAP-seq to identify insertion sites in MARS1 mutants

The protocol was optimized for single-colony DNA sequencing from the original protocol (Li et al., 2016). A pure genomic DNA preparation was assured by running the DNA on a 1.5% agar gel prior to starting. A single-stranded DNA fragment was generated by extending a biotinylated primer from the cassette to the flanking DNA using either primer oMJ598 or primer oMJ1234, which anneals to the 3' or 5' end of the mutagenic cassette, respectively. The linear extension mix was set in the following way: 500 ng of gDNA, 2 ml of 0.25 mM of biotinylated primer, 0.5 ml of Phusion Hot Start Polymerase (Thermo Fisher Scientific), 10 ml of Phusion GC buffer, 3 ml of DMSO, 1 ml of 50 mM MgCl₂, 1 ml of 10 mM dNTPs. Prior to starting the mix, the GC buffer was thawed, heated to 95°C for five minutes, vortexed and then put back on ice until the solution became completely clear. The linear extension reaction was carried out in a thermocycler with the following program: Stage 1) 98° C for 3 min; Stage 2) 98°C for 10 s, 65°C for 30 s, 72°C for 18 s (40 cycles). This program was run twice and, in between the first run and the second run, 0.5 ml of Phusion Hot Start Polymerase was added. The Dynabeads kilobase Binder Kit (Thermo Fisher Scientific) was used to purify the linear extension product. For each reaction, 8 ml of streptavidin-coupled magnetic beads) were transferred into an Eppendorf tube and washed in 100 ml of phosphate-buffered saline (PBS) up to four times using a DynaMag magnet (Thermo Fisher

Scientific). The Dynabeads were then washed once more in 20 ml of binding solution and gently resuspended in 100 ml of binding solution, pipetting up and down only a few times. Next, the beads were transferred in the PCR tube from the linear extension reaction described above. To allow efficient binding of the linear extension product to the streptavidin-coupled magnetic beads, the samples were incubated overnight at RT on an overhead-rotating platform. The following day, the linear extension product was isolated and ligated to a single-strand DNA adaptor, per the following procedure. The beads were washed three times with 100 ml of PBS allowing 8 min incubation in between washes. At the end of the final wash, we ensured that all PBS was carefully removed to avoid interference with the ssDNA ligation reaction. A 20 ml ssDNA ligation reaction was added and gently mixed with the magnetic beads. The ligation mix contained 11.25 ml of H₂O, 1 ml of 25 mM ssDNA adaptor primer (oMJ619), 1 ml of 50 mM MnCl₂, 4 ml of 5 M betaine, 2 ml of CircLigase II reaction buffer, 0.75 ml of CircLigase II (Epicentre). The beads were transferred to the thermocycler, which was pre-heated to 60°C for 10 min. This mixture was incubated for 1 hr at 60°C. The beads were then washed three times with 100 ml of PBS as described above. Next, the ssDNA was converted to a dsDNA using primers annealing to the ligated adaptors at the ends of the ssDNA sequence. 1 ml of 25 mM of Primer 1 (see below), 1 ml of 25 mM of Primer 2 (oMJ621), 0.5 ml of Phusion HotStart, 10 ml of Phusion GC buffer, 32.5 ml of H₂O, 3 ml of DMSO, 1 ml of 50 mM MgCl₂, 1 ml of 10 mM dNTPs and the template DNA (beads) were mixed together. Primer one depended on whether the original extension from the cassette was in the 5' or 3' orientation. If the 3' cassette flanking primer (oMJ598) was used during the linear extension, primer T3_3'oMJ016c 11/ 23 was chosen. Instead, when the 5' cassette flanking primer (oMJ1234) was used during linear extension, oMJ1239 was chosen. Primer 2 (oMJ621) annealed to the ligated adaptor. Both primers were designed to contain a binding site for the mutagenic cassette and a

binding site for a T3 sequencing primer. The following amplification program was used: Stage 1) 98°C for 3 min, Stage 2) 98°C for 10 s, 63°C for 25 s, 72°C for 20 s (10 cycles), Stage 3) 98°C for 10 s, 72°C for 45 s (13 cycles). The dsDNA products were then run on a 1% gel. The DNA smears were cut out of the agarose gel, purified using NucleoSpin Gel and PCR Clean-Up Kit (Takara) according to manufacturer's instructions and subjected to Sanger Sequencing using a standard T3 sequencing primer. Finally, to identify the insertion site of the mutagenic cassette, the sequencing results were blasted in Phytozome, v5.5. The sequence of the aforementioned primers can be found in Table 3.

Mating and tetrad analysis

Note: *mars1-1* and *mars1-2* proved difficult to mate due to their genetic background. Therefore, extra measures were taken to increase the efficiency of mating. *mars1-3* and *mars1-4*, obtained from the Jonikas library, did not have this problem, therefore, these extra measures were not taken. The following protocol will indicate the differences.

Cells were re-streaked onto fresh TAP agar and incubated in low light (<15 mmol photons m⁻² s⁻¹) for five days. They were then transferred onto TAP agar containing 1/10 of the usual NH₄Cl concentration and kept in this medium for four-five days under moderate light (~40 μmol photons m⁻² s⁻¹) to induce starvation. The gametes from each strain were then resuspended in a 24-well sterile transparent plate (Costar) using 150–200 ml of water or M-N/5 solution till a dark green resuspension is obtained. M-N/5 solution was used for the *mars1-1* and *mars1-2* backcrosses, and water was used for *mars1-3* and *mars1-4* backcrosses. M-N5 solution contained 1 ml of 10% sodium citrate, 0.2 ml of 1% FeCl₃, 0.2 ml of 4% CaCl₂, 0.34 ml of 10% K₂HPO₄, 0.2 ml of 10% KH₂PO₄, 0.2 ml of Hutner's Trace elements (Chlamydomonas Resource Center), H₂O to 1.25 liter. The solution was autoclaved in 100 ml aliquots per bottle. The plate was then transferred to

a shaker under moderate light ($\sim 40 \mu\text{mol photons m}^{-2} \text{ s}^{-1}$) and allowed to mix for ~ 1 hr. Gametes of the opposite mating type were mixed (~ 100 ml per gamete) in a separate well and the plate was placed under light with no shaking. For the *mars1-1* and *mars1-2* strains, after one hour of mixing, dibutyryl cyclic AMP (Sigma) was added to each mating mix to a final concentration of 30 mM. Mating efficiency was checked periodically (every 15–30 min) for fusion events and quadriflagellate formation. The gametes were mated for ~ 3 hr. Aliquots (100 ml) of the mating mixture were plated into TAP 4% agar. Plates were exposed to light ($\sim 50 \mu\text{mol photons m}^{-2} \text{ s}^{-1}$) overnight and the next day wrapped in aluminum foil. After ~ 1 – 2 weeks, the vegetative cells were scraped off using a small rectangular soft razor blade (Personna, .009'', two-facet aluminum blade) with gentle pressure on the agar. Zygotes adhere to the agar surface and can be recognized under a light microscope due to their darker and larger appearance. A 100 ml aliquot of liquid TAP medium was then added on top of the zygotes and a more rigid scalpel (Feather, N.2) was used to scrape the zygotes off the agar. A line was drawn onto the center of a fresh TAP 1.5% agar plate, and the zygotes were spotted along this line. The cells were then allowed to dry. For *mars1-1* and *mars1-2*, but not for *mars1-3* and *mars1-4*, vegetative cells were killed by treating the plate with chloroform vapor for ~ 15 – 30 s. The plate was incubated under light ($\sim 80 \mu\text{mol photons m}^{-2} \text{ s}^{-1}$) overnight to 1.5 days. At 24°C , germination typically occurred after ~ 20 hr. Under the dissection scope, tetrads and octads were found and dissected. Incomplete tetrads, full tetrads and octads were then re-arrayed onto TAP agar in a 96-array format and then replicated onto the appropriate drug resistances. When necessary, mating type specific PCRs (Werner and Mergenhagen, 1998) were carried out to ensure that the progeny were in fact due to a sporulation event and were not mistakenly parental strains.

Check-PCRs on genomic DNA to verify the causative mutation in *mars1-1*

Genomic DNA from progeny derived upon crossing *mars1-1* to CC-124 was obtained as outlined in ‘Genomic DNA extraction’ section. The insertion of the mutagenic cassette in the MARS1 locus was verified by PCR by using primers SR773 and T3_5’_oMJ016c 11/24, which anneal to exon 17 of MARS1, and to the 5’ side of the mutagenic cassette, respectively. The PCR reaction was run on 1– 1.5% agarose, cut out of the agarose gel, purified using NucleoSpin Gel and PCR Clean-Up Kit (Takara) according to manufacturer’s instructions and subjected to Sanger sequencing to verify the expected sequence identity. The sequence of the aforementioned primers can be found in Table 3.

Whole Genome Sequencing (WGS)

Progeny derived upon crossing *mars1-2* x CC-124 were re-arrayed onto 96-well plates and replicated onto TAP supplemented with hygromycin, paromomycin or spectinomycin to determine the segregation patterns of the progeny. Mating type specific PCRs were performed on almost all progeny (Werner and Mergenhagen, 1998). The progeny was then tested in high light and by Vipp2 immunoblot analysis two or three times to determine which one had silencing vs. wild-type phenotypes. Genomic DNA was extracted as described above in the section ‘Genomic DNA extraction’ and was subsequently pooled per the progeny’s phenotype, i.e. *mars1*-like or WT-like. Additional pools containing the parental strains were also analyzed likewise. The size of the pools of gDNA were of different proportions depending on the amount of progeny in that group (WT vs. *mars1*-like). The pooled gDNA was then fragmented using Covaris and Bioruptor Pico. The sequencing libraries were prepared with the aid of the PrepX DNA library kit (Takara). One cycle of PCR was used to linearize the library molecules. Fragment analyzer traces and Qubit values were assessed for each sequencing library as quality control checks. Sequencing was performed

on the HiSeq2500 Rapid sequencer. The *C. reinhardtii* reference genome was downloaded from Phytozome, v5.5 onto the Geneious software (Kearse et al., 2012). The reads from each library were then aligned to the reference genome.

Check-PCRs on genomic DNA to verify the causative mutation in *mars1-2*

Genomic DNA from progeny of meiotic tetrads derived upon crossing *mars1-2* to CC-124 was obtained as outlined in ‘Genomic DNA extraction’ section. The MARS1 locus was amplified by using primers SR789 and KP235, which anneal to exon 15 and the intron 19 - exon 20 junction of MARS1, respectively. The MARS1 deletion locus was amplified by using primers KP346, which anneals to intron 1 of the MARS1 gene, and KP347, which was derived from the WGS read found only in the ‘*mars1*-like’ progeny pool. The KP347 primer sequence is a hybrid of telomeric sequence and MARS1 gene sequence: this sequence seems to have arisen after a genomic deletion at the end of chromosome 16 in *mars1-2*. The PCR reactions were then purified and sequenced as described above. The sequence of the aforementioned primers can be found in Table 3.

MARS1 gene cloning

A MARS1 ‘midigene’ was generated by amplifying four different portions of this gene either from gDNA or cDNA using KOD Hot Start DNA Polymerase (Thermo Fisher Scientific) or Phusion Hotstart II polymerase (Thermo Fisher Scientific). In particular, the region spanning the promoter, the 5’UTR and the first 5 exons of this gene was amplified from gDNA using Phusion polymerase and the following primers: SR828 and SR818; the region spanning exon 5 to exon 15 was amplified from gDNA using KOD polymerase and the following primers: SR819 and HT7; the region spanning exon 15 to exon 28 was amplified from cDNA using KOD polymerase and the following primers: SR789 and SR797 and the 3’UTR was amplified from gDNA using KOD polymerase and the following primers: SR793 and SR829.

All PCR products were gel extracted and purified as described above in the section regarding the pPW3217 cloning. Next, these 4 PCR fragments were mixed with a purified and linearized and pRAM118/pPW3216 vector, previously digested by EcoRV and NotI, and incubated in presence of the In-Fusion reagents (Takara) as per manufacturer's instructions. The resulting plasmid is notated as pPW3218. The sequence of the aforementioned primers can be found in Table 3.

The Phytozome v5.5 MARS1 transcript annotation is Cre16.g692228.t1.1.

MARS1 gene tagging

Generation of MARS1-A transgene (pPW3219):

To insert a 3x-Flag epitope after Arg1167 of the Mars1 protein sequence, a dsDNA gene block was synthesized by IDT with the following sequence:

```
GGTACGACGGCTGGGCTGGGGCGCCGGCGTCCGCCCCCTGCTCCCAAGTTGTCATTG
CCATCAGCGGCAGGCGTGGGGCATCGGTTGCAGCCGGTTTCGCCGGCTTCCACCGTG
TCCGGGCTTCCTTGGGGCCAGGCTGCGCACCCGTCGCACACAGCTCCGCAGCTGCTC
CGCGCGCCGCATCAACAGTTCGGGAGCATTGCTGCAGCAGCAGCGAGTGCCGCTCC
AAGCTGGGCTGCAAGCTCGAGCAGTGCTGCACTGGTAGCAGCTGAGCTTGGGGCAG
CTGCAGTAGCAGCTGCAGCGGCAGCGGCGGCTTGCACCTCGGCTTCTGTGGGGCGTAG
ACCCGGGATCATCGGCTGTGAACACACATGCCGCCGCTGCCGTCGCTCCCTCCATGT
GGAAGGCGGCCCTGCTGGCACCCGGTGGGGAGGCTCCGCGTGGGAATGGCTCAGCC
CGGAGCAGCTTTGAGGCGGGGGAGCCATCACCGTCGGAGCGGGCACGCAGGCAGCA
AGAGCAGCTGGCAGCGGCGGCAGCATCGGAGGGGGCGGCCTGCGGCTAGCACAGGCC
AGAAGCCGGCAGCGTCTTCGGCTGTTGCAACCACGTCCAGCTCAACCTCCACTGCCA
GGCGGAGAGACCAGCAGGGTAACTCGCAGTCACGGCCAGTAGTGGAGCGTGGTTTCG
GGCGGTggtggctccgactacaaggaccatgacggtgactataaggatcacgacatcgactacaaggacgatgacgacaagggtg
```

gcggcggcagtGGGAGAGGTGCTGCTCGCGGCGGCATGTCCACACGGGGCGGGGGA
GGAGGCCGGGGCAGTGGACGCCTGTTCGGCAGAGGACGTGGGAGACTGGACCGCGG
AGATGACGACAACGGTTACGCGGAGGAGAACCAGCCATCTGCAATCGGCGCCGCGA
GCAATTCCGAACAGCTGGAGCACGGCCGACAGCGCCGTGAGGGTGCGGGAGGTGAC
GGCGCTCACGAGCAGGGGGCTGGGGCTGCCAGCAGCTCGGCCAGCCCAAGCTGCC
TCTCGCAACTACGGGCACAGCAGCTGCCTCGGAGCACTCTGGCGCTGTTGATTCTTC
AACAGCTACCGCCGGCGCTCCCGACGCAGCTAGCCCT

Lower case letters indicate the Flag epitope encoding insertion. Note that, in this fragment of DNA, often a MARS1 codon ending with G or C was mutated to a synonymous codon ending in A or T as a strategy to decrease the amount of GC in the sequence.

Next, this gene block was mixed with a purified and linearized pPW3218 vector, previously digested by MreI and dephosphorylated by Calf Intestinal Phosphatase (CIP, NEB), and incubated in presence of In-Fusion reagents (Takara) as per manufacturer's instructions. The resulting plasmid is notated as pPW3219.

Generation of MARS1-D transgene (pPW3222)

To insert a 3x-Flag DNA sequence downstream of the second in-frame translation start codon, ATG (ii), (actual position: Met139), two partially overlapping regions of the MARS1 gene were amplified by PCR using as template pPW3218. The following primer pairs were used: KP337/KP344 and KP345/KP342, to enable the insertion of the 3x-Flag epitope after Met139 of the Mars1 protein. Next, these two PCR products were gel-purified as already described above and mixed with a purified and linearized pPW3218 vector, previously digested by AvrII and XbaI. These three DNA fragments were incubated in presence of In-Fusion reagents (Takara) according

to manufacturer's instructions. The resulting plasmid is notated as pPW3222. The sequence of the aforementioned primers can be found in Table 3.

Generation of MARS1-E transgene (pPW3223)

The insertion of a 6x-Flag epitope after Leu402 of the Mars1 protein sequence was a fortuitous byproduct of a cloning strategy in which a 3x-Flag dsDNA sequence was inserted twice rather than once. This 3x-Flag dsDNA, with BglIII-compatible sticky ends, was generated upon annealing of the two following single-stranded DNA fragments:

3x-Flag_UP:

GATCTGGACTACAAGGACCATGACGGTGACTATAAGGATCACGACATCGACTACAA
GGACGATGACGACAAG;

3x-

Flag_DOWN:GATCCTTGTCGCATCGTCCTTGTAGTCGATGTCGTGATCCTTATAGTCA
CCGTCATGGTCCTTG TAGTCCA

and it was mixed with a linearized and purified pPW3218, digested by BglI and dephosphorylated by Calf Intestinal Phosphatase (CIP, NEB) and incubated in presence of In-Fusion reagents (Takara) according to manufacturer's instructions. A clone containing a plasmid with a double insertion of the 3x-Flag DNA sequence at the BglIII site was identified by analytical digestion and confirmed by Sanger sequencing. The resulting plasmid is notated as pPW3223.

Generation of MARS1-A KD, MARS1-D KD and MARS1-E KD transgenes (pPW3224, pPW3226 and pPW3225)

pPW3226, pPW3224 and pPW3225 were all constructed using a three-piece In-Fusion assembly technique. For the kinase-dead version of the MARS1-E transgene, the backbone pPW3223 was digested with EcoRV and BstXI and the D→A point mutation was introduced by generating two

DNA fragments by PCR using pPW3223 as template and Phusion Hotstart II polymerase (Thermo Fisher Scientific) with the following primers pairs: SR852/SR853 and SR829/SR851. The three DNA fragments were incubated in presence of In-Fusion reagents (Takara) according to manufacturer's instructions. A clone containing the D!A mutation was identified by Sanger sequencing. The resulting plasmid is notated as pPW3226.

Similarly, for the kinase-dead (KD) version of the MARS1-A transgenes, the backbone pPW3219 was digested with EcoRV and BstXI. The primers to introduce the D!A mutation and the strategy to generate and identify the correct plasmid clone were the same as for pPW3226. The resulting plasmid was notated as pPW3224.

To introduce the D!A point mutation in the MARS1-D transgene, two partially overlapping regions of the MARS1 gene were amplified by PCR using as template pPW3218 and the following primer pairs: KP337/KP344 and KP345/KP342 as already described above in the case of pPW3222 cloning. Next, these two PCR products were mixed with a purified and linearized pPW3226 vector, previously digested by AvrII and XbaI. These 3 DNA fragments were incubated in presence of In-Fusion reagents (Takara) according to manufacturer's instructions. The resulting plasmid is notated as pPW3225. The sequence of the aforementioned primers can be found in Table 3.

MARS1 transgene nuclear integration

Given the large size of the MARS1 transgene (>10 kbp), a different electroporation protocol was used to successfully integrate each aforementioned MARS1 transgene into the nuclear genome. The electroporation was performed using a NEPA21 electroporator (Nepagene) (Yamano et al., 2013). A 4–8 ml aliquot of purified, non-linearized, plasmid DNA at a concentration of 0.5–1 µg/ml was used per transformation. In each case, the plasmid DNA was mixed together with 5 ml of a ready-to-use, sheared solution of salmon sperm DNA at a concentration of 10 µg/ml (Thermo

Fisher Scientific) prior electroporation. The electroporation parameters were set as follows: Poring Pulse (300 V; length = 6 ms; Interval = 50 ms; No = 1; D.Rate = 40%; + Polarity), Transfer Pulse (20 V; length = 50 ms; Interval = 50 ms; No = 5; D.Rate = 40%; +/- Polarity). Usually, during the electroporation, the impedance was measured to be around 400–700 ohms. Transformants were isolated on TAP agar containing 20 µg/ml hygromycin and screened by Flag immunoblot analysis to identify MARS1 transgene expressors.

Dual immunofluorescence (IF)

Due to the low abundance of the Mars1 protein, the Alexa Fluor 488 Tyramide SuperBoost Kit (Thermo Fisher Scientific) was utilized to amplify the signal. WT (mock control) and Flag-tagged strains were grown in TAP medium to logarithmic phase and a 5 ml aliquot of each cell cultures was harvested at 500 x g for 5 min at RT. The supernatant medium was decanted and the cell pellet was resuspended in 1.5 ml of PBS. A 35 ml cell suspension was added to wells on a slide pre-treated with 0.1% poly-L-lysine and allowed to adhere for 7 min. To solubilize the chlorophyll and maintain cell structure, slides were incubated in 100% methanol 2 times for 4 min at 20°C. Excess methanol was removed and the slides were dried for 2 min at RT. Slides were incubated in PBS supplemented with 0.1% Tween 20 (PBS-T) for 10 min to permeabilize the cell before adding the manufacturer provided 3% H₂O₂ solution to quench endogenous peroxidase activity for 1 hr. Following three washes with PBS, non-specific signal was blocked with 10% goat serum in PBS (Jackson ImmunoResearch Laboratories) for 1 hr. Samples were incubated with commercial monoclonal mouse anti-Flag antibody (M2 Sigma, F1804, diluted 1:500) in combination with one of three subcellular markers: anti-Histone H3 (Agrisera, AS10 710, diluted 1:500), anti-AtpD (Agrisera, AS10 1590, diluted 1:500), or anti-Nab1 (Agrisera, AS08 333, diluted 1:500), and left overnight at 4°C in a humid chamber. The remaining steps were performed as per manufacturer's

instructions. In brief, samples were washed for 10 min in PBS for a total of three washes. Alexa Fluor 488 poly horseradish peroxidase (HRP)-conjugated goat anti-mouse and Alexa Fluor 546 goat anti-rabbit secondary antibodies were utilized for detection of the Flag and subcellular marker signals respectively. Alexa Fluor 546 was diluted 1:500 in the manufacturer prepared Alexa Fluor 488 solution and added to each well for 1 hr at RT protected from light. Slides were washed 3 times in PBS before the amplification step. To amplify the Flag signal, 35 ml of the Tyramide Working Solution was added to the cells and the reaction proceeded for 4 min before an equal volume of Stop Solution was added to end the reaction. Slides were rinsed in 1x PBS and covered with a thin layer of 0.5% low-melting point agarose dissolved in TAP medium before observation by 3D-Structured Illumination Microscopy (3D-SIM).

3D-Structural illuminated microscopy (3D-SIM)

The microscopy samples were observed using an Elyra PS.1 SIM microscope (Zeiss) with objective lens alpha Plan-Apochromat 100x/1.46 oil (Immersol 518F/30°C, Zeiss), as described previously (Iwai et al., 2018). The fluorophores Alexa Fluor 488 and Alexa Fluor 546 were excited with a 488 nm laser and 561 nm laser, and the fluorescence was acquired through a 495–550 nm and 570–620 nm bandpass filters, respectively. Image acquisition was performed with ZEN software (Zeiss). Each focal plane for 3D-SIM image was captured sequentially by the excitation with the patterned light of 3 rotated angled, each of which contains five shifted phases. The optimal z-interval distance was set to 101 nm. Raw SIM images were processed to reconstruct 3D-SIM images using ZEN software. Extraction of the intensity data was done using the SIMcheck plugin for ImageJ software (Ball et al., 2015).

Cytosolic fractionation

For localization studies, cytosol-enriched and cytosol-depleted fractions were isolated from *mars1-3* cells (a cell-wall deficient strain) complemented with the MARS1-A transgene, according to the protocol described below, incorporating guidelines previously described in Klein et al., 1983 and Zerges and Rochaix (1998). A one liter liquid culture, synchronized by growth in dark-light cycles in minimum media and in early exponential phase (1–2 10⁶ ml⁻¹), was harvested at 3000 x g for 5 min at RT. Upon media removal, the cell pellet was resuspended by gentle hand-shaking of the centrifugation tube without using a pipette in 15 ml of autolysin freshly supplied with 1 mM potassium phosphate buffer (pH 6.0) and 0.5 mg/ml BSA (Solution A). Solution A was pre-warmed at 30°C for 30 min prior to use and, after resuspending the pellet in this solution, cells were transferred to a 200 ml 30°C-prewarmed beaker immersed in a water bath and incubated at 30°C for 50 min. Next, cells were transferred to a 50 ml Falcon tube and collected by centrifugation at 2000 x g for 5 min at RT. The autolysin was quickly removed using a 25 ml plastic pipette and the cell pellet was very gently resuspended in 20 ml of ice-cold Solution B consisting of 5 mM K-phosphate buffer (pH 6.5), 6% PEG (w/w) and 4 mg/ml BSA.

Cells were then transferred to a 32°C-prewarmed beaker immersed in a water bath at 32°C and 80 ml of freshly-prepared 1% digitonin (Calbiochem) (0.004% final concentration) was quickly added and well-mixed with the cell suspension.

Cells were then subjected to two rapid warming-cooling cycles using 32°C pre-warmed or ice pre-chilled beakers to induce plasma membrane rupture and cytosolic protein release without intracellular organelles breakage. Cycling was performed for 2 min at 32°C, 5 min on ice, 1 min at 32°C, 5 min on ice. Next, this suspension of permeabilized cells and released cytosolic proteins was transferred to a 50 ml pre-chilled Falcon tube and centrifuged at 800 x g for 3 min at 4°C.

After centrifugation, the cytosol-enriched fraction was further purified from the supernatant fraction, while the cytosol-depleted fraction containing chloroplasts and mitochondria was further purified from the cell pellet.

To remove potential cell debris and obtain a clean cytosolic fraction, the supernatant was subjected to two further consecutive rounds of centrifugation: first, at 5000 x g for 15 min at 4°C and then at 23,000 x g for 1 hr at 4°C. Finally, the cytosol-enriched fraction was precipitated in ice cold acetone containing 10% of trichloroacetic acid (TCA).

To enrich the cytosol-depleted fraction with organelles, the pellet of permeabilized cells was kept in ice and resuspended in 2 ml of ice-cold 2x isotonic solution consisting of 0.6 M sorbitol, 10 mM MgCl₂ and 20 mM Tricine pH 7.8. At this point, a rather dark-green aggregate formed in the falcon tube. To resuspend this aggregate, a cut plastic pipette tip was used to gently pipette the pellet up/down for 20 times. Then, 2 ml of ice-cold milliQ water were added to bring the isotonic solution to 1x and the aggregates were further dissolved as described above.

Next, this suspension was loaded on a Percoll step gradient (10 ml 75% Percoll in isotonic solution/10 ml 45% Percoll in isotonic solution/4 ml cell lysate) in a Corex glass tube. The gradient was subjected to centrifugation using the HB4 swinging-rotor at 7000 x g for 15 min at 4°C. Chloroplasts and contaminating mitochondria were recovered from the interface between 45% and 75% Percoll and diluted in 20 ml of 1x ice-cold isotonic solution. The organelles were collected by 5 min centrifugation at 4000 x g at 4°C and, after removing the supernatant, the pellet was resuspended in 2 ml ice-cold isotonic solution and run through a second Percoll gradient as described above. Finally, the cytosolic-depleted fraction was precipitated in ice-cold acetone containing 10% TCA. Denatured proteins from each fraction were extracted after TCA

precipitation, as described below. Prior to gel electrophoresis, the protein content of each fraction was normalized using a bicinchoninic acid (BCA) assay as described in the section below.

Denaturing protein extraction, immunoblot analysis and BCA assay

Proteins were extracted from whole cell lysate using a denaturing SDS extraction protocol for all experiments except for immunoblots that include the Mars1 protein, in which case TCA precipitation was used. For the SDS protein extraction, cells from a 5 ml culture in exponential growth phase were harvested at 3000 x g for 5 min and resuspended in 150 ml of SDS-lysis buffer (100 mM Tris-HCl pH 8.0, 600 mM NaCl, 4% SDS, 20 mM EDTA, freshly supplied with Roche Protease Inhibitors). Samples were vortexed for 10 min at RT and centrifuged at maximum speed for 15 min at 4°C to remove cell debris. The supernatant, containing a total extract of denatured proteins was transferred to a new Eppendorf tube, a 5 ml aliquot was saved for BCA quantification and 1/4 vol of 5X SDS-loading buffer (250 mM Tris-HCl pH 6.8, 5% SDS, 0.025% bromophenol blue, 25% glycerol), freshly supplied with 500 mM DTT or 5% of 2-mercaptoethanol prior use, was added to the extract and denatured at 37°C for >30 min. For the TCA precipitations, cell pellets were resuspended in 1 ml of 10% TCA in acetone, freshly supplemented with 0.5% beta-mercaptoethanol. Samples were vortexed for 10 min at 4°C then left at 20°C for 1–2 hr for efficient protein precipitation. Samples were centrifuged at maximum speed for 10 min at 4°C and the TCA solution was carefully aspirated. Three washes with 1 ml of cold 100% acetone were performed (5 min of vortexing followed by 5 mins of maximum speed centrifugation) and the remaining pellet was dried for 5–10 min before resuspension in Lysis Buffer (same as above), achieved through vigorously shaking of the Eppendorf tube with the aid of a vortex at RT or with the aid of a thermomixer at 50°C for 10–15 min. The resuspended protein extract was isolated by a quick centrifugation and was transferred to a new Eppendorf tube. A 5 ml aliquot was saved for BCA

quantification and 1/4 vol of 5x SDS loading buffer was added to the rest and denatured at 37°C for at least 30 min. Immunoblot analysis was performed on 20–60 mg of denatured protein extract. Proteins were separated by SDS-PAGE using Mini-PROTEAN or Criterion Precast Gels) (Bio-Rad) and transferred onto Protran nitrocellulose membrane, 0.2 mm pore (Perkin Elmer). Non-specific signal was blocked with PBS-T supplemented with 5% instant nonfat dry milk (Carnation, Nestle) for 1 hr at RT or overnight at 4°C. All primary and secondary antibodies were diluted in this blocking buffer. The following antibodies (at the indicated dilution) were used for this publication: monoclonal mouse anti-Flag (1:3,000) (M2, Sigma F1804), monoclonal mouse anti-alpha-tubulin (1:5,000) (Sigma #T6074), polyclonal rabbit anti-DnaK (provided by Jean David Rochaix) (1:10,000) (H.Naver, K.Wilson and J.D.Rochaix, unpublished results) (Dauvillee, 2003), polyclonal rabbit anti-RpoA (1:10,000) (Ramundo et al., 2013), polyclonal rabbit anti-ClpP1 (provided by Francis-Andre' Wollman and Olivier Vallon) (1:5,000) (Majeran et al., 2000), polyclonal rabbit anti-Hsp22E/F (provided by Michael Schroda) (1:5,000) (Rutgers et al., 2017), polyclonal rabbit anti-Vipp2 (1:3,000) (raised against a –CDPLERELEELRRRARE- peptide, developed during this study by Yenzym, South San Francisco), polyclonal rabbit anti-Aox1 (1:2,000) (Agrisera AS06 152), polyclonal rabbit anti-Sultr2 (provided by Arthur Grossman) (1:3,000) (Pootakham et al., 2010), polyclonal rabbit holo-Rubisco (provided by Jean David Rochaix) (1:10,000) (Borkhsenius et al., 1998), polyclonal rabbit anti-Hsp90C (1:10,000) (Agrisera AS06 174) and anti-Histone H3 (1:10,000) (Agrisera AS10 710). To detect the primary antibodies, HRP-conjugated anti-rabbit and anti-mouse secondary antibodies (Promega) were used at dilution 1:10.000 in PBS-T supplemented with 5% instant nonfat dry milk for 1 hr at RT. In between the incubation with primary and secondary antibody and after the incubation with the secondary antibody, three washes of about 10 min each time, at RT, were performed using PBS-T

supplemented with 5% instant nonfat dry milk. The membranes were quickly rinsed three times with milliQ-water and a luminol-based enhanced chemiluminescence (ECL) method was applied to develop the signal. For most immunoblot analysis, the SuperSignal West Dura Extended Duration Substrate kit (Thermo Fisher Scientific) was used according to manufacturer's directions. By contrast, for Flag immunoblot analysis to detect Mars1 protein, the SuperSignal West Femto Maximum Sensitivity Substrate kit (Thermo Fisher Scientific) was chosen, given the low expression level of this protein. The ECL signal was detected with the LI-COR Odyssey imaging system or using clear-blue X-ray films (CL-Xposure, Thermo Fisher Scientific).

To carry out the BCA assay, 5 ml of protein extract was added to 200 ml of BCA/copper sulfate solution (1:50 dilution of 4% CuSO₄ into BCA solution, Sigma) and incubated at 50°C for 5 min.

Protein concentration was estimated by measuring the absorbance at 562 nm and comparing it to a BSA standard.

Note: for Figure 6—figure supplement 1B, the denaturing protein extraction was carried out as follows: cell cultures started in 7 ml of TAP were grown to mid-log phase and subsequently spun down at 3000 x g for 8 min. The pellets were resuspended in 150 ml of TAP. Then, an equal volume of 0.2M NaOH was added to the pellets, vortexed at RT for 5 min and pelleted at 15,000 x g for 5 min. The supernatant was removed, the pellet was resuspended in 280 ml of SDS samples buffer (0.06 M Tris-HCl pH 6.8, 5% glycerol, 2% SDS, 4% 2-Mercaptoethanol, 0.0025% bromophenol blue), boiled for 5 min and then pelleted again. A 28 ml aliquot was loaded onto a Criterion gel.

High light (HL) assays

The following protocol was used for the HL assay described in Figure 4A–B. Slight modifications were applied during the HL assays described in Figure 6E and will be underscored below. Liquid

cultures were started from TAP plates that had all been grown in dim light and in the same conditions. A small slab of cells was taken from the agar plate and resuspended in 28 ml of TAP media in 50 ml falcon tubes (Sarstedt). The Olympus Plastics brand product line from Genesee Scientific was avoided because there was a higher propensity for the cells to adhere to this plastic material. An equal slab of cells was used for each culture to approximate the same level of starting cells. Typically, the strains had been growing in fresh TAP agar for ~3–5 days. The cells were pre-conditioned in low light ($\sim 20\text{--}50 \mu\text{mol photons m}^{-2} \text{ s}^{-1}$) for about 38–44 hr. For the HL assays shown in Figure 6E, the cells were preconditioned for slightly longer period, ~3 days. The chlorophyll concentration of the cell cultures was measured using the methanol extraction method as described in Porra et al. (1989). At the above described time points, it was found to be ~13–18 mg/ml (HL assays described in Figure 4A–B), or ~25 mg/ml (in the HL assays described in Figure 6E). Cell cultures were then equally diluted to ~10 mg chlorophyll ml⁻¹ (in the case of the HL assays described in Figure 4A–B), or to 7 mg chlorophyll ml⁻¹ (HL assays described in Figure 6E). Chlorophyll concentrations were confirmed and, if needed, re-adjusted after dilution before HL was started. The final volume of cell culture used for high light treatment was ~26 ml in 50 ml Falcon tubes. During the high light treatment, the distance between the light source (Phlizon 2017, 2000W Plant LED Growth light) and the shaker was set to 25 cm. The HL intensity was measured at $1100 \mu\text{mol photons m}^{-2} \text{ s}^{-1}$ at the beginning of the experiment but was reduced to $\sim 900 \mu\text{mol photons m}^{-2} \text{ s}^{-1}$ by the end of the experiment. On the right and left side of the shaker, two fans were turned on to keep the samples at RT and a Smart Sensor (SensorPush) was used to monitor temperature in real-time. Typically a 4°C increase in temperature (from 24.5°C to about 28.5°C) was measured after the cultures were shifted from the dim light growth setup to this HL setup. The light intensity at each position of the culture on the shaker was measured to ensure cells were

getting the same number of photons (~50,000 LUX). The cultures in the Falcon tubes were taped (clear tape) onto the shaker and the shaker was set at 150 rpm. Chlorophyll measurements were taken at multiple time points of HL treatment (during HL assays described in Figure 4A and Figure 4—figure supplement 1A) and after 27 hr or 50 hr of HL treatment (during HL assays described in Figure 4B and Figure 6E, respectively). Serial dilutions performed on cultures before and after the HL treatment were spotted onto TAP plates. Photographs of these plates were taken over time to track cell recovery.

Metronidazole assays

For immunoblot analyses, as shown in Figure 4D, cell cultures were grown in liquid TAP medium in a 50 ml Falcon tube for about two days to a chlorophyll concentration of 11 mg/ml in a volume of 30 ml. Cells were spun down and the pellet was resuspended in 1.5 ml of TAP. 0.3 ml of the resuspended pellet was then added to 10 ml of TAP with or without 1.1 mM metronidazole (Sigma). These cultures were then placed under white light ($20\text{--}50 \mu\text{mol photons m}^{-2} \text{s}^{-1}$) for 12–15 hr and then spun down and saved at 20°C or directly used for denaturing protein extraction as described above.

For growth tests on TAP agar supplemented with metronidazole, as shown in Figure 4C and Figure 4—figure supplement 1B–E, strains were either manually re-streaked or robotically replicated from TAP agar plate to +/- 1.5 mM metronidazole TAP agar plates.

For dilution spot tests, shown in Figure 6D, cells were freshly inoculated from a 3-4 days old agar plate and grown in in falcon tubes for 2 days in a starting volume of 30 ml of TAP. After these 2 days of preconditioning, chlorophyll concentrations were normalized to be at ~18 mg/ml and serial dilutions of 1.5-fold were done in liquid TAP using a 96-well plate. Finally, 6 ml cells from each

dilution series were spotted onto TAP agar plates with or without 2.2 mM metronidazole. Photographs were taken periodically to track growth over time.

Metronidazole is rather insoluble in aqueous solutions; therefore, it was always added (as powder) directly to the autoclaved liquid TAP medium at final concentrations of 1.1 mM, 1.5 mM or 2.2 mM.

Flag affinity purification and mass spectrometry (MS) analysis

Mars1-D and Mars1-D KD strains were subjected to metronidazole treatment for 15 hr. Culture were then harvested and subjected to Flag affinity purification followed by MS analysis according to the protocol described by {Mackinder, 2017 #30} and publically available through :<https://docs.google.com/viewer?a=v&pid=sites&srcid=ZGVmYXVsdGRvbWFpbXjaGxhbXlzcGF0aWFsaW50ZXJ-hY3RvbWV8Z3g6NzlkNjUzMTM0ZWYyYmI5>. Preparation of samples for MS analysis and processing of MS raw data was performed by the Stanford Mass Spectrometry Facility in Palo Alto.

RNA extraction

A 10-ml aliquot of a cell culture in early-mid exponential phase ($1-5 \times 10^6$ ml⁻¹), was harvested at 3000x g for 5 min at RT. After decanting the media, 1 ml of Trizol Reagent (ThermoFisher Scientific) was added to the cells. The cells were lysed in sample by vigorous shaking with the aid of a vortex for 5-8 min. Chloroform (1/5 vol, ~200 μ l) was then added to the lysate and the tube was vigorously shaken up and down by hand for 60 s. The sample was then centrifuged at 11,000 x g for 7 min at RT. The upper aqueous phase (~350 μ l) was removed with care to not draw any of the organic layer, transferred in a nuclease-free 1.5 ml tube (Ambion) and mixed well with 1 vol of 100% ethanol (Fisher Scientific) at RT. From this point onwards, the RNA purification was carried out with the aid of the Direct-zol RNA MiniPrep Plus kit (ZymoResearch) following the

manufacturer's protocol, including in-column DNase I treatment prior to RNA washing and elution steps.

Analysis of gene expression by RT-PCR

A semi-quantitative RT-PCR was carried out to qualitatively determine the presence or absence of MARS1 gene transcripts. Total RNAs were extracted as described in the previous section. Complementary DNA was synthesized from 1 mg of total RNA using PrimeScript 1st strand cDNA Synthesis Kit (Takara) as per manufacturer's instructions. Subsequently, RNA/DNA hybrids were removed by ribonuclease H treatment (NEB) as per manufacturer's instructions. cDNAs were diluted two-fold and 1–2 µl were used as template for a 20 µl PCR reaction by Phusion High-Fidelity DNA Polymerase (Thermo Fisher Scientific) with the following parameters: initial melting 98°C for 30 s, amplification cycles 98°C for 10 s, 68°C for 30 s, 72°C for 1 min 15 s (35 times), final extension 72°C for 5 min. Primers SR834 and SR835 were used to amplify a fragment of the MARS1 coding sequence spanning from exon 16 to exon 28. Primers SR836 and SR837 were used to amplify the GBLP coding sequence, used as loading and positive control during the RT-PCR analysis. The sequence of the primers can be found in Table 3.

Analysis of gene expression by quantitative polymerase chain reaction (qPCR)

For qPCR analyses, the cDNA was prepared as described above but the cDNA was diluted six to eight-fold in nuclease-free water prior to use. Primers to amplify the target transcripts are indicated in Table 3. The qPCR reactions were carried out using the iQ Sybr green supermix as per manufacturer's instructions (Bio-Rad). To determine whether there was DNA contamination in the mix or whether there was primer dimer formation or misannealing, the same volume of the master mix, without cDNA, was added to a well in the 96-well plate. The raw Ct values were analyzed per the 'eleven golden rules', as previously described (Udvardi et al., 2008). GBLP was chosen as

reference housekeeping transcript during normalization. Standard deviation was obtained for the 2–5 technical replicates and a minimum of 2 biological replicates were done per experiment, except for the experiment in Figure 3—figure supplement 1B, where only one biological replicate was analyzed.

The Phytozome v5.5 gene annotation for the target transcripts is as follows: VIPP2 (Cre11.g468050.t1.2), SULTR2 (Cre17.g723350.t1.2), LHCBM9 (Cre06.g284200.t1.2), HSP22F (Cre14.g617400.t1.1), SNOAL (Cre11.g478100.t1.2), LHCSR3.1 (Cre08.g367500.t1.1), PSBS1 (Cre01.g016600.t1.2), CPLD29 (Cre02.g088500.t1.1), GBLP (Cre06.g278222.t1.1).

RNA-Seq: sample preparation and processing

Prior to RNA-seq analyses, the *mars1-1* strain was backcrossed to the wild-type CC-124 (Chlamydomonas Resource Center). A full tetrad was selected and analyzed as shown in Figure 2E. A wild-type and MARS1 mutant progeny (CrPW8, indicated as E12, and CrPW9, indicated as F2 respectively, in Figure 2E and Figure 2—figure supplement 2B) were chosen for follow-up studies, based on the retention of the ClpP1 repressible system in their genetic background.

For each strain, two cultures (biological replicates) were inoculated in 30 ml liquid TAP medium using 50 ml Falcon tubes, starting from a fresh re-streak of cells propagated on TAP agar. These cultures were grown with mild agitation (150 rpm) on a shaker at around 22°C, under an illumination of 30–40 $\mu\text{mol photons m}^{-2} \text{s}^{-1}$ for about three-four days till they reach mid-late exponential phase ($4-7 \times 10^6$ cells ml⁻¹). Next, cells were diluted to about 1×10^6 cells ml⁻¹ in 30 ml of liquid TAP medium using 50 ml Falcon tubes and they were subjected to three different treatments: a) low light, i.e. they were kept at the same light intensity used during conditioning; b) HL, i.e. they were shifted to very high light ($1200 \mu\text{mol photons m}^{-2} \text{s}^{-1}$) for 40 min or 70 min; and

c) ClpP1 repression, i.e. they were diluted in liquid TAP medium containing 100 mM thiamine and 40 ng ml⁻¹ vitamin B12 and incubated for 68 hr at the same light intensity used during conditioning. Cells were then shifted to ice and quickly harvested by centrifugation at 3000 x g for 5 min at 4°C. Cell pellets were snap-frozen in liquid nitrogen and saved at -80°C till use. RNA extraction was carried as described in the previous section. The following extra measures were taken to ensure a complete removal of DNA contaminants: An additional round of in-solution Dnase I treatment was performed using 1 unit of Rnase-free Dnase I (Roche)/1 mg of total RNA at RT for 20 min in presence of 1 unit of recombinant ribonuclease inhibitors (RNaseOUT, Thermo Fisher Scientific). Next, the RNA was re-purified using the same extraction protocol described above.

Each total RNA preparation was ran on an Agilent Bioanalyzer RNA 6000 Nano chip for quantification and quality control. PolyA mRNAs were purified and RNAseq libraries were prepared using the Kapa mRNA HyperPrep kit (Roche, KK8540) following manufacturer's protocols. Libraries were pooled based on fragment analyzer concentrations. Sequencing was performed on Nextseq high-output flowcell, 1 75 bp run (Illumina).

RNA-Seq: data analysis

We used a combination of publicly available tools and custom scripts for the processing of the raw demultiplexed Illumina sequencing data. Illumina adapter sequences were first trimmed off with TrimGalore! (version_0.4.1) (www.bioinformatics.babraham.ac.uk/projects/trim_galore) and contaminating ribosomal reads were removed by mapping against the Silva rRNA database using bbdut v37.32 (part of the BBTools suite, <https://jgi.doe.gov/data-and-tools/bbtools/bb-tools-user-guide/>). Quality control of raw and processed fastq files was performed using FastQC version 0.11.3 ([https://www.bioinformatics.babraham.ac.uk/projects/fastqc/](http://www.bioinformatics.babraham.ac.uk/projects/fastqc/)). The remaining reads were aligned to the unmasked *C. reinhardtii* genome (Phytozome, v5.5) using STAR v.2.5.3a (Dobin et

al., 2013) and bam files were sorted with samtools 1.1 (Li et al., 2009). Count generation and downstream analysis were done in R (R project v3.4.0, www.R-project.org) using a combination of the packages Rsubread (Liao et al., 2013) EdgeR (Robinson et al., 2010) plyr, ggplot2, gplots, and heatmap2. For differential expression analysis, genes with less than 0.5 counts per million reads in less than two samples were discarded, the data were fit to a negative binomial generalized linear model, and differential expression was determined using the quasi likelihood F-test with Benjamini-Hochberg correction of multiple testing in EdgeR. To subdivide genes into groups of MARS1-dependent and -independent genes, weakly-expressed genes (average RPKM <2.5 in at least two conditions) were discarded. Stress-responsive genes (defined as log₂-fold change $\geq |2|$ at FDR 0.001 upon treatment - high light, ClpP repression, or both as noted – in WT background) were considered MARS1-dependent when treatment in the MARS1 mutant did not lead to a greater than 2-fold change in expression (log₂-fold change $< |1|$). MARS1-independent genes were defined as genes with an at least 4-fold (log₂-fold change $\geq |2|$) change upon treatment in the mars1 background, in the same direction (up or down) as the response in WT cells. For analysis of functional categories in MapMan 10.0 (Thimm et al., 2004, Usadel et al., 2005) the *C. reinhardtii* v5.5 proteome (downloaded from Phytozome, v5.5, protein sequences from primary transcript only) was binned using Mercator4 (www.pla-bipd.de/portal/web/guest/mercator4) and MARS1-dependent and MARS1-independent gene subsets were mapped onto plant pathways in MapMan.

REFERENCES

1. Blaby IK, Blaby-Haas CE, Perez-Perez ME, Schmollinger S, Fitz-Gibbon S, Lemaire SD, Merchant SS. 2015. Genome-wide analysis on *Chlamydomonas reinhardtii* reveals the impact of hydrogen peroxide on protein stress responses and overlap with other stress transcriptomes. *The Plant Journal* 84:974–988. DOI: <https://doi.org/10.1111/tpj.13053>
2. Bobik K, Burch-Smith TM. 2015. Chloroplast signaling within, between and beyond cells. *Frontiers in Plant Science* 06:781. DOI: <https://doi.org/10.3389/fpls.2015.00781>
3. Borkhsenius ON, Mason CB, Moroney JV. 1998. The intracellular localization of ribulose-1,5-bisphosphate carboxylase/Oxygenase in *Chlamydomonas reinhardtii*. *Plant Physiology* 116:1585–1591. DOI: <https://doi.org/10.1104/pp.116.4.1585>, PMID: 9536077
4. Chan KX, Phua SY, Crisp P, McQuinn R, Pogson BJ. 2016. Learning the languages of the chloroplast: retrograde signaling and beyond. *Annual Review of Plant Biology* 67:25–53. DOI: <https://doi.org/10.1146/annurev-arplant-043015-111854>, PMID: 26735063
5. Correa-Galvis V, Redekop P, Guan K, Griess A, Truong TB, Wakao S, Niyogi KK, Jahns P. 2016. Photosystem II Subunit PsbS Is Involved in the Induction of LHCSR Protein-dependent Energy Dissipation in *Chlamydomonas reinhardtii*. *Journal of Biological Chemistry* 291:87–17487. DOI: <https://doi.org/10.1074/jbc.M116.737312>
6. Croft MT, Moulin M, Webb ME, Smith AG. 2007. Thiamine biosynthesis in algae is regulated by riboswitches. *PNAS* 104:20770–20775. DOI: <https://doi.org/10.1073/pnas.0705786105>, PMID: 18093957
7. Dauvillee D. 2003. Tab2 is a novel conserved RNA binding protein required for translation of the chloroplast *psaB* mRNA. *The EMBO Journal* 22:6378–6388. DOI: <https://doi.org/10.1093/emboj/cdg591>

8. Davies JP, Yildiz F, Grossman AR. 1994. Mutants of *Chlamydomonas* with aberrant responses to sulfur deprivation. *The Plant Cell* 6:53–63. DOI: <https://doi.org/10.2307/3869674>, PMID: 12244220
9. Dent RM, Sharifi MN, Malnoe A, Haglund C, Calderon RH, Wakao S, Niyogi KK. 2015. Large-scale insertional mutagenesis of *Chlamydomonas* supports phylogenomic functional prediction of photosynthetic genes and analysis of classical acetate-requiring mutants. *The Plant Journal* 82:337–351. DOI: <https://doi.org/10.1111/tpj.12806>, PMID: 25711437
10. Dobin A, Davis CA, Schlesinger F, Drenkow J, Zaleski C, Jha S, Batut P, Chaisson M, Gingeras TR. 2013. STAR: ultrafast universal RNA-seq aligner. *Bioinformatics* 29:15–21. DOI: <https://doi.org/10.1093/bioinformatics/bts635>, PMID: 23104886
11. Dogra V, Duan J, Lee KP, Kim C. 2019. Impaired PSII proteostasis triggers a UPR-like response in the *var2* mutant of *Arabidopsis*. *Journal of Experimental Botany* 70:3075–3088. DOI: <https://doi.org/10.1093/jxb/erz151>, PMID: 30989223
12. D’Andrea L, Simon-Moya M, Llorente B, Llamas E, Marro M, Loza-Alvarez P, Li L, Rodriguez-Concepcion M. 2018. Interference with *clp* protease impairs carotenoid accumulation during tomato fruit ripening. *Journal of Experimental Botany* 69:1557–1568. DOI: <https://doi.org/10.1093/jxb/erx491>
13. Emanuelsson O, Nielsen H, von Heijne G. 1999. ChloroP, a neural network-based method for predicting chloroplast transit peptides and their cleavage sites. *Protein Science* 8:978–984. DOI: <https://doi.org/10.1110/ps.8.5.978>, PMID: 10338008
14. Erickson E, Wakao S, Niyogi KK. 2015. Light stress and photoprotection in *Chlamydomonas reinhardtii*. *The Plant Journal* 82:449–465. DOI: <https://doi.org/10.1111/tpj.12825>

15. Gonzalez-Ballester D, Pollock SV, Pootakham W, Grossman AR. 2008. The central role of a SNRK2 kinase in sulfur deprivation responses. *Plant Physiology* 147:216–227. DOI: <https://doi.org/10.1104/pp.108.116137>
16. Gonzalez-Ballester D, Casero D, Cokus S, Pellegrini M, Merchant SS, Grossman AR. 2010. RNA-seq analysis of sulfur-deprived *Chlamydomonas* cells reveals aspects of acclimation critical for cell survival. *The Plant Cell* 22: 2058–2084. DOI: <https://doi.org/10.1105/tpc.109.071167>, PMID: 20587772
17. Helliwell KE, Scaife MA, Sasso S, Araujo AP, Purton S, Smith AG. 2014. Unraveling vitamin B12-responsive gene regulation in algae. *Plant Physiology* 165:388. DOI: <https://doi.org/10.1104/pp.113.234369>, PMID: 24627342
18. Heredia-Martínez LG, Andre´s-Garrido A, Martínez-Force E, Pérez-Pérez ME, Crespo JL. 2018. Chloroplast damage induced by the inhibition of fatty acid synthesis triggers autophagy in *Chlamydomonas*. *Plant Physiology* 178:1112–1129. DOI: <https://doi.org/10.1104/pp.18.00630>, PMID: 30181343
19. Huang C, Wang S, Chen L, Lemieux C, Otis C, Turmel M, Liu XQ. 1994. The *Chlamydomonas* chloroplast clpP gene contains translated large insertion sequences and is essential for cell growth. *MGG Molecular & General Genetics* 244:151–159. DOI: <https://doi.org/10.1007/BF00283516>, PMID: 8052234
20. Iwai M, Roth MS, Niyogi KK. 2018. Subdiffraction-resolution live-cell imaging for visualizing thylakoid membranes. *The Plant Journal* 96:233–243. DOI: <https://doi.org/10.1111/tpj.14021>
21. Kajikawa M, Yamauchi M, Shinkawa H, Tanaka M, Hatano K, Nishimura Y, Kato M, Fukuzawa H. 2019. Isolation and Characterization of *Chlamydomonas* Autophagy-Related

- Mutants in Nutrient-Deficient Conditions . *Plant and Cell Physiology* 60:126–138. DOI: <https://doi.org/10.1093/pcp/pcy193>
22. Kearse M, Moir R, Wilson A, Stones-Havas S, Cheung M, Sturrock S, Buxton S, Cooper A, Markowitz S, Duran C, Thierer T, Ashton B, Meintjes P, Drummond A. 2012. Geneious basic: an integrated and extendable desktop software platform for the organization and analysis of sequence data. *Bioinformatics* 28:1647–1649. DOI: <https://doi.org/10.1093/bioinformatics/bts199>
23. Klein U, Chen C, Gibbs M, Platt-Aloia KA. 1983. Cellular fractionation of *Chlamydomonas reinhardtii* with emphasis on the isolation of the chloroplast. *Plant Physiology* 72:481–487. DOI: <https://doi.org/10.1104/pp.72.2.481>, PMID: 16663028
24. Kropat J, Hong-Hermesdorf A, Casero D, Ent P, Castruita M, Pellegrini M, Merchant SS, Malasarn D. 2011. A revised mineral nutrient supplement increases biomass and growth rate in *Chlamydomonas reinhardtii*. *The Plant Journal* 66:770–780. DOI: <https://doi.org/10.1111/j.1365-313X.2011.04537.x>, PMID:
25. Kuroda H, Maliga P. 2003. The plastid clpP1 protease gene is essential for plant development. *Nature* 425:86–89. DOI: <https://doi.org/10.1038/nature01909>, PMID: 12955146
26. Li H, Handsaker B, Wysoker A, Fennell T, Ruan J, Homer N, Marth G, Abecasis G, Durbin R, 1000 Genome Project Data Processing Subgroup. 2009. The sequence alignment/Map format and SAMtools. *Bioinformatics* 25:2078–2079. DOI: <https://doi.org/10.1093/bioinformatics/btp352>, PMID: 19505943
27. Li X, Zhang R, Patena W, Gang SS, Blum SR, Ivanova N, Yue R, Robertson JM, Lefebvre PA, Fitz-Gibbon ST, Grossman AR, Jonikas MC. 2016. An Indexed, Mapped Mutant Library

Enables Reverse Genetics Studies of Biological Processes in *Chlamydomonas reinhardtii* .
The Plant Cell 28:367–387. DOI: <https://doi.org/10.1105/tpc.15.00465>

28. Li X, Patena W, Fauser F, Jinkerson RE, Saroussi S, Meyer MT, Ivanova N, Robertson JM, Yue R, Zhang R, Vilarrasa-Blasi J, Wittkopp TM, Ramundo S, Blum SR, Goh A, Laudon M, Srikumar T, Lefebvre PA, Grossman AR, Jonikas MC. 2019. A genome-wide algal mutant library and functional screen identifies genes required for eukaryotic photosynthesis. *Nature Genetics* 51:627–635. DOI: <https://doi.org/10.1038/s41588-019-0370-6>, PMID: 30886426
29. Liao Y, Smyth GK, Shi W. 2013. The subread aligner: fast, accurate and scalable read mapping by seed-and-vote. *Nucleic Acids Research* 41:e108. DOI: <https://doi.org/10.1093/nar/gkt214>, PMID: 23558742
30. Llamas E, Pulido P, Rodriguez-Concepcion M. 2017. Interference with plastome gene expression and clp protease activity in *Arabidopsis* triggers a chloroplast unfolded protein response to restore protein homeostasis. *PLOS Genetics* 13:e1007022. DOI: <https://doi.org/10.1371/journal.pgen.1007022>, PMID: 28937985
31. Mackinder LC, Meyer MT, Mettler-Altmann T, Chen VK, Mitchell MC, Caspari O, Freeman Rosenzweig ES, Pallesen L, Reeves G, Itakura A, Roth R, Sommer F, Geimer S, Muhlhaus T, Schroda M, Goodenough U, Stitt M, Griffiths H, Jonikas MC. 2016. A repeat protein links rubisco to form the eukaryotic carbon-concentrating organelle. *PNAS* 113:5958–5963. DOI: <https://doi.org/10.1073/pnas.1522866113>, PMID: 27166422
32. Majeran W, Wollman F-A, Vallon O. 2000. Evidence for a role of ClpP in the degradation of the chloroplast cytochrome b 6 f complex. *The Plant Cell* 12:137. DOI: <https://doi.org/10.2307/3871035>

33. Nordhues A, Schottler MA, Unger A-K, Geimer S, Schonfelder S, Schmollinger S, Rutgers M, Finazzi G, Soppa B, Sommer F, Muhlhaus T, Roach T, Krieger-Liszkay A, Lokstein H, Crespo JL, Schroda M. 2012. Evidence for a Role of VIPP1 in the Structural Organization of the Photosynthetic Apparatus in *Chlamydomonas*. *The Plant Cell* 24:637–659. DOI: <https://doi.org/10.1105/tpc.111.092692>
34. Pootakham W, Gonzalez-Ballester D, Grossman AR. 2010. Identification and regulation of plasma membrane sulfate transporters in *Chlamydomonas*. *Plant Physiology* 153:1653–1668. DOI: <https://doi.org/10.1104/pp.110.157875>
35. Porra RJ, Thompson WA, Kriedemann PE. 1989. Determination of accurate extinction coefficients and simultaneous equations for assaying chlorophylls a and b extracted with four different solvents: verification of the concentration of chlorophyll standards by atomic absorption spectroscopy. *Biochimica Et Biophysica Acta (BBA) - Bioenergetics* 975:384–394. DOI: [https://doi.org/10.1016/S0005-2728\(89\)80347-0](https://doi.org/10.1016/S0005-2728(89)80347-0)
36. Ramundo S, Rahire M, Schaad O, Rochaix JD. 2013. Repression of essential chloroplast genes reveals new signaling pathways and regulatory feedback loops in *Chlamydomonas*. *The Plant Cell* 25:167–186. DOI: <https://doi.org/10.1105/tpc.112.103051>, PMID: 23292734
37. Ramundo S, Casero D, Muhlhaus T, Hemme D, Sommer F, Cre`vecoeur M, Rahire M, Schroda M, Rusch J, Goodenough U, Pellegrini M, Perez-Perez ME, Crespo JL, Schaad O, Civic N, Rochaix JD. 2014. Conditional depletion of the *Chlamydomonas* chloroplast ClpP protease activates nuclear genes involved in autophagy and plastid protein quality control. *The Plant Cell* 26:2201–2222. DOI: <https://doi.org/10.1105/tpc.114.124842>, PMID: 24879428

38. Ramundo S, Rochaix JD. 2014. Loss of chloroplast ClpP elicits an autophagy-like response in *Chlamydomonas*. *Autophagy* 10:1685–1686. DOI: <https://doi.org/10.4161/auto.29960>, PMID: 25046108
39. Robinson MD, McCarthy DJ, Smyth GK. 2010. edgeR: a bioconductor package for differential expression analysis of digital gene expression data. *Bioinformatics* 26:139–140. DOI: <https://doi.org/10.1093/bioinformatics/btp616>, PMID: 19910308
40. Rudella A, Friso G, Alonso JM, Ecker JR, van Wijk KJ. 2006. Downregulation of ClpR2 leads to reduced accumulation of the ClpPRS protease complex and defects in chloroplast biogenesis in *Arabidopsis*. *The Plant Cell* 18:1704–1721. DOI: <https://doi.org/10.1105/tpc.106.042861>, PMID: 16766689
41. Rutgers M, Muranaka LS, Muhlhaus T, Sommer F, Thoms S, Schurig J, Willmund F, Schulz-Raffelt M, Schroda M. 2017. Substrates of the chloroplast small heat shock proteins 22E/F point to thermolability as a regulative switch for heat acclimation in *Chlamydomonas reinhardtii*. *Plant Molecular Biology* 95:579–591. DOI: <https://doi.org/10.1007/s11103-017-0672-y>, PMID: 29094278
42. Schmidt GW, Matlin KS, Chua NH. 1977. A rapid procedure for selective enrichment of photosynthetic electron transport mutants. *PNAS* 74:610–614. DOI: <https://doi.org/10.1073/pnas.74.2.610>, PMID: 265526
43. Schneider CA, Rasband WS, Eliceiri KW. 2012. NIH image to ImageJ: 25 years of image analysis. *Nature Methods* 9:671–675. DOI: <https://doi.org/10.1038/nmeth.2089>, PMID: 22930834

44. Shpilka T, Haynes CM. 2018. The mitochondrial UPR: mechanisms, physiological functions and implications in ageing. *Nature Reviews Molecular Cell Biology* 19:109–120. DOI: <https://doi.org/10.1038/nrm.2017.110>
45. Sjogren LL, MacDonald TM, Sutinen S, Clarke AK. 2004. Inactivation of the *clpC1* gene encoding a chloroplast Hsp100 molecular chaperone causes growth retardation, leaf chlorosis, lower photosynthetic activity, and a specific reduction in photosystem content. *Plant Physiology* 136:4114–4126. DOI: <https://doi.org/10.1104/pp.104.053835>, PMID: 15563614
46. Thimm O, Blasing O, Gibon Y, Nagel A, Meyer S, Kruger P, Selbig J, Muller LA, Rhee SY, Stitt M. 2004. MAPMAN: a user-driven tool to display genomics data sets onto diagrams of metabolic pathways and other biological processes. *The Plant Journal* 37:914–939. DOI: <https://doi.org/10.1111/j.1365-313X.2004.02016.x>, PMID: 14996223
47. Udvardi MK, Czechowski T, Scheible WR. 2008. Eleven golden rules of quantitative RT-PCR. *The Plant Cell* 20: 1736–1737. DOI: <https://doi.org/10.1105/tpc.108.061143>, PMID: 18664613
48. Usadel B, Nagel A, Thimm O, Redestig H, Blaesing OE, Palacios-Rojas N, Selbig J, Hannemann J, Piques MC, Steinhauser D, Scheible W-R, Gibon Y, Morcuende R, Weicht D, Meyer S, Stitt M. 2005. Extension of the visualization tool MapMan to allow statistical analysis of arrays, display of corresponding genes, and comparison with known responses. *Plant Physiology* 138:1195–1204. DOI: <https://doi.org/10.1104/pp.105.060459>
49. Walter P, Ron D. 2011. The unfolded protein response: from stress pathway to homeostatic regulation. *Science* 334:1081–1086. DOI: <https://doi.org/10.1126/science.1209038>, PMID: 22116877

50. Werner R, Mergenhagen D. 1998. Mating type determination of *Chlamydomonas reinhardtii* by PCR. *Plant Molecular Biology Reporter* 16:295–299. DOI: <https://doi.org/10.1023/A:1007583508766>
51. Yamano T, Iguchi H, Fukuzawa H. 2013. Rapid transformation of *Chlamydomonas reinhardtii* without cell-wall removal. *Journal of Bioscience and Bioengineering* 115:691–694. DOI: <https://doi.org/10.1016/j.jbiosc.2012.12.020>
52. Yamaoka Y, Choi BY, Kim H, Shin S, Kim Y, Jang S, Song WY, Cho CH, Yoon HS, Kohno K, Lee Y. 2018. Identification and functional study of the endoplasmic reticulum stress sensor IRE1 in *Chlamydomonas reinhardtii*. *The Plant Journal* 94:91–104. DOI: <https://doi.org/10.1111/tpj.13844>, PMID: 29385296
53. Zerges W, Rochaix JD. 1998. Low density membranes are associated with RNA-binding proteins and thylakoids in the chloroplast of *Chlamydomonas reinhardtii*. *The Journal of Cell Biology* 140:101–110. DOI: <https://doi.org/10.1083/jcb.140.1.101>, PMID: 9425158
54. Zhang Z, Shrager J, Jain M, Chang CW, Vallon O, Grossman AR. 2004. Insights into the survival of *Chlamydomonas reinhardtii* during sulfur starvation based on microarray analysis of gene expression. *Eukaryotic Cell* 3:1331–1348. DOI: <https://doi.org/10.1093/eukcel/3.12.1331>
55. Zybailov B, Friso G, Kim J, Rudella A, Rodriguez VR, Asakura Y, Sun Q, van Wijk KJ. 2009. Large scale comparative proteomics of a chloroplast clp protease mutant reveals folding stress, altered protein homeostasis, and feedback regulation of metabolism. *Molecular & Cellular Proteomics* 8:1789–1810. DOI: <https://doi.org/10.1074/mcp.M900104-MCP200>, PMID: 19423572

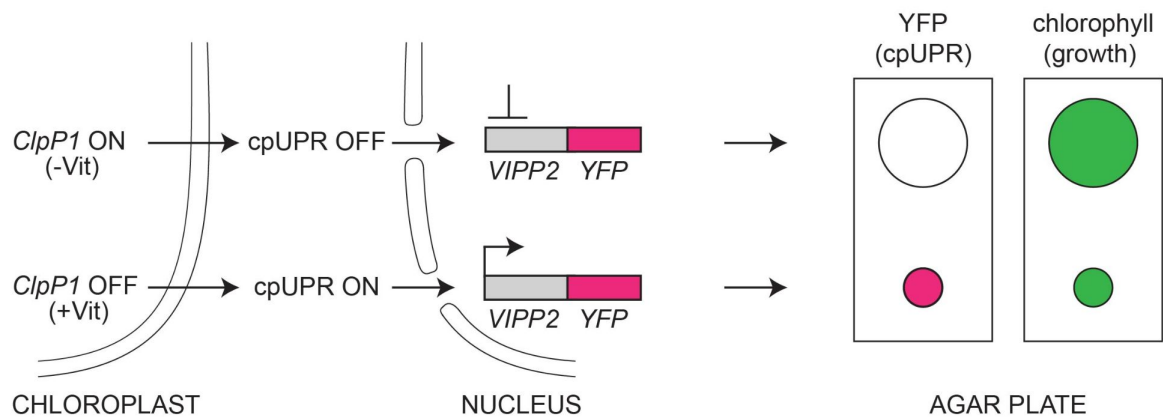
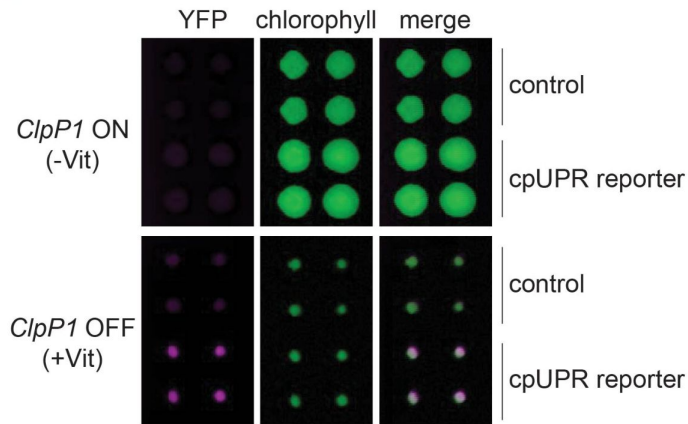
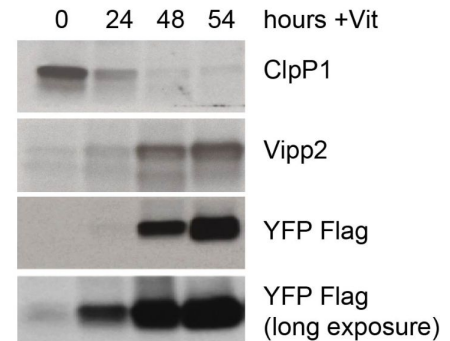
A**B****C**

Figure 1-1. Reporter strain for high-throughput screening for cpUPR mutants.

(A) Schematic of cpUPR regulation in the reporter strain. Under homeostatic conditions (-Vit), chloroplast ClpP1 is expressed and the cpUPR pathway is OFF, as indicated by the lack of VIPP2 expression; upon ClpP1 depletion (+Vit), the cpUPR is induced leading to VIPP2 expression. The cells contain an inducible reporter gene consisting of the VIPP2 promoter fused to the coding sequence of YFP tagged with a 3x-Flag epitope at its C-terminus. When the reporter gene is activated, YFP fluorescence is induced (magenta circles), and the reporter strain's growth is inhibited, as indicated by the smaller colony size (green circles) measured in the chlorophyll-imaging channel. (B) Plate-based real-time imaging assay to detect cpUPR activation. Four technical replicates of control cells (containing only the ClpP1-repressible system) and of cpUPR reporter cells (additionally containing the YFP reporter gene) were imaged after 6 days of growth on agar plates under ClpP1-permissive or ClpP1-nonpermissive conditions (-/+Vit, respectively). Induction of the YFP fluorescence is observed exclusively in the reporter strain replicates, while growth inhibition is observed in both control and cpUPR reporter strains in ClpP1-nonpermissive conditions. (C) Immunoblots of reporter cell extracts upon ClpP1 repression (+Vit) for 0, 24, 48, and 54 hr were probed with anti-ClpP1, anti-Vipp2, and anti-Flag antibodies.

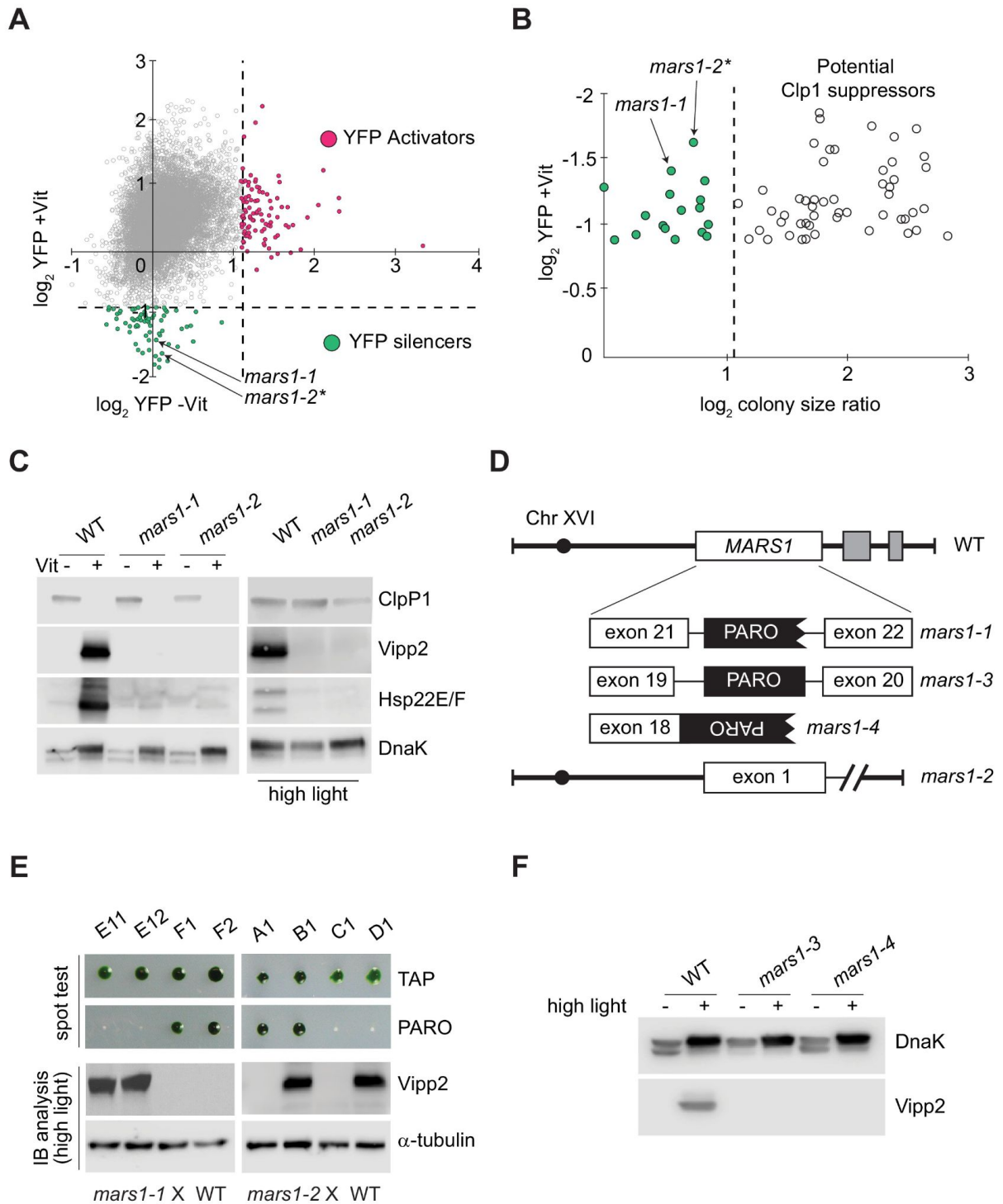


Figure 1-2. Genetic screen identifying *mars1-1* and *mars1-2*.

(A) Scatter plot of changes in YFP fluorescence for each mutant relative to reporter cells in ClpP1-permissive (-Vit) and ClpP1-nonpermissive (+Vit) conditions. Mutants exhibiting YFP fluorescence at least three standard deviations lower or higher than the mean (dotted lines) were categorized as YFP silencers and activators. Positions of the cpUPR silencers *mars1-1* and *mars1-2** are indicated (for details on *mars1-2** refer to the note in Supplementary Materials). (B) Scatter plot of colony size ratio over fold-changes in YFP fluorescence for each mutant relative to reporter cells under ClpP1-

nonpermissive conditions (+Vit). Colony size ratio was calculated as a fold-change of the colony area between 2 and 6 days after plating. The average colony size increase is indicated by the dashed line. Colonies that increased in size more than average represent potential suppressors of ClpP1 repression. (C) Immunoblot analysis of cpUPR reporter cell (WT) extracts, mars1-1 and mars1-2 cells grown in ClpP1-permissive or ClpP1-nonpermissive conditions (-/+Vit, respectively) or exposed to high light, using antibodies against ClpP1, Vipp2, Hsp22E/F and DnaK (loading/stress control). (D) Diagram of MARS1 indicating the insertion site of the mutagenic cassette (PARO) in each respective MARS1 mutant allele. Gray boxes indicate neighboring genes and the interrupted line a deletion. (E) Analysis of representative meiotic tetrads from backcrosses of mars1-1 and mars1-2 to WT (CC-124) (E11-F2 and A1-D1 correspond to the plate coordinates in Figure 2—figure supplement 2B, Figure 2—figure supplement 3B). Tetrads were spotted on acetate agar (TAP) and on acetate agar supplemented with paromomycin (PARO). Samples prepared from the strains grown under HL were immunoblotted with antibodies against Vipp2 and α -tubulin (loading control). (F) Immunoblot samples prepared from WT, mars1-3 and mars1-4 cells grown under control or HL conditions were probed with antibodies against Vipp2 and DnaK as a loading/stress control.

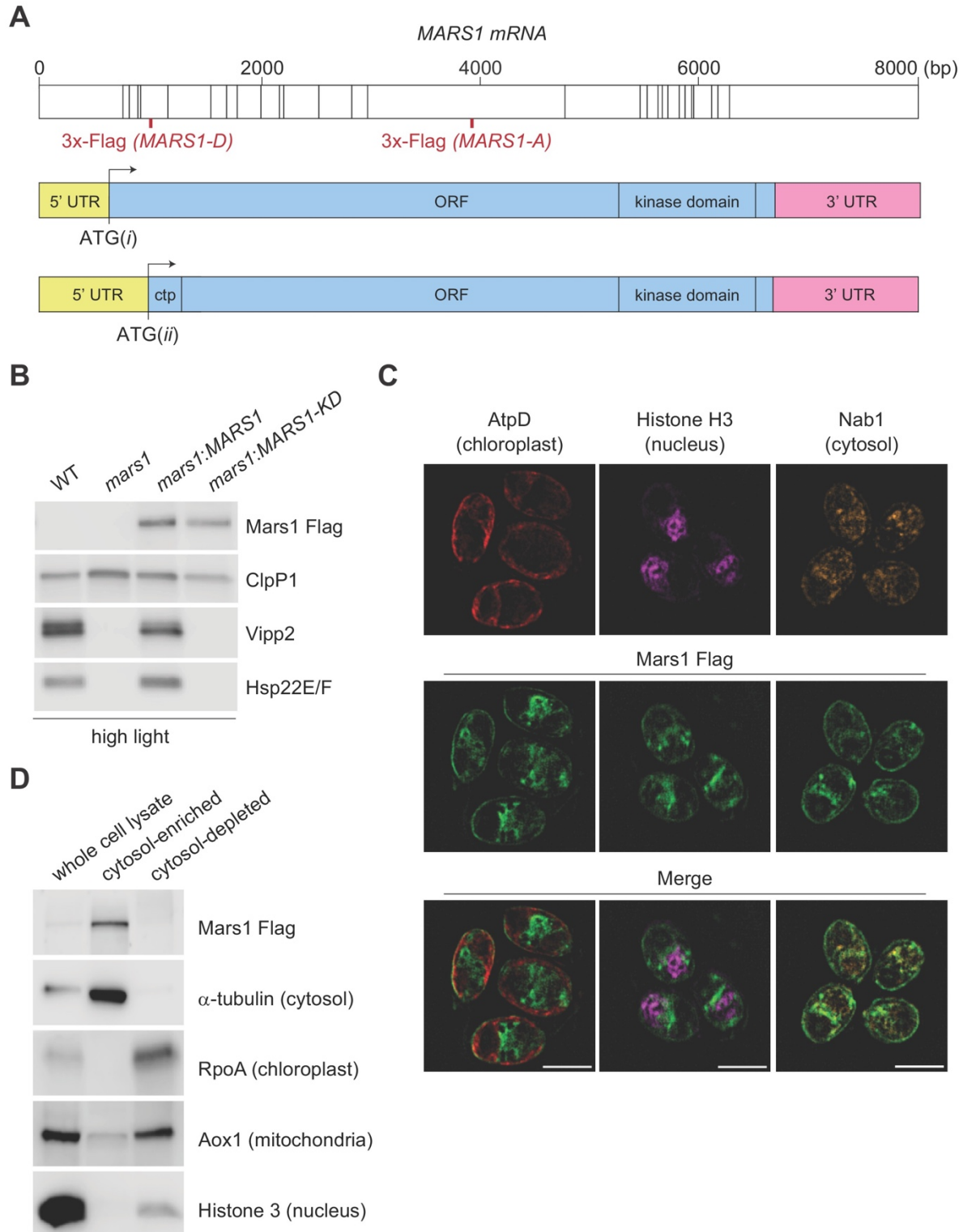


Figure 1-3. Characterization of Mars1.

(A) In the upper diagram, the length of MARS1 transcript is shown, the position of exon-exon boundaries is indicated with vertical lines while the different locations of the triple Flag epitope engineered in MARS1-A and MARS1-D transgenes are highlighted in red. In the lower diagrams, alternative models

for the 5' untranslated region (5' UTR) (yellow) and open reading frame (ORF) (light blue) in MARS1 transcript are shown as predicted for translation starts ATG(i) and ATG(ii). The N-terminal chloroplast transit peptide (ctp) is predicted by ChloroP (Emanuelsson et al., 1999) only if ATG(ii) is used as the translation start site. In both models, the position of the 3' UTR (pink) and the kinase domain is the same. (B) Immunoblot analysis of samples prepared after HL treatment using antibodies against Flag for Mars1 detection, Vipp2, Hsp22E/F, and ClpP1 (loading control). Strains analyzed: mars1 = mars1-3; mars1:MARS1-A = mars1-3 transformed with a MARS1-A transgene containing a 3x-Flag epitope after Arg1167 of Mars1 (as shown in Figure 3A); mars1:MARS1-A KD = mars1-3 transformed with a catalytically-inactive MARS1-A transgene bearing the kinase active site D1871A mutation. (C) Representative dual immunofluorescence images obtained by structured illumination microscopy of mars1-3:MARS1-A cells. Mars1 was detected with anti-Flag. Anti-AtpD, anti-Histone H3 and anti-Nab1 staining served as controls for the localization of the chloroplast, nucleus and cytosol, respectively. Scale bar: 5 μ m. For imaging conditions and negative controls, see Supplementary Materials and Figure 3—figure supplement 2. (D) Immunoblot analysis of lysates fractionated by differential centrifugation from mars1-3:MARS1-A cells probed with the indicated antibodies against known markers of the cytosol (α -tubulin), chloroplast (RpoA, α -subunit of chloroplast RNA polymerase), nucleus (Histone H3) and mitochondria (Aox1, alternative oxidase 1).

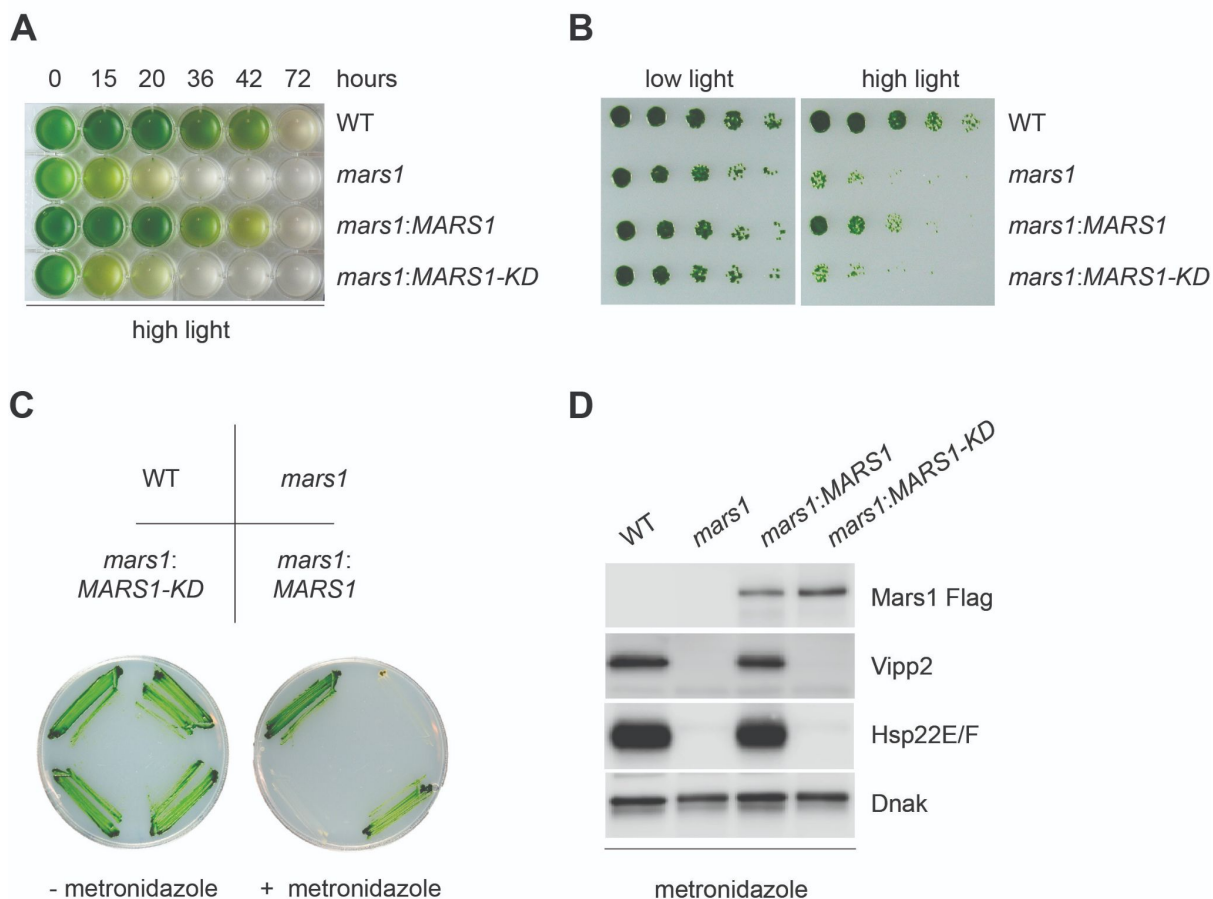


Figure 1-4. *mars1* cells are hypersensitive to photooxidative stress.

(A) Liquid TAP cultures of WT, *mars1*, *mars1:MARS1-D* and *mars1:MARS1-D KD* at different time points upon HL exposure. Alleles used: *mars1* = *mars1-3*; *mars1:MARS1-D* = *mars1-3* transformed with the MARS1-D transgene containing a 3x-Flag epitope after Met139; *mars1:MARS1-D KD* = *mars1-3* transformed with a catalytically-inactive MARS1-D bearing the kinase active site D1871A mutation. (B) Strains described in Figure 4A were spotted onto TAP agar plate in 4-fold serial dilutions before and after exposure to high light for 27 hr. Photographs of untreated and treated cells were taken after 6 and 7 days, respectively, of growth in low light. (C) Strains described in Figure 4A were streaked on +/- 1.5 mM metronidazole TAP agar plates. Photographs were taken after 4 days of growth in normal light. (D) Immunoblot analysis of samples prepared from strains described in Figure 4A treated with 1.1 mM metronidazole for 15 hours. Detection with antibodies against Flag (Mars1), Vipp2, Hsp22E/F, and ClpP1 (loading control).

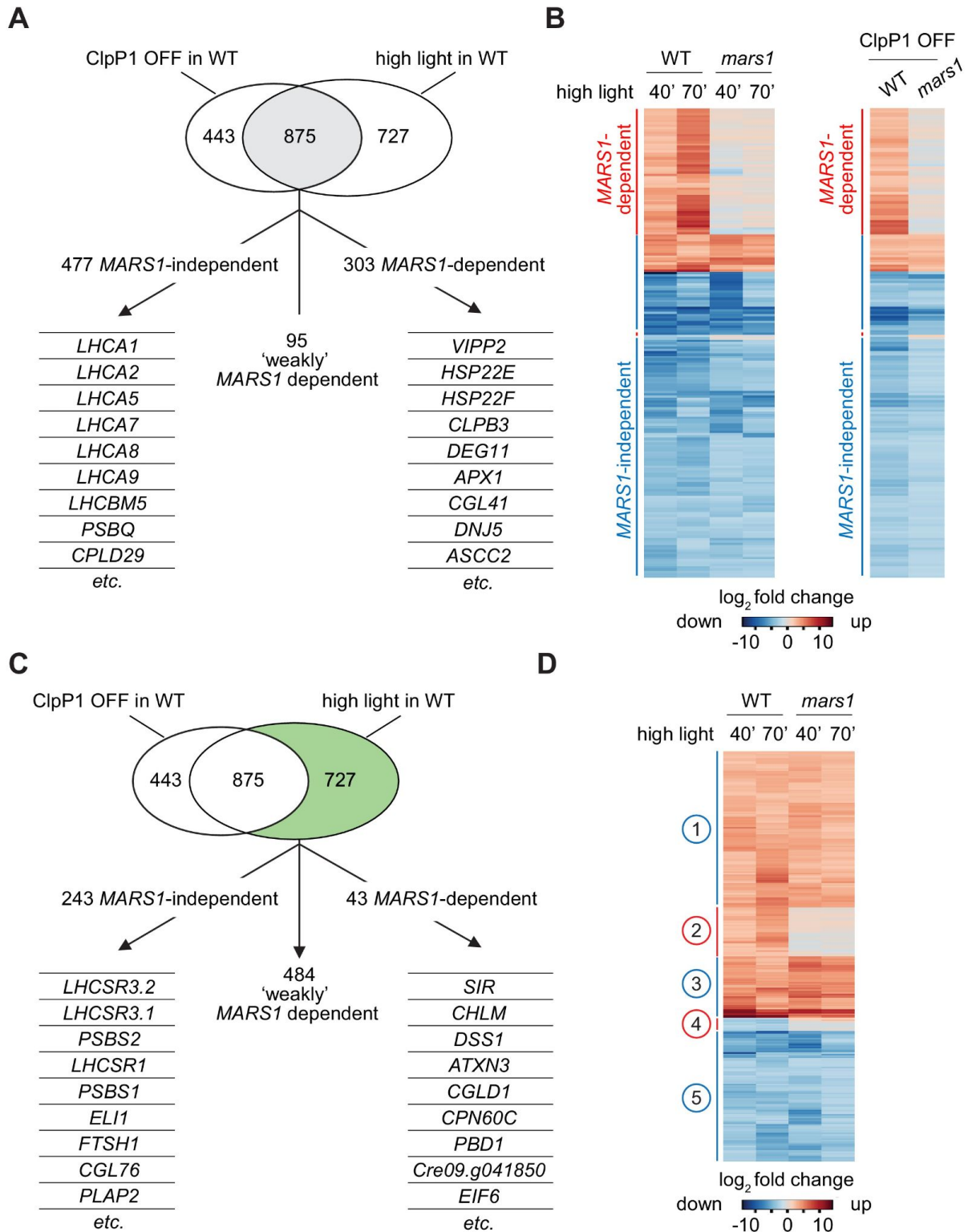


Figure 1-5. *mars1* cells do not activate the cpUPR transcriptional program.

(A) Venn diagram highlighting the transcriptional changes elicited genetically (ClpP1 repression) or physiologically (HL exposure) in *Chlamydomonas* cells, as determined by RNA sequencing (overlap in gray). The 875 common stress-responsive genes are defined as genes whose expression showed at least a 4-fold change upon stress ($p < 0.001$) and were consistently up- or down-regulated in both high light and

ClpP1 repression. These genes are further subdivided in three groups: 1) *MARS1*-dependent, being unresponsive (<2-fold change) when *MARS1* was disrupted; 2) ‘weakly’ *MARS1* dependent, being only mildly induced or inhibited (<4-fold but >2-fold) upon stress in the *mars1* background; and 3) *MARS1*-independent, being still responsive (<2-fold change) in absence of *MARS1* expression. A short list of genes belonging to each category (*MARS1*-dependent and *MARS1*-independent) is provided. Full lists of *MARS1*-dependent and *MARS1*-independent genes are available through Figshare (<https://figshare.com/s/992706a610ce6b71f03c>, <https://figshare.com/s/66417c2b28f3110b8077>). (B) Heatmap comparing gene expression patterns of the 875 common stress-responsive genes (as defined in Figure 5A) in WT and *mars1* cells upon exposure to HL (for 40 or 70 min) or in ClpP1-nonpermissive conditions (+Vit). (C) The same Venn diagram shown in Figure 5A highlighting (in green) genes that are preferentially responsive to HL exposure (>4-fold change only upon HL stress, $p < 0.001$, and consistently up- or down-regulated in both time points during HL stress). These 727 genes are further categorized based on their gene expression dependency on *MARS1*. A short list of genes belonging to each category (*MARS1*-dependent and *MARS1*-independent) is provided. *MARS1*-dependent genes are related to chloroplast protein folding and degradation, protein translation or are poorly characterized. By contrast, the list of *MARS1*-independent genes includes key regulators of nonphotochemical quenching such as *LHCSR* and *PSBS* genes. HL = high light; ClpP1 OFF = ClpP1 repression. (D) Heatmap showing genes that are preferentially responsive to HL exposure. Five clusters of genes are highlighted on the side. Numbers circled in blue and red indicate gene clusters not affected and affected by *MARS1* disruption, respectively.

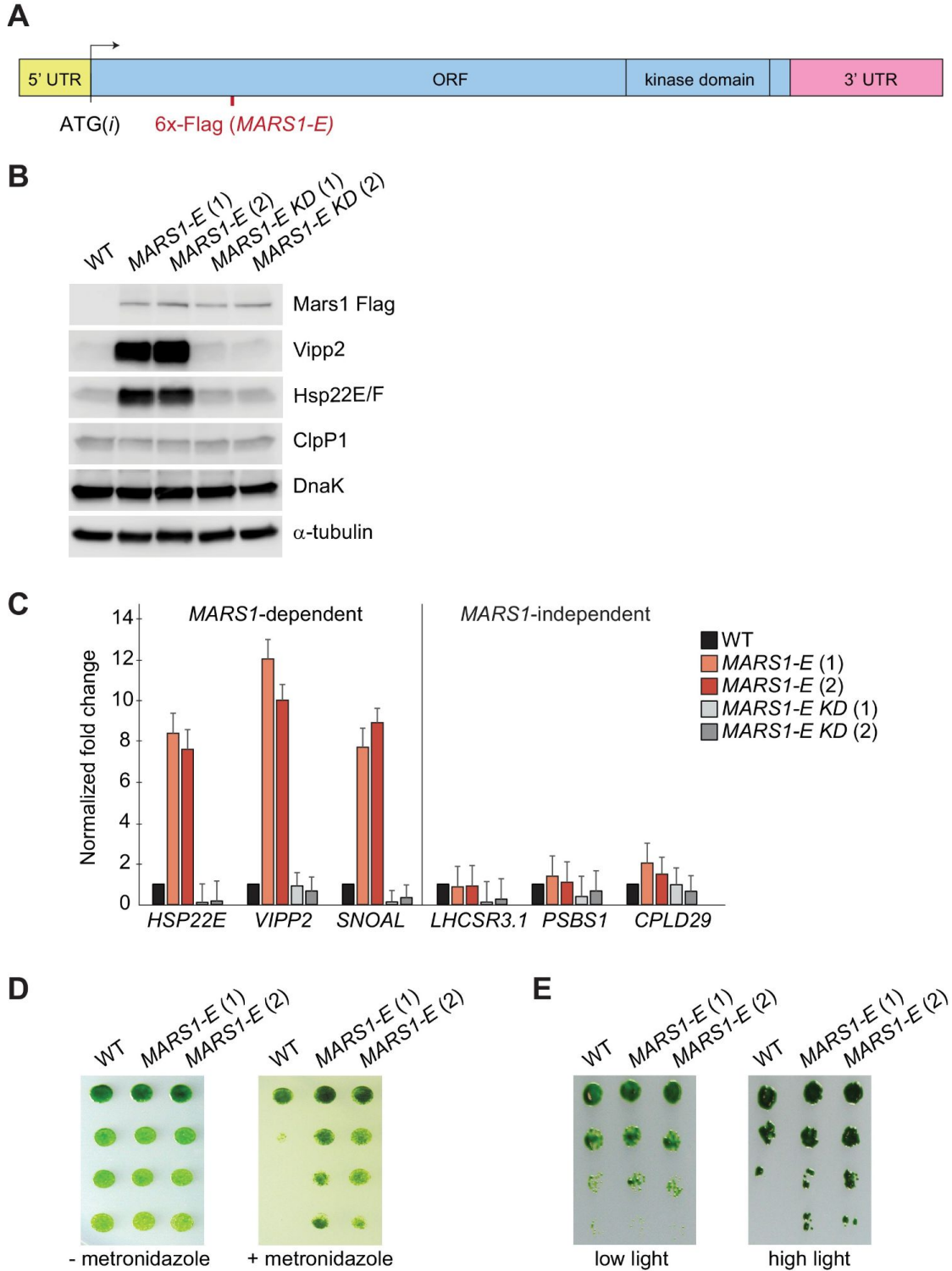
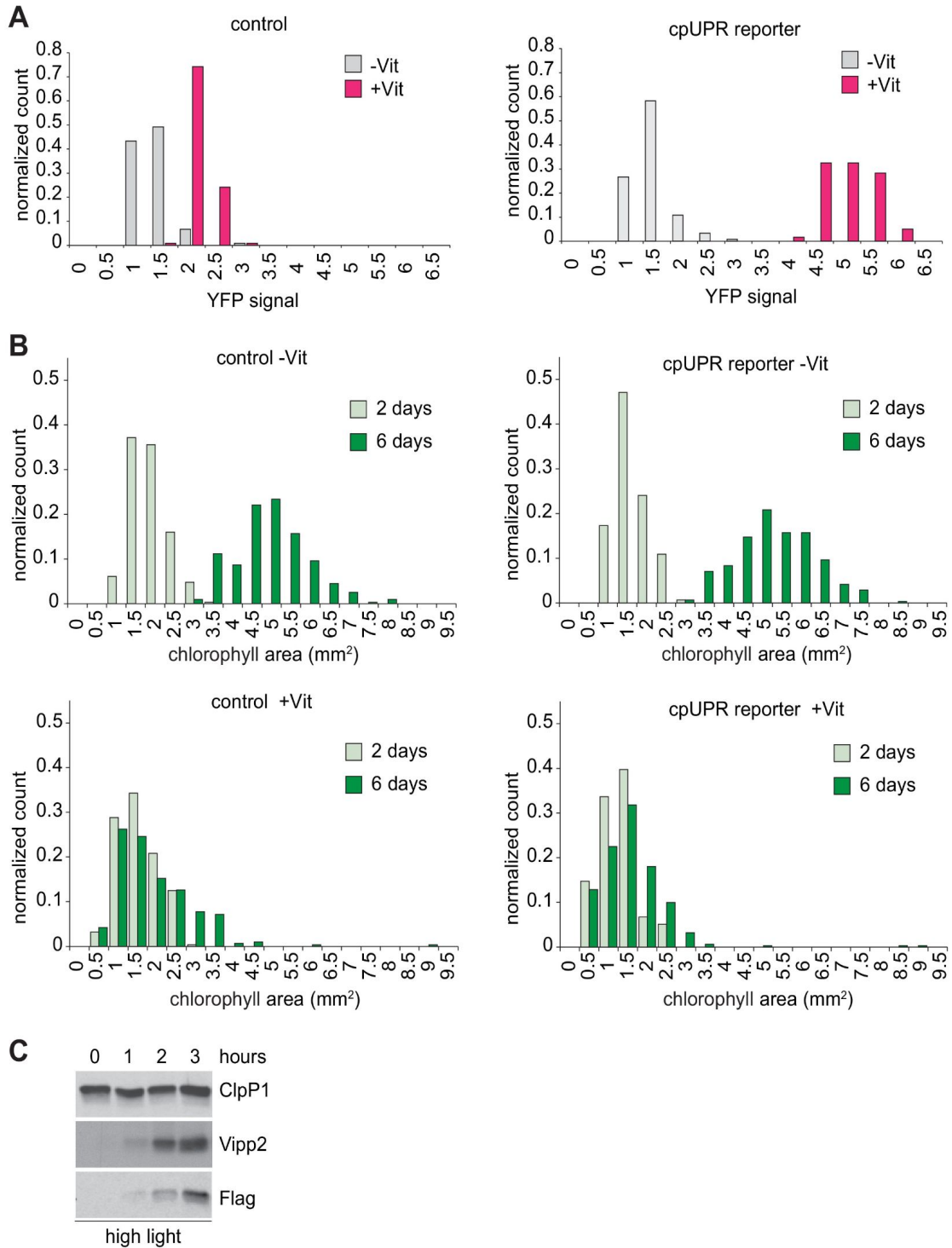


Figure 1-6. Basal induction of the cpUPR renders cells more resistant to chloroplast stress.

(A) A diagram of *MARS1-E* transcript showing the position of the 6x-Flag epitope inserted after Leu402 of Mars1. (B) Immunoblot analysis of samples prepared from cells grown under normal conditions, using antibodies described in Figure 3. Strains used: *MARS1-E* (1) and (2) = WT cells expressing a *MARS1-*

E transgene; *MARSI-E KD* (1) and (2) = WT cells expressing a catalytically-inactive *MARSI-E* transgene bearing the D1871A mutation. (C) Expression level of *MARSI*-dependent or *MARSI*-independent transcripts determined by quantitative PCR under normal growth conditions in cpUPR constitutive-active cells described in Figure 6B. Reference gene for normalization: *GBLP*. (D) cpUPR constitutive-active cells (described in Figure 6B) were grown in liquid TAP until logarithmic phase, diluted to the same cell count and spotted onto +/- 2.2 mM metronidazole agar plates using 1.5-fold dilutions between spots. Photographs of untreated and treated cells were taken after 3 and 6 days, respectively, of growth in normal light. (E) Cells as in Figure 6D spotted onto TAP agar using 4-fold serial dilutions before or after exposure to HL. Photographs were taken after 7 days of growth in normal light.



(A) Histograms of the normalized Yellow Fluorescent Protein (YFP) maximum intensity signal after 2 days in ClpP1-permissive (-Vit) or ClpP1-nonpermissive media (+Vit) for control and cpUPR

reporter cell colonies ($N = 120$ for each strain). The control strains contain only the ClpP1 repressible system, while the cpUPR reporter strain also harbors the reporter construct described in Figure 1B. (B) Histograms of colony area measurements (in mm^2) for control and for the cpUPR reporter cell colonies described in Figure 1—figure supplement 1A after 2 or 6 days in ClpP1-permissive (-Vit) or ClpP1-nonpermissive media (+Vit). (C) Immunoblot analysis of samples prepared from the reporter strain exposed to high light for 1, 2, and 3 hr using antibodies against Vipp2, Flag for YFP detection and ClpP1 as loading control.

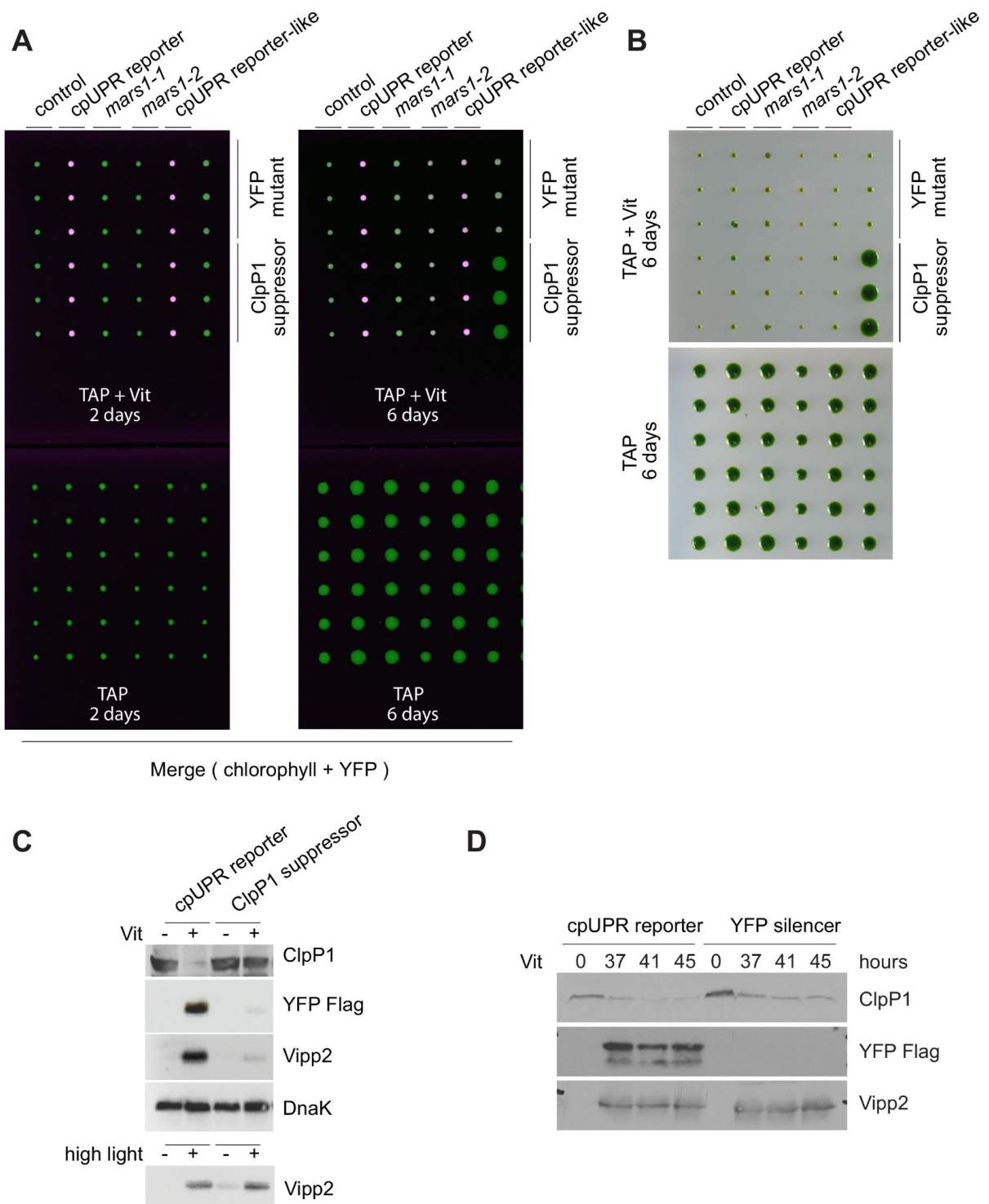


Figure 1-2S1. The genetic screen yields two cpUPR silencing mutants, mars1-1 and mars1-2.

(A) A merge of the chlorophyll (green) and YFP (magenta) channel for each of the following cell colonies: control cells (containing only the ClpP1 repressible system), cpUPR reporter cells (containing both the ClpP1 repressible system and the YFP reporter construct described in Figure 1B), mars1-1, mars1-2 (described in Figure 2A–C), a cpUPR reporter-like cell line (mutant strain performing like the parental

cpUPR reporter used as a positive control) (technical replicates N = 6), a YFP mutant and a ClpP1 suppressor cell colony (technical replicates N = 3). Colonies were grown in acetate media (TAP) in ClpP1-permissive (-Vit) or nonpermissive conditions (+Vit) for 2 and 6 days. In +Vit, the ClpP1 suppressor exhibits a YFP-silencing phenotype, but its colony size is comparable to that in -Vit. (B) Photographs of the same cell colonies shown in Figure 2—figure supplement 1A, grown in ClpP1-permissive (-Vit) or ClpP1-nonpermissive conditions (+Vit) for 6 days. (C) Immunoblot analysis of samples prepared from the cpUPR reporter cell line and the ClpP1 suppressor mutant grown in ClpP1-permissive (-Vit) and ClpP1-nonpermissive (+Vit, 2 days) conditions or upon exposure to HL (3 hr) using antibodies against ClpP1, Vipp2, Flag for YFP detection and DnaK for loading control. As expected, the ClpP1 suppressor mutant expresses ClpP1 in +Vit. (D) Immunoblot analysis of samples prepared from the cpUPR reporter cell line and the YFP mutant grown in ClpP1-permissive and ClpP1-nonpermissive conditions (-/ +Vit, respectively), using antibodies against ClpP1, Vipp2 and Flag for YFP detection.

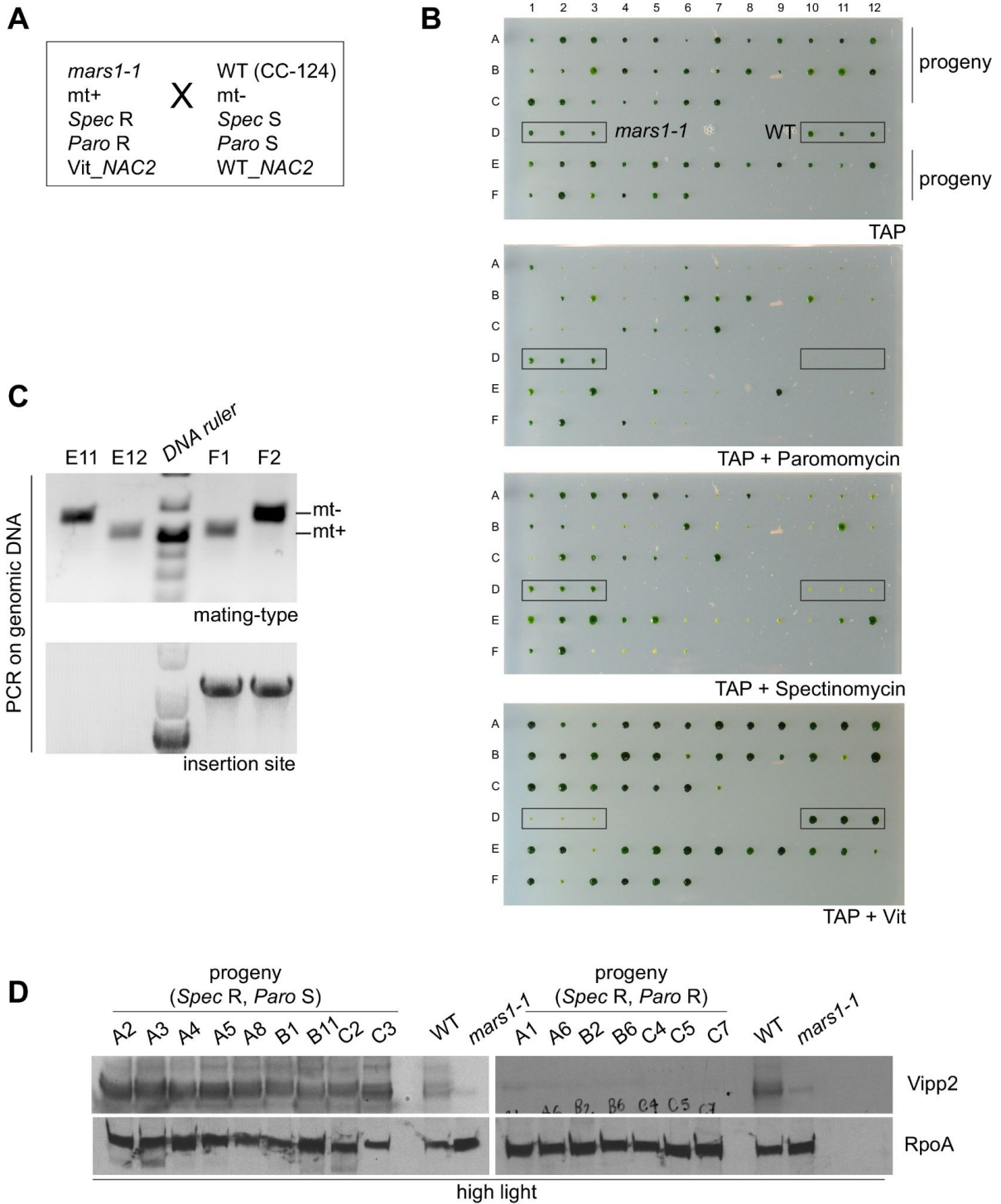


Figure1-2S2. Genetic analysis of *mars1-1*.

(A) Diagram showing the backcross of *mars1-1* to CC-124 (WT) and indicating the mating-type and other genetic markers of these two cell lines. The spectinomycin resistance (*Spec R*) and the Vit-driven NAC2 transgene (Vit-NAC2) are linked to the genetic modifications introduced into the chloroplast and in

the nuclear genome, respectively, to generate a Vit-driven ClpP1 repressible cell line (Ramundo et al., 2014; Ramundo et al., 2013). The paromomycin resistance (Paro R) is linked to the insertion of the mutagenic cassette into the nuclear genome. (B) Photographs of offspring from the mars1-1 x CC-124 (WT) backcross along with the parental controls, mars1-1 and CC-124, re- arrayed in a 96-well format and replicated on TAP agar or on TAP agar supplemented with Vit, with paromomycin or with spectinomycin. Due to difficulties in the cross, most isolated tetrads were incomplete. However, among the spectinomycin resistant offspring, about 50% of the cells were found to be paromomycin resistant as expected in the case of Mendelian inheritance of a single nuclear locus. (C) Mating type and insertion site PCR products from genomic DNA samples prepared from a full tetrad progeny obtained from the backcross of mars1-1 to CC-124 (WT) (Werner and Mergenhagen, 1998). The phenotypes of the progeny are shown in Figure 2E. Both the mating-type and the mutagenic cassette, disrupting the MARS1 gene locus, segregated 2:2. (D) Immunoblot analysis of samples prepared from the indicated progeny and exposed to HL, using antibodies against Vipp2 and RpoA as a loading control. Only spectinomycin-resistant progeny were selected, and they were named after their coordinates in the 96-well plates shown in panel B.

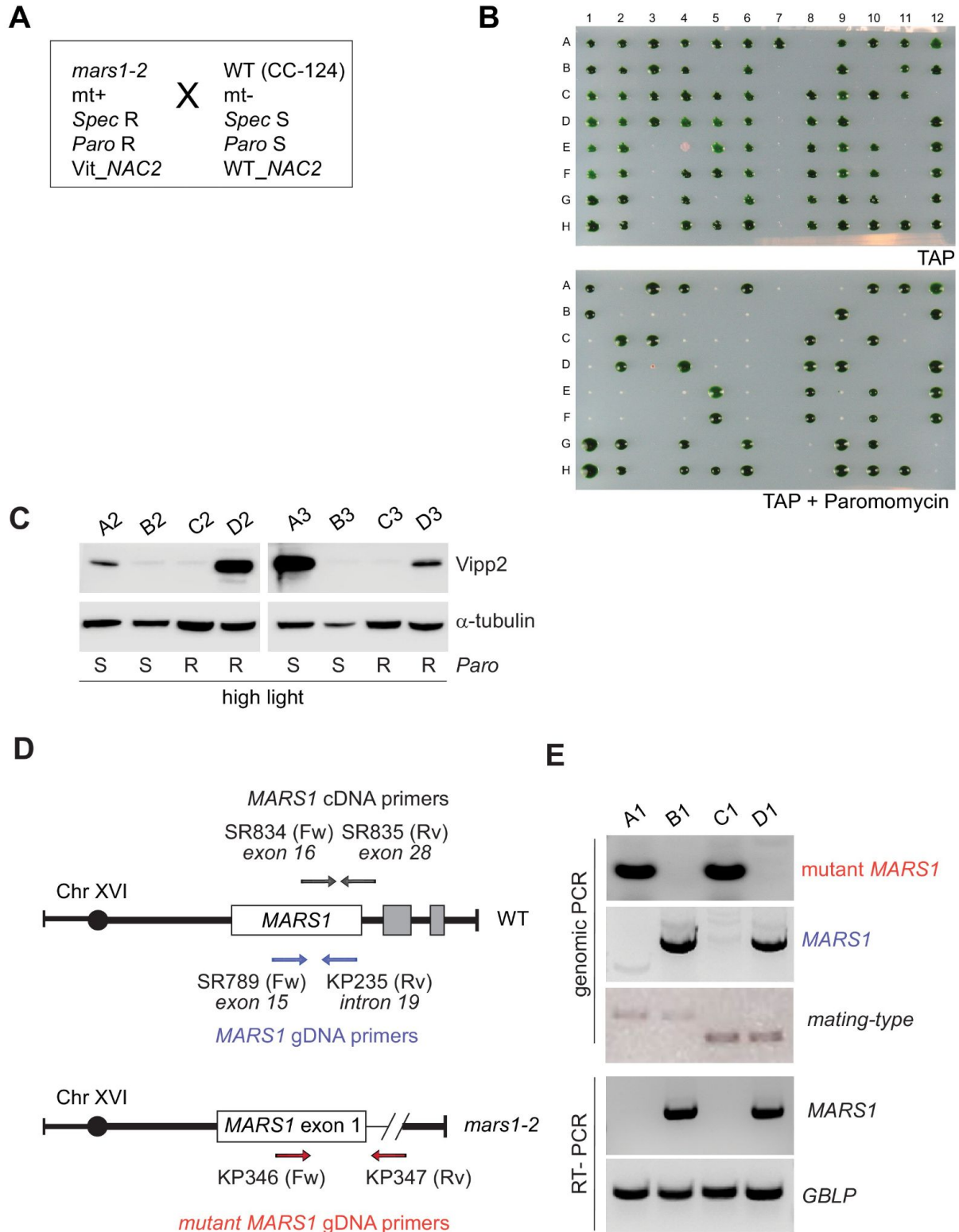
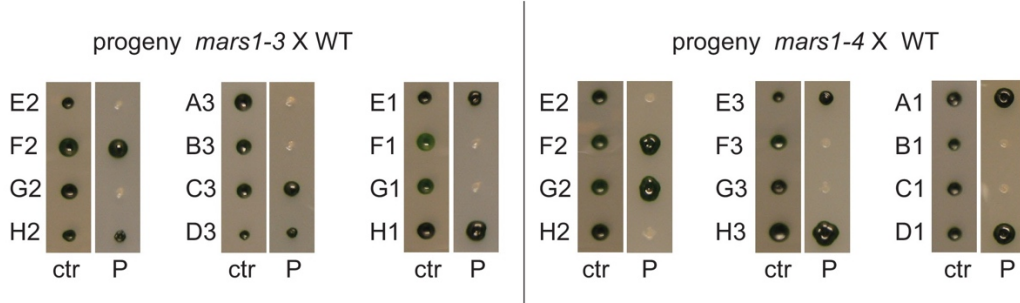
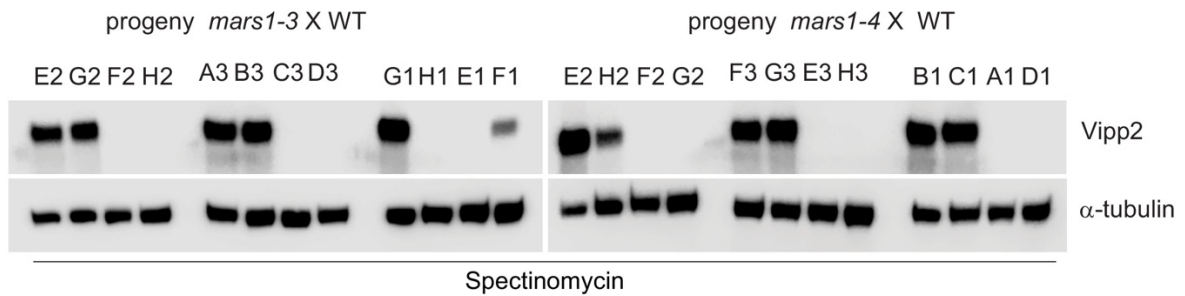
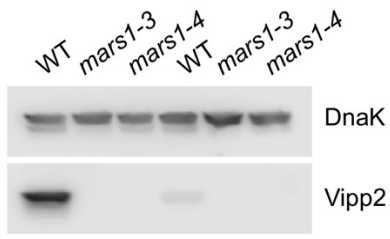
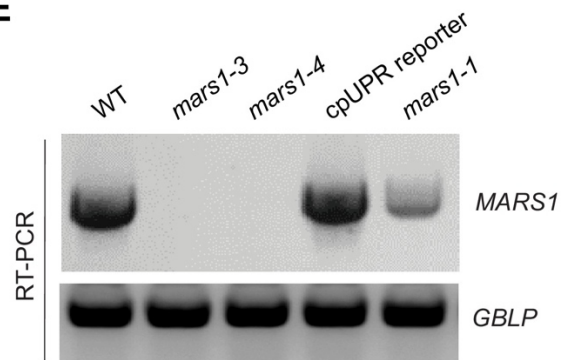


Figure 1-2S3. Genetic analysis of *mars1-2*.

(A) Diagram showing the backcross of *mars1-2* to CC-124 (WT) and indicating the mating-type and other genetic markers of these two cell lines. (B) Photographs of offspring from the *mars1-2* to CC-124

(WT) backcross along with the parental controls, mars1-2 and CC-124, re-arrayed in a 96-well format and replicated on TAP agar or on TAP agar supplemented with paromomycin. (C) Immunoblot analysis of samples prepared from tetrads obtained from the mars1-2 to CC-124 backcross and exposed to HL, using antibodies against Vipp2 and α -tubulin as a loading control. Sensitivity (S) or resistance (R) to Paromomycin (Paro) is also indicated. (D) Cartoon indicating the deletion of the MARS1 gene locus in mars1-2 and the annealing position of the primers at different regions of the MARS1 gene locus and chromosome 16. These primers were used for PCR amplification on cDNA and/or genomic DNA prepared from WT and mars1-2 (in Figure 2—figure supplement 3E), mars1-1, mars1-3 and mars1-4 (in Figure 2—figure supplement 4E). (E) Detection of MARS1 gene deletion and abrogation of MARS1 transcript in mars1-2. Genomic DNA and cDNA samples obtained from the meiotic tetrad shown in Figure 2E were analyzed by PCR and RT-PCR, respectively, using the primers indicated in Figure 2—figure supplement 3D. GBLP was used as a loading control for cDNA amplification. Progeny containing the MARS1 deletion correlated with having no MARS1 transcript.

A**B****C****D****E****Figure 1-2S4. Genetic analysis of *mars1-3* and *mars1-4*.**

(A) Diagram showing the backcross of *mars1-3* or *mars1-4* x CC-125 (WT) and indicating the mating-type and other genetic markers of these cell lines. (B) Photographs of offspring from the backcross of *mars1-3* or *mars1-4* to CC-125 (WT), re-arrayed in a 96-well format and replicated on TAP agar (‘ctr’, control) or on TAP agar supplemented with paromomycin (‘P’). Three representative tetrads are shown for each mutant. (C) Immunoblot analysis of samples prepared from tetrads obtained from the backcross of *mars1-3* or *mars1-4* to CC-125 (WT) (shown in Figure 2—figure supplement 4B) and treated with

spectinomycin, using antibodies against Vipp2 and a-tubulin for loading control. Since these cell lines do not harbor a spectinomycin resistance cassette, this antibiotic was used as a chloroplast translation inhibitor to trigger the activation of the chloroplast unfolded protein response. (D) Immunoblot analysis of samples prepared from wild-type cells and mars1-3 and mars1-4 cells, upon treatment with either spectinomycin or hydrogen peroxide, using antibodies against Vipp2 and DnaK as a loading control. (E) MARS1 RT-PCRs performed on cDNA extracted from wild-type cells (CC-4533, the parental line used to generate the mars1-3 and mars1-4 mutants), mars1-3 and mars1-4 cells, cpUPR reporter cells (the parental line used to generate mars1-1) and mars1-1 cells using primers indicated in Figure 2— figure supplement 3D. RT-PCRs of the housekeeping gene GBLP served as loading controls. The insertion of the mutagenic cassette in different regions of the MARS1 gene (as indicated in Figure 2D) impairs expression of MARS1 transcript to different degrees in each mutant (completely in mars1-4, almost completely in mars1-3 and partially in mars1-1).

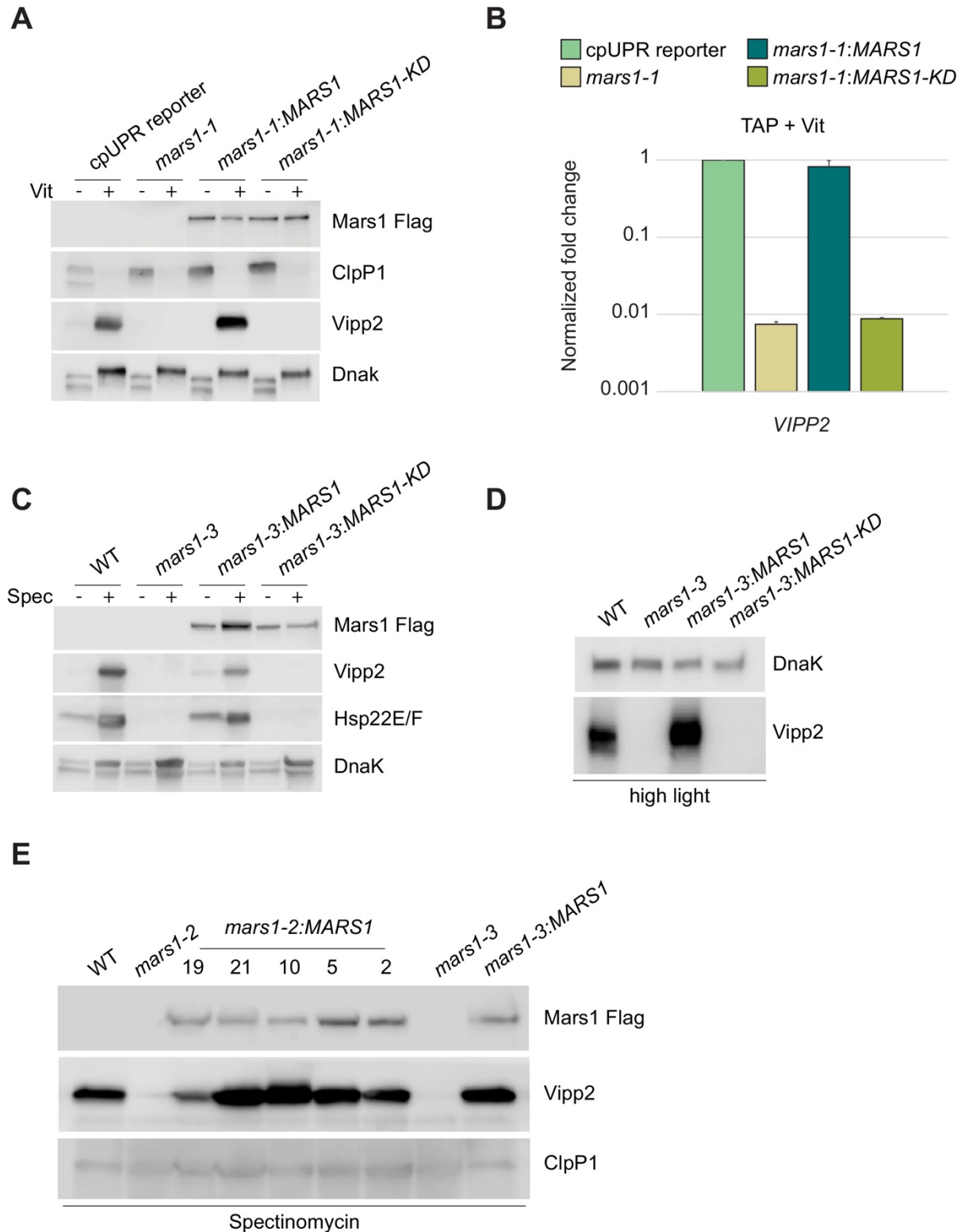


Figure 1-3S1. A catalytic active Mars1 kinase is required for signaling during the cpUPR.

(A) Immunoblot analysis of samples prepared from cell lines described below grown in ClpP1-permissive (-Vit) and ClpP1-nonpermissive conditions (+Vit) using antibodies against Flag for Mars1

detection, Vipp2, Hsp22E/F, ClpP1, and DnaK for loading control; WT = backcrossed wild-type (E12 offspring from tetrad shown in Figure 2E); mars1 1 = backcrossed mars1-1 (F2 offspring from tetrad shown in Figure 2E); mars1-1:MARS1 = backcrossed mars1-1 transformed with a MARS1-A transgene containing a 3x-Flag epitope after Arg1167 of Mars1; mars1:MARS1-KD = backcrossed mars1-1 transformed with a catalytically-inactive MARS1-A transgene (mutated at D1871A) (for more details about MARS1 tagging, see diagrams in Figure 3A and Supplementary Materials). (B) The same cell lines described in Figure 3—figure supplement 1A were subjected to quantitative PCR analysis and the level of expression of the VIPP2 transcripts was measured in ClpP1-nonpermissive conditions (TAP +Vit). GBLP was chosen as a reference gene during normalization. (C) Immunoblot analysis of samples prepared from cell lines described in Figure 3B treated in -/+ spectinomycin using antibodies against Flag for Mars1 detection, Vipp2, Hsp22E/F and DnaK for loading/stress control. (D) Immunoblot analysis of samples prepared from cell lines described in Figure 3E exposed to HL using antibodies against Vipp2 and DnaK for loading control. (E) Immunoblot analysis of WT, mars1-2 and several mars1-2:MARS1 samples treated with spectinomycin, using antibodies against Flag for Mars1 detection, Vipp2, and ClpP1 for loading control. Both WT (CrPW10) and mars1-2 (CrPW11), indicated in the figure, were obtained upon 3 backcrosses of mars1-2 to CC-124. mars1-2:MARS1 (19, 21, 10, 5, 2) are independently complemented cell lines obtained upon genomic integration of a wild-type MARS1-A transgene in mars1-2 (CrPW11). mars1-3 and mars1-3:MARS1 from Figure 3B were used as control cell lines.

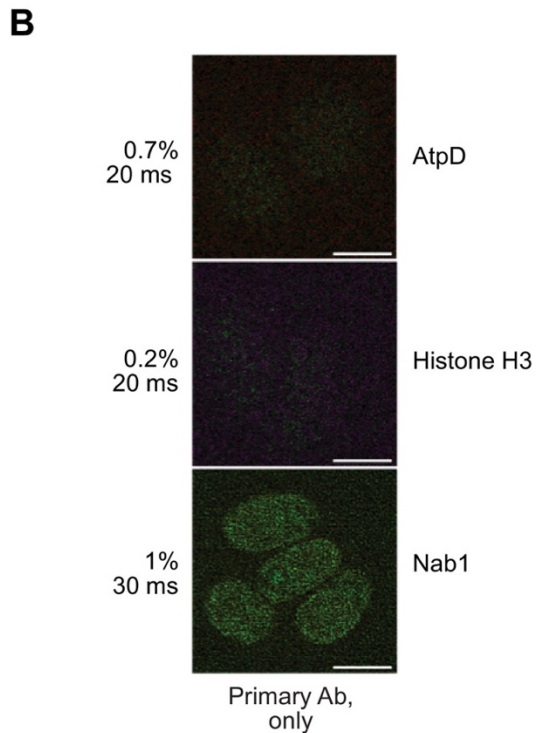
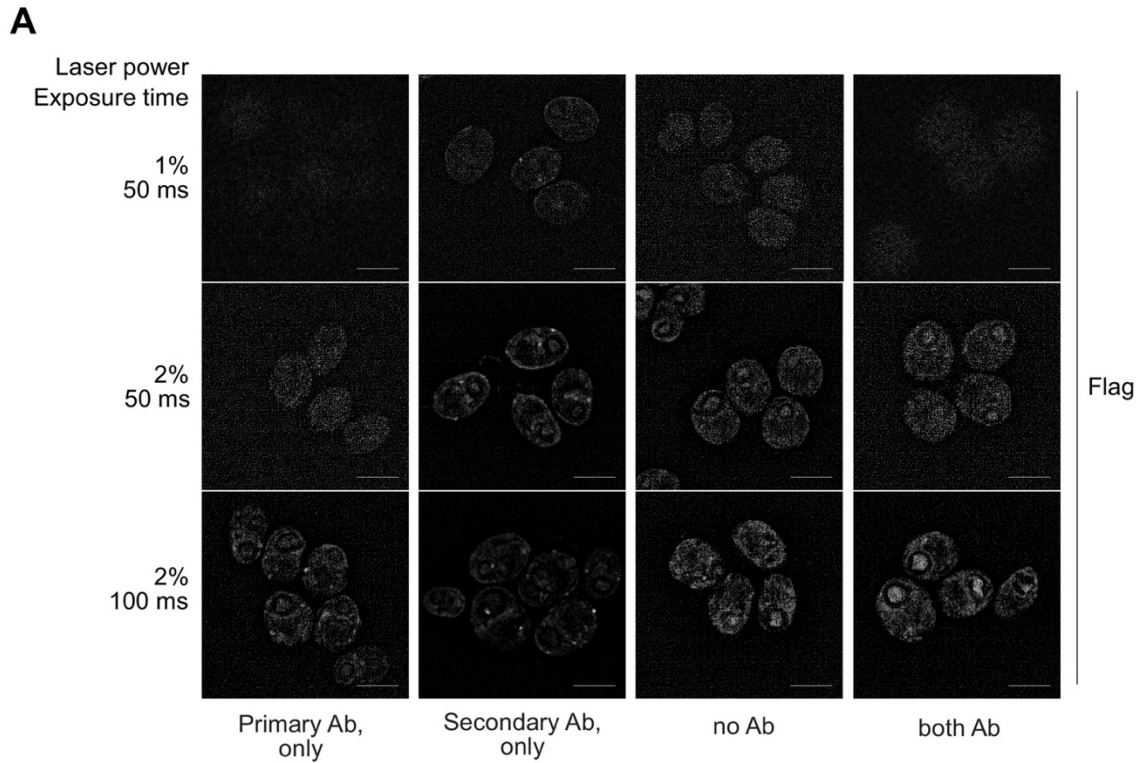


Figure 1-3S2. Specific immunodetection of the Mars1 Flag protein.

(A) WT cells (CC-4533) were grown in TAP medium, fixed for immunofluorescence (IF) staining with the indicated antibodies and imaged by structured illumination microscopy with the indicated laser

intensity and exposure time. Scale bar: 5 mm. No specific signal was detected in any of the tested conditions, thus supporting the specificity of the Flag IF signal observed for Mars1, shown in Figure 3C. (B) mars1-3:MARS1-A cells were grown in TAP medium, fixed for immunofluorescence (IF) staining with the indicated antibodies and imaged by structured illumination microscopy with the indicated laser intensity and exposure time. Scale bar: 5 mm. No specific signal was detected in the absence of the secondary antibody, thus supporting the specificity of the IF signal observed for AtpD, Histone H3 and Nab1 shown in Figure 3C.

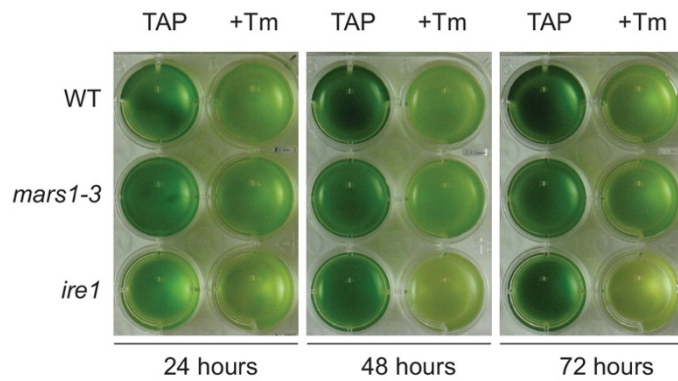
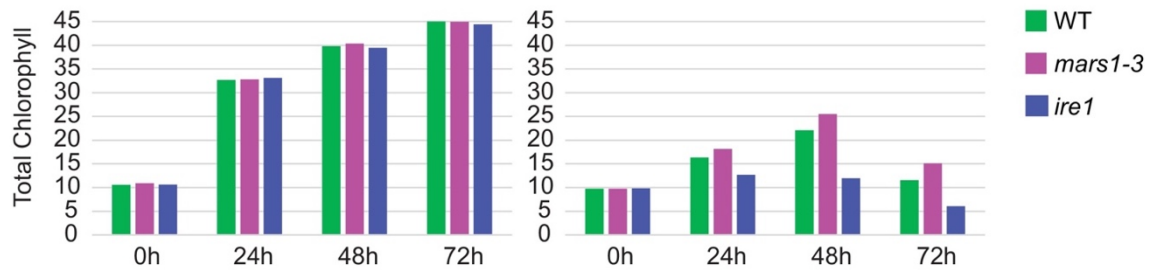
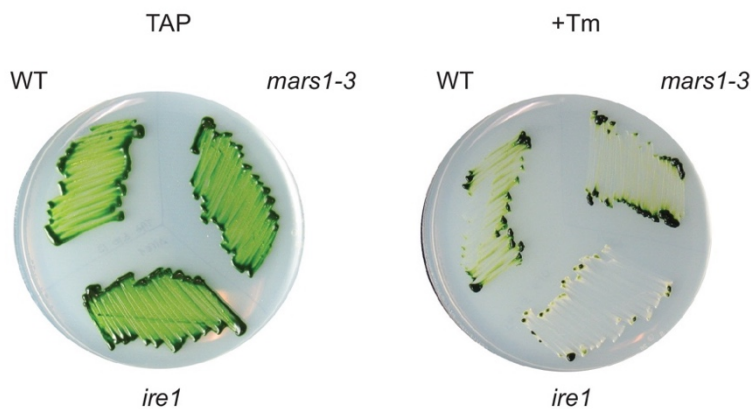
A**B****C**

Figure 1-4S1. Mars1 confers protection against photooxidative stress.

(A) Line charts of total chlorophyll concentrations measured from liquid TAP cultures of cell lines described in Figure 4A during high light treatment, at the indicated time points. (B) The following cell lines: cpUPR reporter (CrPW1), *mars1-1*, *mars1-2*, WT (WT CC-4533), *mars1-3* and *mars1-4* were replica plated in \pm 1.5 mM metronidazole (MZ) TAP agar. Photographs were taken after 9 days of growth in normal light. (C) Metronidazole assay with WT (CC-4533) and *mars1-3*. The cell lines were replica plated on TAP agar with or without 1.5 mM metronidazole (MZ), in the presence or absence of light (i.e.

photoheterotrophic or heterotrophic conditions). Photographs were taken after 7 days. (D) Metronidazole assay with cell lines shown in Figure 3—figure supplement 1E. The cell lines were replica plated on TAP agar with or without 1.5 mM metronidazole (MZ). Photographs were taken after 9 days of growth in normal light. The insertion of a 3x-Flag-tagged MARS1 transgene (MARS1-A) rescues the metronidazole-sensitivity of the *mars1-2* mutant. (E) Side-by-side comparison of metronidazole-sensitivity of *mars1:3* transformed with wild-type or kinase-dead versions of MARS1-A or MARS1-D transgenes. WT (CC-4533) and *mars1-3* are used as negative and positive controls, respectively. Both wild-type MARS1 transgenes can rescue the metronidazole-sensitivity of the *mars1-3* mutant, although at different levels. In both cases, the rescue is dependent on the kinase activity. Since the best rescue was observed with MARS1-D transgene, this cell line was chosen for the high light and metronidazole assays shown in Figure 4A–D. (F) Metronidazole assay with cell lines used in Figure 4A–D, using minimal media where cells can only grow if they are photosynthetic-competent (i.e. phototrophic conditions). In the absence of metronidazole, all cell lines grew equally well. However, in the presence of metronidazole, only WT cells (CC-4533) and *mars1-3* cell lines complemented with a MARS1-D transgene survived.

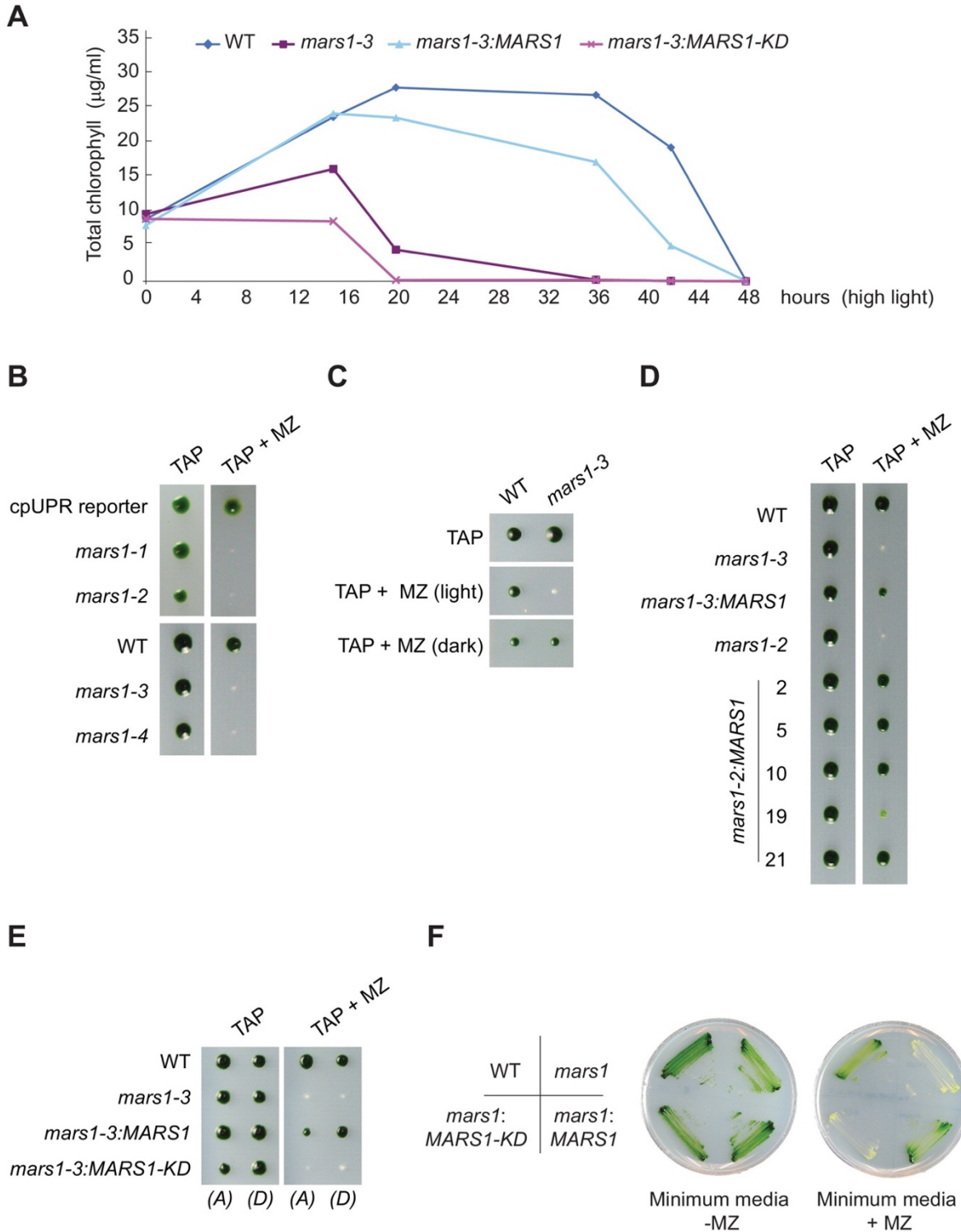


Figure 1-4S2. *mars1* cells can cope with ER stress.

(A) WT, *mars1-3* and *ire1* cells grown till log phase were harvested and resuspended to a final chlorophyll concentration of ~10 mg/ml in liquid TAP with or without 5 mg/ml of tunicamycin (Tm), a chemical ER stressor. Cultures were sampled at 24, 48 and 72 hr to take photographs and measure total

chlorophyll concentration. *ire1* cells were used as a positive control given the essential role of the Ire1 kinase in the activation of the erUPR (Yamaoka et al., 2018). (B) Histograms of total chlorophyll concentrations (mg/ ml) measured from TAP liquid cultures collected during the experiment described in Figure 4—figure supplement 2A. (C) WT, *mars1-3* and *ire1* cells were streaked on TAP agar plates with or without 0.2 mg/ml of tunicamycin. Photographs were taken after 5 days of growth in normal light.

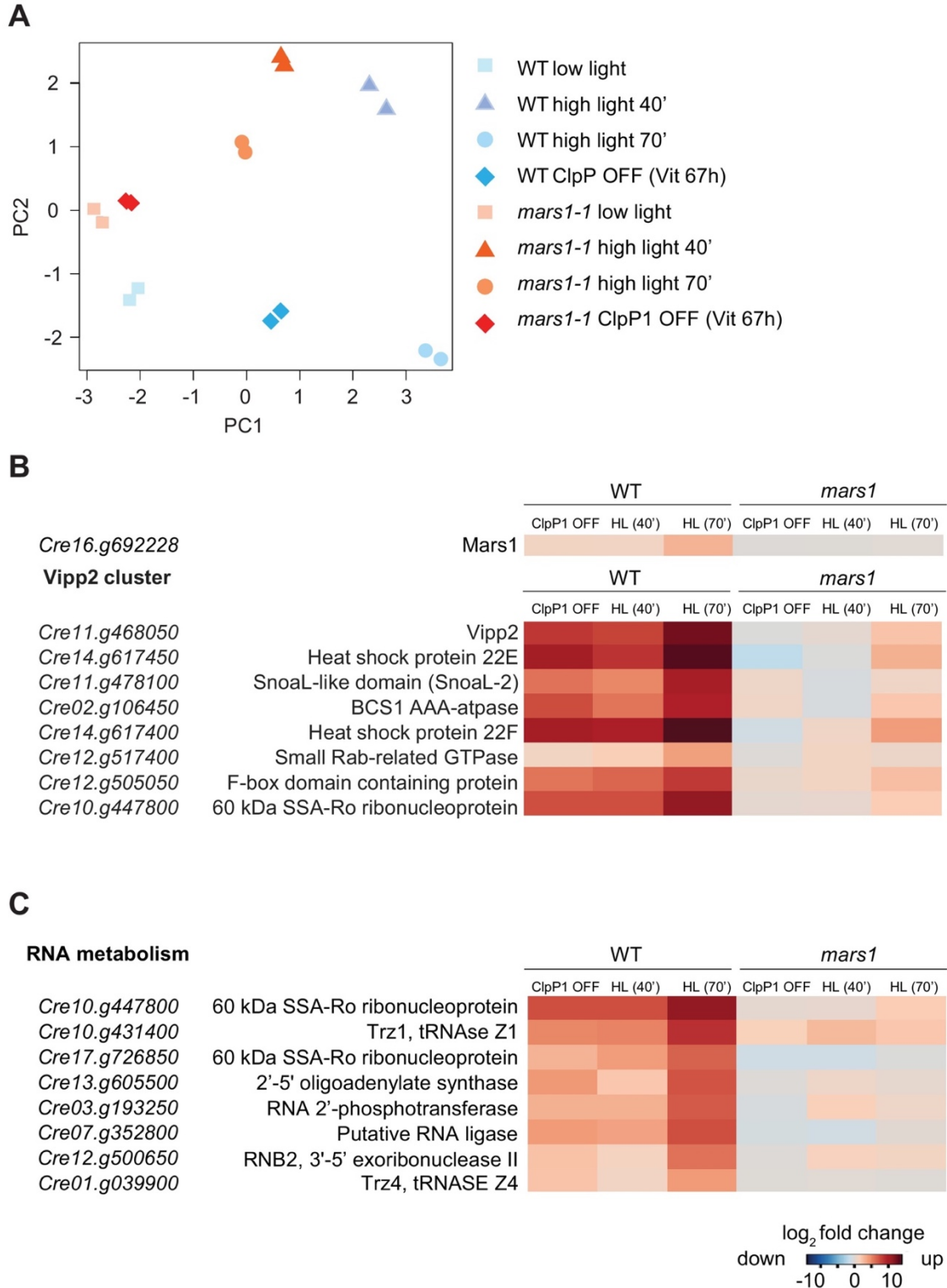


Figure 1-5S1. *mars1* cells do not induce the cpUPR transcriptional program.

(A) The multidimensional scaling plot illustrates the distance between RNA-seq samples, calculated as leading biological coefficient of variation between samples, based on the log₂-fold change of

top genes. WT, stressed and unstressed cells are more dispersed than those in the mars1-1 background, indicating that the MARS1 gene deletion affects both high light and ClpP1 repression responses. High light 40'=exposed to high light for 40 min; high light 70'=exposed to high light for 70 min; ClpP OFF = ClpP repression. PC1 = dimension 1; PC2 = dimension 2. (B) Heatmap comparing the VIPP2 cluster gene expression patterns in WT and mars1-1 upon HL exposure (40 and 70 min) and ClpP1 repression. MARS1 disruption abrogates the induction of almost every gene in the VIPP2 cluster. HL = high light; ClpP1 OFF = ClpP1 repression. (C) Heatmap comparing expression pattern of manually-selected genes involved in RNA metabolism in WT and mars1-1 upon HL exposure (40 and 70 min) and ClpP1 repression. MARS1 disruption impairs the induction of these genes. HL = high light.

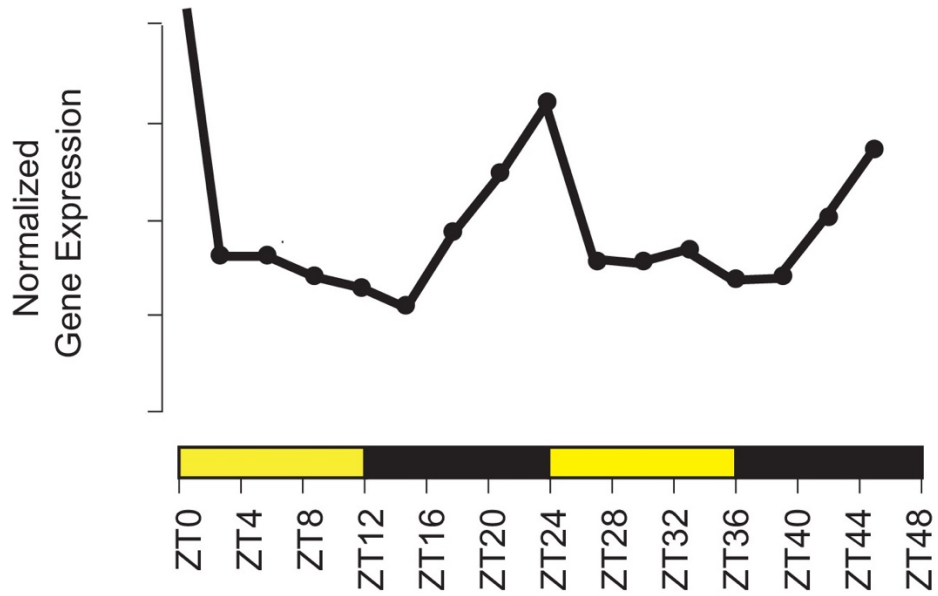
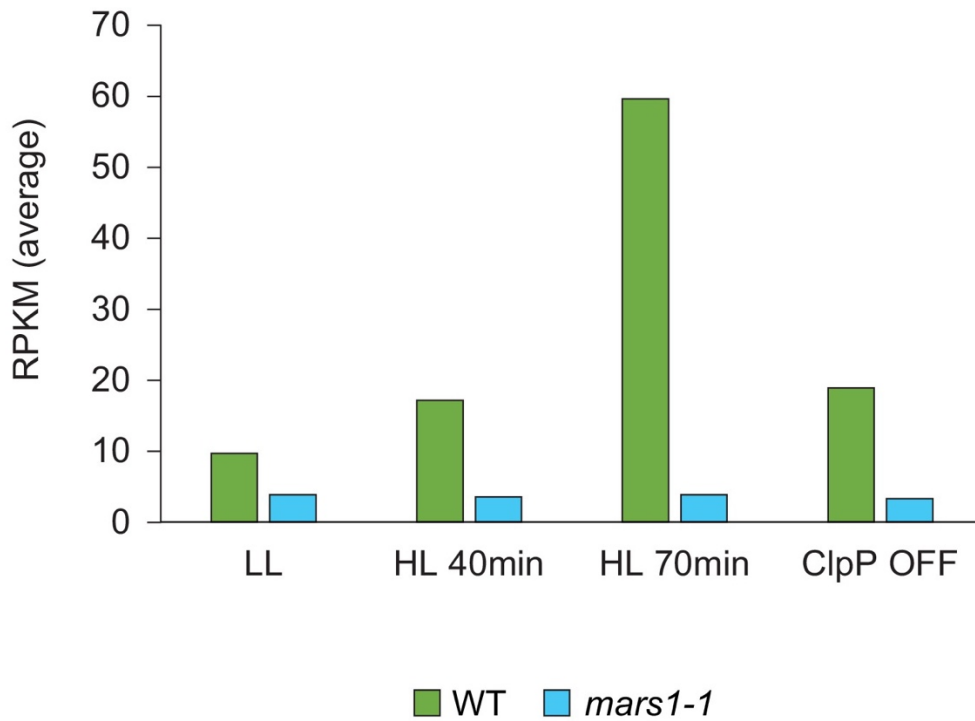
A**B**

Figure 1-5S2. MARS1 gene expression pattern.

(A) MARS1 mRNA expression profile according to CircadiaNET, a web-based developed tool integrating RNA-Seq data generated over 24 hr periods in neutral day conditions (12 hr light/12 hr dark)

from the eudicot *Arabidopsis thaliana* and the microalgae *Chlamydomonas reinhardtii* and *Ostreococcus tauri*. (<http://viridiplantae.ibvf.csic.es/circadiaNet/index.html>). MARS1 gene shows a circadian expression pattern (p-value of 1.53×10^{-11}) and clusters with a group of 1212 genes exhibiting their expression peaks at dawn and their expression troughs at night (http://viridiplantae.ibvf.csic.es/circadiaNet/clusters/cre/cre_trough_dark_peak_dark_light.html). (B) MARS1 mRNA expression level (average Reads Per Kilobase Million –RPKM-) in WT and *mars1-1* mutant subjected to high light treatment for 40 or 70 min or to ClpP1 down-regulation for 68 hr. (Raw values are available in Figure 5—figure supplement 2—source data 1 and Supplementary file 2).

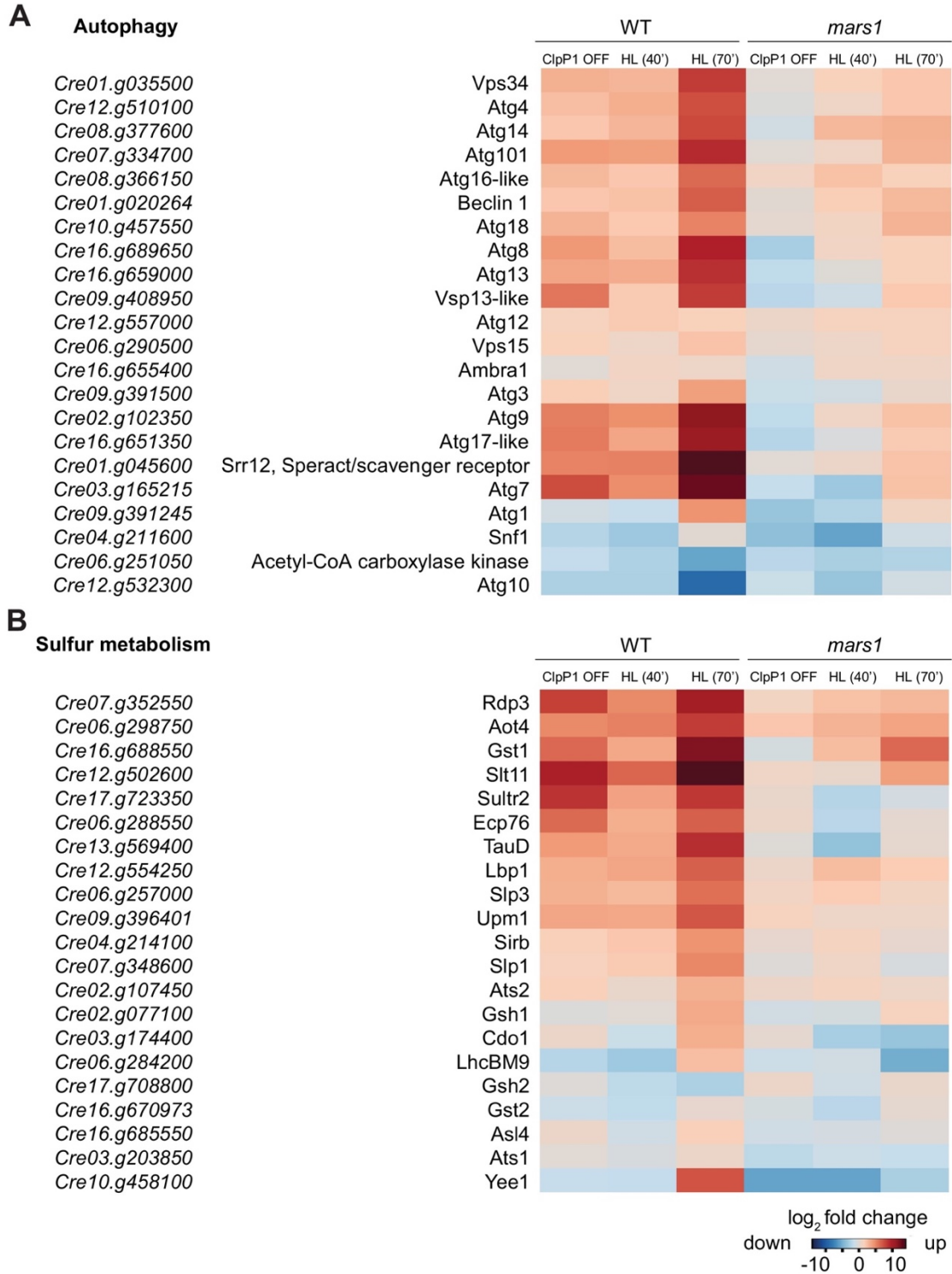


Figure 1-5S3. *mars1* cells do not activate autophagy and sulfur starvation genes during cpUPR inducing conditions.

(A) Heatmap comparing expression pattern of manually-selected genes involved autophagy in WT and *mars1-1* mutant upon HL exposure (40 and 70 min) and ClpP1 repression. MARS1 disruption impairs

the induction of a small subset of autophagy genes. HL = high light; ClpP1 OFF = ClpP1 repression. (B) Heatmap comparing expression pattern of manually-selected genes involved sulfur assimilation and metabolism in WT and mars1-1 mutant upon high light exposure (40 and 70 min) and ClpP1 repression. Surprisingly, both chloroplast stresses induce many of these genes and MARS1 disruption impairs induction of a subset of them. HL = high light; ClpP1 OFF = ClpP1 repression.

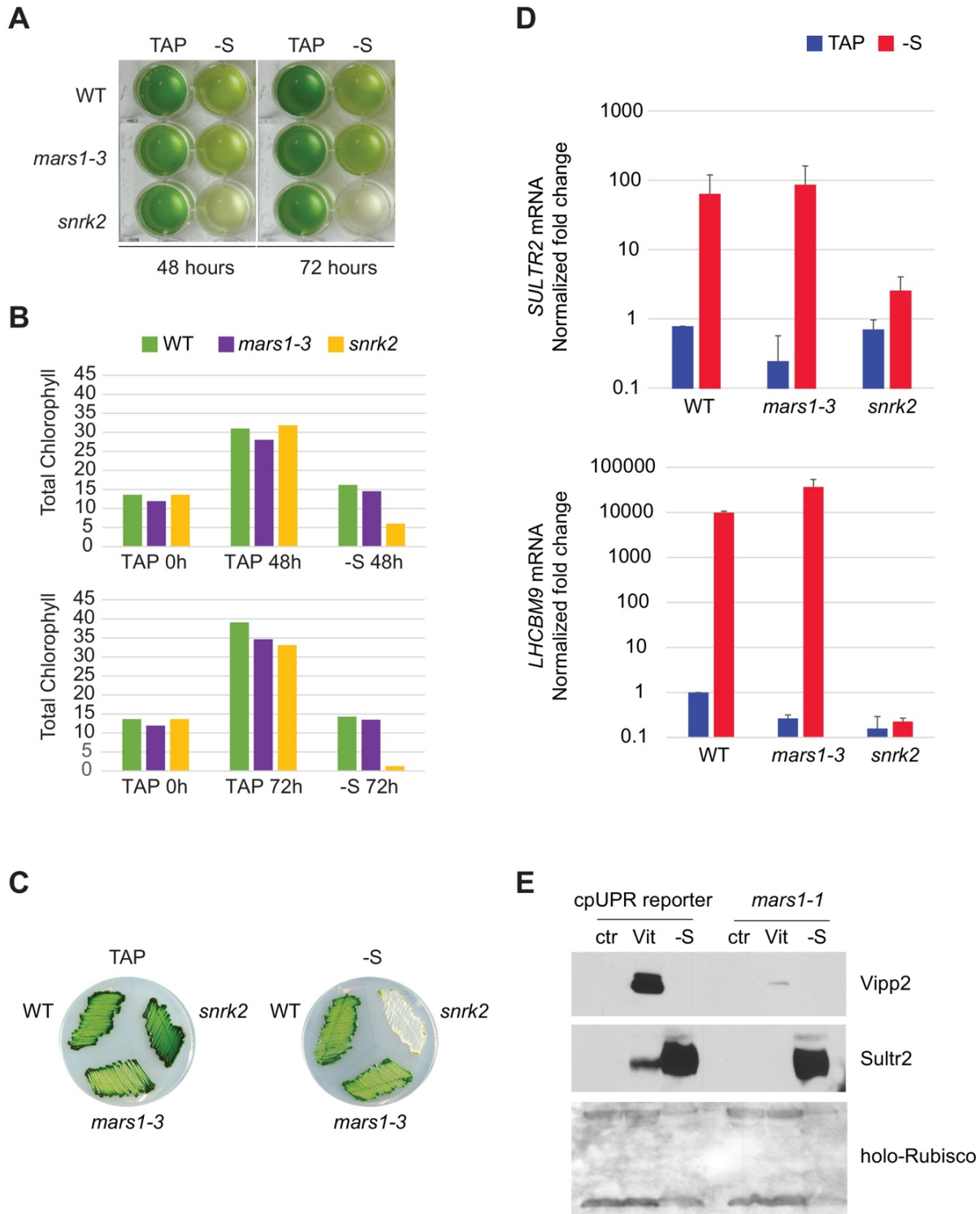


Figure 1-5S4. *mars1* cells activate sulfur starvation genes and survive in sulfur-limiting conditions.

(A) WT, *mars1-3* and *snrk2* cells grown till saturation were harvested, washed twice in sulfur-depleted TAP (-S) and resuspended in TAP or sulfur-depleted TAP to a final chlorophyll concentration of ~13 mg/ml. Cultures were sampled at 48 and 72 hr to take photographs and measure total chlorophyll

concentration. *snrk2* cells were used as a positive control given the essential role of the Snrk2/Stpk12 kinase in the activation of the sulfur starvation response (Gonzalez-Ballester et al., 2010; Gonzalez-Ballester et al., 2008). (B) Histograms of total chlorophyll concentrations (mg/ml) measured from TAP liquid cultures collected during the experiment described in Figure 5—figure supplement 4A. (C) WT, *mars1-3* and *snrk2* cells were streaked on TAP or sulfur-depleted TAP (-S) agar plates. Photographs were taken after 12 days of growth in normal light. (D) The same cell lines described in Figure 5—figure supplement 4A were subjected to quantitative PCR analysis and the level of expression of SULTR2 and LHCBM9 transcripts, encoding two sulfur starvation-responsive proteins (Gonzalez-Ballester et al., 2010; Pootakham et al., 2010), was measured after 24 hours of growth in TAP or sulfur-depleted TAP (-S). GBLP was chosen as reference gene during normalization. (E) Immunoblot analysis of samples prepared from the cpUPR reporter and *mars1* cells grown in ClpP1-permissive (ctr) and ClpP1-nonpermissive (Vit) conditions or subjected to sulfur starvation (-S) for 2 days using antibodies against Vipp2, Sultr2 and holo-Rubisco (as loading control).

Photosynthesis

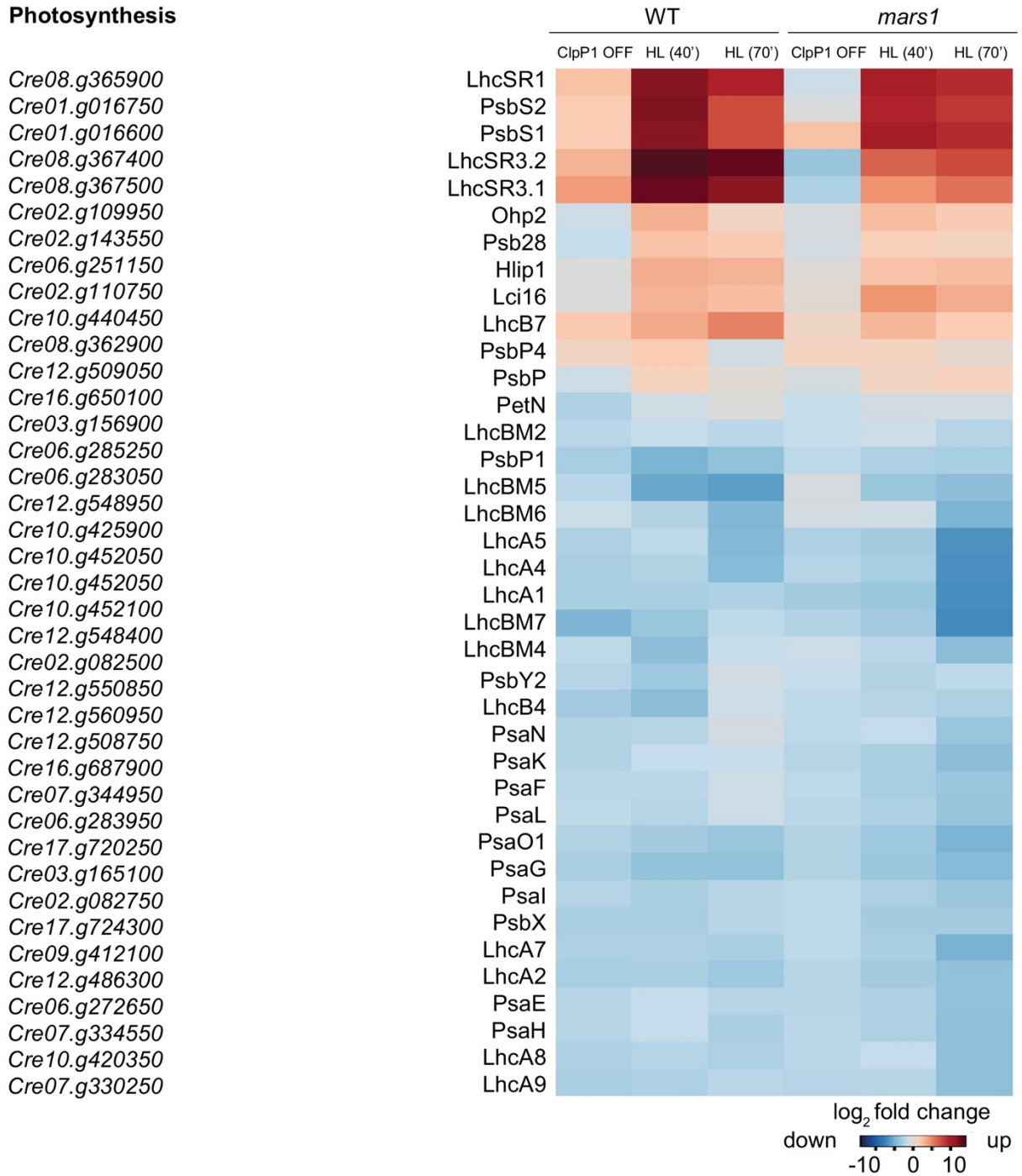


Figure 1-5S5. Regulation of photosynthesis-associated genes is not affected in *mars1* cells.

Heatmap comparing expression patterns of manually-selected genes involved in photosynthesis in WT and *mars1-1* mutant upon high light exposure (40 and 70 min) and ClpP1 repression. HL = high light; ClpP1 OFF = ClpP1 repression.

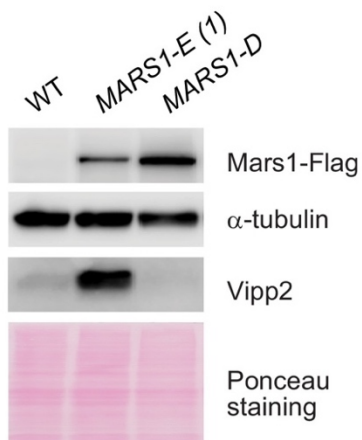
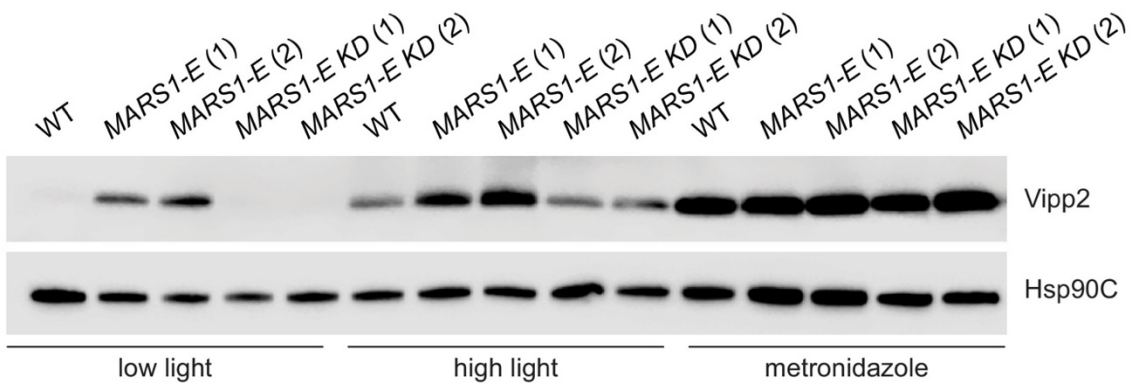
A**B**

Figure 1-6S1. The MARS1-E transgene causes mild induction of cpUPR signaling.

(A) Immunoblot analysis of samples prepared from WT cells (CC-4533) and WT cells expressing MARS1-E, MARS1-A or MARS1-D transgene, using antibodies against Flag for Mars1 detection, Vipp2, and α -tubulin for loading control. (B) Immunoblot analysis of samples prepared from cell lines shown in Figure 6B–C in basal conditions (low light), upon high light or metronidazole treatment, using antibodies against Vipp2 and Hsp90C for loading control.

Table 1-2: Strain Table

CrPW #	Cell Line Name	Short description	Reference
	CC-4533	parental cell lines used to generate <i>mars1-3</i> and <i>mars1-4</i>	<i>Li et al., 2016</i>
	CC-124	wild-type used for <i>mars1-1</i> and <i>mars1-2</i> genetic backcrosses	<i>(available at the Chlamydomonas Resource Center)</i>
	CC-125	wild-type used for <i>mars1-3</i> and <i>mars1-4</i> genetic backcrosses	<i>(available at the Chlamydomonas Resource Center)</i>
	A31	parental cell line of DCH16	<i>Ramundo et al., 2013</i>
	DCH16	ClpP1 repressible cell line	<i>Ramundo et al., 2013</i>
CrPW 1	A1N5	cpUPR reporter cell line	<i>(generated in this study)</i>

CrPW #	Cell Line Name	Short description	Reference
CrPW 2	ACT C6	YFP positive cell line	<i>(generated in this study)</i>
CrPW 3	DRB1	YFP positive cell line	<i>(generated in this study)</i>
CrPW 4	<i>mars1-1</i>	<i>Cre16.g692228</i> mutant allele	<i>(generated in this study)</i>
CrPW 5	<i>mars1-2</i>	<i>Cre16.g692228</i> mutant allele*-Full genotype described below	<i>(generated in this study)</i>
CrPW 6	<i>mars1-3</i>	<i>Cre16.g692228</i> mutant allele Clip ID: LMJ.RY0402.195536	<i>(available at the Chlamydomonas Resource Center)</i>
CrPW 7	<i>mars1-4</i>	<i>Cre16.g692228</i> mutant allele Clip ID: LMJ.RY0402.189144	<i>(available at the Chlamydomonas Resource Center)</i>

CrPW #	Cell Line Name	Short description	Reference
CrPW 8	E12	wild-type like progeny from backcross of <i>mars1-1</i> to CC124 (used for RNA-seq analysis)	<i>(generated in this study)</i>
CrPW 9	F2	<i>mars1</i> mutant progeny from backcross of <i>mars1-1</i> to CC124 (used for RNA-seq analysis)	<i>(generated in this study)</i>
CrPW 10	D2C4	wild-type like progeny from backcross of <i>mars1-2</i> to CC124 (used for complementation analysis)**	<i>(generated in this study)</i>
CrPW 11	D2C3	<i>mars1</i> mutant progeny from backcross of <i>mars1-2</i> to CC124 (used for complementation analysis)**	<i>(generated in this study)</i>
CrPW 12	M22	<i>mars1-3:MARSI-A</i> cell line	<i>(generated in this study)</i>
CrPW 13	NS1	<i>mars1-3:MARSI-B</i> cell line	<i>(generated in this study)</i>

CrPW #	Cell Line Name	Short description	Reference
CrPW 14	USM26	<i>mars1-3:MARS1-C</i> cell line	<i>(generated in this study)</i>
CrPW 15	FMW1 4	<i>mars1-3:MARS1-D</i> cell line	<i>(generated in this study)</i>
CrPW 16	KDM1 4	<i>mars1-3:MARS1-A KD</i> cell line	<i>(generated in this study)</i>
CrPW 17	FMD17	<i>mars1-3:MARS1-D KD</i> cell line	<i>(generated in this study)</i>
CrPW 18	189 N25	<i>mars1-1:MARS1-A</i> cell line	<i>(generated in this study)</i>
CrPW 19	FKD7	<i>mars1-1:MARS1-D</i> cell line	<i>(generated in this study)</i>
CrPW 20	pKP29 B30	<i>mars1-1:MARS1-D KD</i> cell line	<i>(generated in this study)</i>

CrPW #	Cell Line Name	Short description	Reference
CrPW 22	DCM2	<i>mars1-2:MARS1-A</i> cell line	<i>(generated in this study)</i>
CrPW 23	DCM5	<i>mars1-2:MARS1-A</i> cell line	<i>(generated in this study)</i>
CrPW 24	DCM1 0	<i>mars1-2:MARS1-A</i> cell line	<i>(generated in this study)</i>
CrPW 25	DCM1 9	<i>mars1-2:MARS1-A</i> cell line	<i>(generated in this study)</i>
CrPW 26	DCM2 1	<i>mars1-2:MARS1-A</i> cell line	<i>(generated in this study)</i>
CrPW 27	W153	CC-4533 transformed with <i>MARS1-E</i> transgene, cell line (a)	<i>(generated in this study)</i>
CrPW 28	W155	CC-4533 transformed with <i>MARS1-E</i> transgene, cell line (b)	<i>(generated in this study)</i>

CrPW #	Cell Line Name	Short description	Reference
CrPW 29	WKD4	CC-4533 transformed with <i>MARS1-E KD</i> transgene, cell line (a)	<i>(generated in this study)</i>
CrPW 30	WKD1 6	CC-4533 transformed with <i>MARS1-E KD</i> transgene, cell line (a)	<i>(generated in this study)</i>
CrPW 31	WFM2	CC-4533 transformed with <i>MARS1-D</i> transgene, cell line (a)	<i>(generated in this study)</i>
CrPW 43	$\Delta ire1$	<i>Cre08.g371052</i> mutant allele Clip ID: LMJ.RY0402.122895	<i>(available at the Chlamydomonas Resource Center)</i>
CrPW 44	$\Delta snrk2$	<i>Cre02.g075850</i> mutant allele Clip ID: LMJ.RY0402.187019	<i>(available at the Chlamydomonas Resource Center)</i>

**mars1-2* has a total of three mapped genomic disruptions.

1. The chromosome 16 deletion which encompasses *Cre16.g692228* (*MARS1*), *Cre16.g692340*, and *Cre16.g692452*.

2. The full Paromomycin cassette was found in an intergenic region on chromosome 7, 958bp downstream of gene Cre07.g336300. A portion of a gene- Cre02.g108450 (5'UTR-intron 4) was found directly upstream of this Paromomycin cassette (in intergenic region of Chromosome 7).
3. The locus for the Cre02.g108450 gene itself has a deletion spanning the 5'UTR-intron 4.

**D2C3 and D2C4 were offspring isolated upon backcrossing *marsI-2* to CC-124 three times. D2C4 contains the *W.T MARS1* gene and D2C3 contains the *MARS1* deletion. In both strains all other markers (Hygromycin, Paromomycin, and Spectinomycin) as well as the abovementioned Cre02.g108450 deletion were crossed out.

Table 1-3: Plasmids table

Plasmid Name (nickname / official name)	Purpose	Reference
pLM005	for amplification of the <i>YFP</i> coding sequence	<i>Mackinder et al., 2016</i>
pHyg3	for amplification of the <i>RBCS2</i> 3'UTR sequence and cloning of the Hygromycin resistance cassette	<i>Berthold et al., 2002</i>
pMJ016c	for insertional mutagenesis	<i>Li et al., 2016</i>
pRAM118 / pPW3216	for gene tagging and subcloning	<i>Li et al., 2019</i>
pRAM103.5 / pPW3217	For generation of the cpUPR reporter cell line	<i>(generated during this study)</i>
pRAM185.2 / pPW3218	For <i>MARSI</i> cloning (untagged <i>MARSI</i> transgene)	<i>(generated during this study)</i>
pRAM189 M2 / pPW3219	For <i>MARSI</i> cloning (<i>MARSI-A</i> transgene)	<i>(generated during this study)</i>
pRAM199.5 / pPW3220	For <i>MARSI</i> cloning (<i>MARSI-B</i> transgene)	<i>(generated during this study)</i>
pRAM200.4/ pPW3221	For <i>MARSI</i> cloning (<i>MARSI-C</i> transgene)	<i>(generated during this study)</i>

Plasmid Name (nickname / official name)	Purpose	Reference
pKP29/ pPW3222	For <i>MARSI</i> cloning (<i>MARSI-D</i> transgene)	<i>(generated during this study)</i>
pRAM184.1/ pPW3223	For <i>MARSI</i> cloning (<i>MARSI-E</i> transgene)	<i>(generated during this study)</i>
pHT20.1/ pPW3224	For <i>MARSI</i> cloning (catalytically-dead <i>MARSI-A</i> transgene)	<i>(generated during this study)</i>
pKP30 / pPW3225	For <i>MARSI</i> cloning (catalytically-dead <i>MARSI-D</i> transgene)	<i>(generated during this study)</i>
pHT6 / pPW3226	For <i>MARSI</i> cloning (catalytically-dead <i>MARSI-E</i> transgene)	<i>(generated during this study)</i>

Table 1-4: Primers table

Primer Name	5'--> 3' sequence
oMJ598	b-CAGGCCATGTGAGAGTTTGC (b = biotynilated)
oMJ619	/5Phos/ AGATCGGAAGAGCGTCGTGTAGGGAAAGAGTGTAGATCTCG GTGGTCGCCGTATCATTACTCAGTAGTTGTGCGATGGATTGA TG/3ddc/ (/5Phos/=phosphorylated; /3ddc/=dideoxycytidine (to prevent self-ligation)
oMJ621	AATGATACGGCGACCACCGAGATCTACACTCTTCCCTACAC GACGCTCTTCCGATCT
oMJ1234	b-GCAGCCAAACCAGGATGATG (b= biotynilated)
oMJ1239	aattaaccctcactaaagCAATCATGTCAAGCCTCAGC
T3_3'_oMJ016c 11/23	aattaaccctcactaaagGGTCGAGCCTTCTGGCAGA
T3_5'_oMJ016c 11/24	aattaaccctcactaaaggGCGGAGACGTGTTTCTGAC
SR502	tgctcacatACTAGTGAGCACGCTGCGA
SR503	gctcactagtATGGTGAGCAAGGGCGAG
SR504	gggatcctaagatctTACTTGTCGTCATCGTCCTT
SR505	cgacaagtaaagatctTAAGGATCCCCGCTCCGTG
SR506	gcgcaagaaagaagcttgatatcCGCTTCAAATACGCCAGC

Primer Name	5'--> 3' sequence
SR510	atgtggcggccgcTGGAAAAGCGTTTCGGAAGG
SR773	CGCCTTTAAAGCTGAAGTGG
SR789	CAGCTGCGTCTCCGTTTGC
SR793	CCTTCACCATTTAAGACGGAGCAGTAAACAGTTGCTG
SR797	CTGCTCCGTCTTAAATGGTG
SR818	CGGCATGCCGCTACCCGC
SR819	GGGTAGCGGCATGCCGCC
SR828	tttgctcacatgtggcggccgcCAGCCCTGTACACCAGCTC
SR829	gcgcaagaaagaagcttgatATCTCGGCGCCAGGTTTAC
SR834	ccatatcgaaggtcgtcatatgATGGCAATCGCAGACGCTG
SR835	gctttgtagcagccgatctcaGCCGAGGACGGTCATCAG
SR836	GACGTCATCCACTGCCTGTG
SR837	CGACGCATCCTCAACACACC
SR851	TGTGCGCCTTCAATTTGAGC

Primer Name	5'--> 3' sequence
SR852	GCTCAAATTGAAGGCGCACA
SR853	TAGCCCTTCGTTACCATCGTC
HT7	GCAAACGGAGACGCAGCTG
KP235	CTCCATCACAATTGCCTGCA
KP337	GTGTGGTCGGGCCGTCTAGAA
KP342	TGGTCCGCCGGAACAGATCTTCC
KP344	CTTGTCGTCATCGTCCTTGTAGTCGATGTCGTGATCCTTATAG TCACCGTCATGGTCCTTGTAGTCCATGCCGCTACCCGCCCA
KP345	GGACGATGACGACAAGGGCAGCAGCCCGCCCAGCCCTTGTA GCAGCAG
KP346	GTCAGCCCTGTTCTGCCC
KP347	AACCCTAAACCCGCTGG
qRT_SULTR2_Fw	ACGTGGCATGCAGCTCAT
qRT_SULTR2_Rv	CTTGCCACTTTGCCAGGT
qRT_LHCBM9_Fw	TGGTGGTGCTTTCCTTCAGAC
qRT_LHCBM9_Rv	TGGACACAACACTGCAGGCTTTGC

Primer Name	5'--> 3' sequence
qRT_HSP22F_Fw	TGCGCACGCGACATTATCAAAG
qRT_HSP22F_Rv	GTACAAACCAGCATGCGCTCAG
qRT_VIPP2_Fw	CATCATGCATTTGGCAGGCTCTC
qRT_VIPP2_Rv	AATGAGAGGTGCGACGACCAAC
qRT_SNOAL_Fw	TGCTGTGGGCAACTGTGCATAC
qRT_SNOAL_Rv	TCCGTGCTTGACGCTACCATTC
qRT_LHCSR3.1_Fw	CACAACACCTTGATGCGAGATG
qRT_LHCSR3.1_Rv	CCGTGTCTTGTCAGTCCCTG
qRT_PSBS1_Fw	TAAACCGTGTATTGGA ACTCCG
qRT_PSBS1_Rv	CTCTGCACGCGGCGTGTT
qRT_CPLD29_Fw	AACCGGGTCTTCTTCGCCTTTG
qRT_CPLD29_Rv	GTGTGCCCGCCATTCCAAAGAAC
qRT_GBLP_Fw	CAAGTACACCATTGGCGAGC
qRT_GBLP_Rv	CTTGCAGTTGGTCAGGTTCC

CHAPTER 2

**Late stages of flagellar assembly require the TOG-domain array protein,
Crescerin/SHF1**

**Late stages of flagellar assembly require the TOG-domain array protein,
Crescerin/SHF1.**

Karina Perlaza,¹ Mariya Mirvis,¹ Hiroaki Ishikawa,¹ Wallace Marshall¹

¹Department of Biochemistry and Biophysics, University of California, San Francisco, San Francisco, CA 94158

ABSTRACT

Organelles represent dynamic entities within the cell that change shape depending on fluctuations in cellular conditions, environmental cues, and cell stage. Models for how length control is established has been driven by studies in the flagella of the model organism, *Chlamydomonas reinhardtii*. The intraflagellar transport (IFT) system manages the delivery and removal of axonemal subunits at the tip of the flagella. Since the quantity of IFT particles does not change with length, the rate of arrival of particles and cargo at the tip decreases during the assembly process. One of these cargoes, tubulin, is the major axonemal subunit, and its frequency of arrival at the tip of the flagella has recently become implicated in size control models. Even though the interplay between the pool of available tubulin in the cell body and the ongoing synthesis of the microtubule polymers at the tip of the flagella is known to play a role in length control, the active process of tubulin regulation at the tip is still poorly understood. We used a genetic approach to discover a loss-of-function mutation in a gene that leads to shortened flagella. This gene, which encodes a *Chlamydomonas* ortholog of Crescerin, corresponds to the short flagella gene SHF1. Crescerin/SHF1 has been identified as a cilia-specific TOG-domain array protein that can bind tubulin via its TOG domains and increase tubulin polymerization rates. In this mutant, we found that flagellar regeneration occurs with the same initial kinetics as wild-type cells, but plateaus at a shorter length. This finding led us to propose two models, model A describes Crescerin/SHF1 as a microtubule polymerase at the flagellar tip, whereas Model B focuses on Crescerin/SHF1 binding tubulin dimers in the cytoplasm and transporting them into the flagellum. Using a computational model in which the flagellar microtubules are represented by a differential equation for flagellar length combined with a stochastic model for cytoplasmic microtubule dynamics, we found that our experimental results best align with Model B. We place this finding in the larger context of

tubulin dynamics by suggesting that this TOG-domain array protein is necessary to efficiently and preemptively increase tubulin levels to offset decreasing IFT cargo at the tip as flagellar assembly progresses.

INTRODUCTION

The complex structure of a eukaryotic cell can be broken down into a collection of distinct organelles, such that the question of cell architecture is reduced to the question of organelle size, shape, number, and position. Varying signaling molecules or cellular conditions stimulates changes in organelle size that are characterized by high levels of dynamicity and organization (Chan and Marshall 2012). The mechanisms by which organellar morphologies are maintained or transformed remain largely unknown. Tracking changes in organelle size is typically complicated by inherently complex three-dimensional structures, but the cilium or flagellum (used interchangeably) eases this technical barrier because the only parameter that varies is its length. By reducing the complexity to one-dimension, it is easier to measure and model the dynamics of this protruding organelle (K. A. Wemmer and Marshall 2007).

Eukaryotic flagella are appendages that extend from the surface of the cell. The flagellar membrane is continuous with the membrane of the cell, but it is kept compartmentalized from the cytosol through the transition zone, a segment near the base of the flagella that acts as a protein diffusion barrier which only allows a subset of cellular proteins to enter the flagellum (Czarnecki and Shah 2012). Since there are no ribosomes in the flagella (Rosenbaum and Child 1967), all flagellar structures must be assembled from precursor proteins synthesized in the cell body. Approximately 4-5% of the nuclear-encoded proteins made in the cell body are imported into the flagella (Gregory J. Pazour et al. 2005). Flagellar assembly is accomplished through addition of subunits at the distal tip (Rosenbaum and Child 1967; Witman 1975; Johnson and Rosenbaum 1992). Because the axoneme, the core scaffold of the flagellum, is composed of nine doublet microtubules arranged in radial symmetry, tubulin subunits are critical for the assembly process. Flagellar length is determined by competing processes of assembly and disassembly both

occurring at the flagellar distal tip (Johnson and Rosenbaum 1992; W. F. Marshall and Rosenbaum 2001; Song and Dentler 2001). Assembly and disassembly rates are driven by the arrival of proteins to the tip and base of the flagella. The system dedicated to this bi-directional movement is known as intraflagellar transport (IFT), which is responsible for moving select proteins along the axonemal microtubules via molecular motors (Kozminski et al. 1993) (Kozminski *et al.*, 1993; Taschner *et al.*, 2016). Tubulin is transported by the IFT system mediated by specific binding sites for tubulins on specific IFT proteins (Bhogaraju, Engel, and Lorentzen 2013; Bhogaraju et al. 2014; Taschner et al. 2016; Kubo et al. 2016), and tubulin can be visualized undergoing active IFT towards the assembly site at the tip (Hao et al. 2011; Craft et al. 2015).

Characterization of IFT dynamics led to the simple “balance point” model which describes how steady-state flagellar length is set by a balance between assembly and disassembly rates (Wallace F. Marshall et al. 2005). The disassembly rate has been found to be length-independent whereas the assembly rate decreases as the flagella increase in length. IFT plays a major role in maintaining flagellar length since it balances the ongoing disassembly of the outer doublet microtubules by providing a constant supply of fresh subunits at the distal end, and reduction of IFT using temperature sensitive mutants leads to reduction in steady-state flagellar length (W. F. Marshall and Rosenbaum 2001; Wallace F. Marshall et al. 2005; Engel et al. 2012). Another model derived for flagellar length control is based on differential cargo-loading by IFT. In this model, regulation of the cargo size transported by IFT particles is a decreasing function of length (Wren et al. 2013) such that the cargo-carrying capacity is low in steady-state flagella and high during growth of new flagella.

The crux of these and most flagellar size control models is centered primarily around IFT dynamics, however, other work has pointed to regulation of the cytoplasmic precursor pool as an

additional parameter that is crucial for proper size control (Rosenbaum, Moulder, and Ringo 1969; Lefebvre et al. 1978; Jarvik et al. 1984). The limiting protein component of the precursor pool has been assumed to be tubulin, and this assumption has been confirmed by experiments showing that competition between flagella and cytoplasmic microtubules for a fixed pool of tubulin affects flagellar length. During flagellar regeneration, cytoplasmic microtubules undergo transient shortening, indicating that tubulin is depleted and used for building the flagellum (L. Wang et al. 2013). Loss-of- function in either Kinesin 13, a microtubule depolymerizer located in the cell body (Piao et al. 2009; L. Wang et al. 2013), or katanin, a cytoplasmic microtubule-severing protein (Qasim Rasi et al. 2009; Kannegaard et al. 2014), both lead to shorter flagellar length. These mutant phenotypes can be explained if these microtubule disassembly factors normally act to shift cytosolic microtubule dynamics during flagellar formation so as to favor a more readily available tubulin pool. When these genes are mutated, cytoplasmic microtubules are more stable, and flagella become shorter because they cannot access the cytoplasmic tubulin pool.

Much of what we know about flagellar length, assembly, and precursor pools, has come about through use of the model organism, *Chlamydomonas reinhardtii*. This green unicellular alga has two flagella of equal lengths (10-12 μm) that can easily be detached through pH shock, after which the flagella regenerates back to its normal length . *Chlamydomonas* can be grown as a haploid or diploid and has genetics similar to budding yeast, including tetrad analysis. The ability to easily perform forward genetic screens in *Chlamydomonas* has led to the discovery of many mutants with abnormal flagellar lengths. Length-altering phenotypes in *Chlamydomonas* include such diverse phenotypes such as short-flagella (shf), long-flagella (Lf) and unequal-length flagella (Ulf) (McVittie 1972; Jarvik et al. 1984; Barsel, Wexler, and Lefebvre 1988; Asleson and Lefebvre 1998; Tam, Dentler, and Lefebvre 2003). Although the genes affected in some of these mutants

have been identified and characterized, usually by taking advantage of insertional mutagenesis strategies, in many cases the underlying genetic alleles remain unidentified due to the fact that the mutation was not tagged with an insertion. Identified length altering genes described so far include components of the IFT system (G. J. Pazour, Wilkerson, and Witman 1998; Iomini et al. 2001; Matsuura et al. 2002; Dutcher et al. 2012; Lucker et al. 2010; Lin et al. 2013), kinases that act to regulate IFT (Berman et al. 2003; Tam, Dentler, and Lefebvre 2003; Tam, Wilson, and Lefebvre 2007; Ludington et al. 2013; Tam, Ranum, and Lefebvre 2013; K. Wemmer, Ludington, and Marshall 2020), and microtubule regulators localized in the cytoplasm (Piao et al. 2009; Qasim Rasi et al. 2009; L. Wang et al. 2013; Kannegaard et al. 2014). Until now, factors directly involved in the incorporation of tubulin into the growing flagellum itself have not been reported among existing length-altering mutants of *C. reinhardtii*. As a result, models for flagellar length have generally not included specific representation of active modulators of tubulin dynamics. Here, we use a genetic approach to show that a TOG-domain array protein of the Crescerin family is required to achieve proper flagellar length and we propose that it does so by allowing flagella to continue growth by preemptively increasing tubulin levels at the tip earlier in flagellar regeneration.

RESULTS

During the course of screening mutants obtained from the Chlamydomonas Library Project (CLiP) (X. Li et al. 2019), we found a mutant strain with shorter flagella than wild-type (W.T) cells, that we provisionally refer to as *shf-A* (Figure 1A). Flagella in these mutant cells were on average about 4 μm shorter than W.T cells (Figure 1B), but were not paralyzed since they were capable of swimming. We decided to uncover the genetic lesion leading to the short-flagellar (*shf*) phenotype. After backcrossing the original mutant to W.T, we learned that the mutation was due to a single Mendelian mutation based on the 2:2 segregation pattern of the *shf* phenotype, however, it was not due to a Paromomycin insertion of which there was only one full cassette (2:2 Paromomycin resistance). Given that insertional mutagenesis often leads to multiple and diverse types of genetic disruptions, ranging from large insertions, deletions, SNP's, and global genomic rearrangements (X. Li et al. 2016), we took an unbiased approach to discovering the genetic mutation in question (Figure 1C). One of the short-flagella progeny from the first cross was used to cross once more to W.T. After the second cross, tetrads were analyzed and separated into two pools, one containing DNA of 20 *shf* phenotype-exhibiting spores and one containing DNA of 20 W.T phenotype-exhibiting spores. This approach was used to randomize mutations specific to each background (W.T vs mutant) and enrich for the mutant allele of interest causing the *shf* phenotype. Using a modified bioinformatics workflow similar to Schierenbeck *et al.* (2015) (Figure 1D), we arrived at two filtered lists by variant calling algorithms, Pindel (structural variants- e. g. large deletions, insertions, inversions) and GATK (SNPS and Indels). Of the final filtered lists derived from each software, one variant, a 5 base pair (bp) deletion in Exon 8 of gene Cre06.g278219, was found in both lists (Figure 1E). PCR of this region followed by Sanger sequencing confirmed the existence of the 5 bp deletion in *shf-A*. The *shf* phenotype most likely results from a loss-of-

function mutation since a 5 bp deletion would lead to an early stop codon. To increase our confidence that this was our causative allele of interest, we obtained an additional mutant from the CLiP with a Paromomycin resistance cassette insertion in the exact location where the 5 base-pair deletion started (Figure 1E). This mutant, *shf-B*, phenocopied the short-flagella of our original mutant (Supplementary Figure 1A and 1B), *shf-A*, thus increasing our confidence that this gene, Cre06.g278219, is crucial in maintaining flagella length control.

The mutated gene, Cre06.g278219, designated as sensory, structural and assembly 6 (SSA6) in the *C.reinhardtii* genome database (Merchant et al. 2007) is a homolog of the Crescerin1/CHE-12 gene. CHE-12 was first characterized in *Caenorhabditis elegans*, when it was observed that *che-12* worms exhibited abnormal *chemotaxis* in response to sodium chloride (Bacaj, Lu, and Shaham 2008). Furthermore, *che-12* mutants had cilia formation impairment in a subset of sensory neurons. This gene was later brought into a greater contextual frame when the human homolog, TOGARAM1 (renamed Crescerin for the Latin *creocere*- grow), was found to belong to a large family conserved across ciliated eukaryotes (Das et al. 2015). TOGARAM1 was classified as a TOG (tumor overexpressed gene) domain array-containing protein that regulates cilia microtubule structure. Recently, TOGARAM1 variants were shown to cause Joubert syndrome, a recessive neurodevelopmental ciliopathy (Latour et al. 2020; Morbidoni et al. 2020). TOG domains have been shown to promote microtubule polymerization (Fox et al. 2014; Brouhard et al. 2008; Das et al. 2015; Byrnes and Slep 2017), raising the possibility that the *shf-A* mutant phenotype might reflect the dynamic role of microtubule growth in flagellar length control.

To examine the potential function of Crescerin in flagellar length regulation, we analyzed Crescerin protein domain structure and evolutionary conservation via phylogenetic analysis and sequence alignment. Our analysis on the Crescerin1 and Crescerin2 subfamilies revealed that

Crescerin2 is specific to vertebrates whereas Crescerin1 exists in both ciliated vertebrates and invertebrates (Figure 2A). Interestingly our BLAST searches revealed no clear Crescerin1 homolog in plants, including non-vascular plants such as liverworts, hornworts and mosses closest to ancestral green alga, suggesting that the sperm flagella in Bryophytes do not require Crescerin1 for proper functioning. Sequence alignments and structural predictions of homologs in other organisms indicate that the minimal unit of the Crescerin1 sub-family consists of TOG2, a flexible central linker and TOG3. *C.reinhardtii* Crescerin1 homolog contains a TOG2 domain at the N-terminus followed by a central linker and TOG3 and TOG4 at the C-terminal end. The Crescerin2 subfamily which is exclusive to vertebrates only contains TOG3 and TOG4-like domains. Given that the crystal structure of the Crescerin1 TOG2 domain has been solved and it is the most well characterized, we compared the *C.reinhardtii* TOG2 domain to the *M.musculus* (mouse) TOG2 domain (Figure 2B). TOG domains contain six conserved HEAT (Huntington, elongation factor 2, phosphatase A2, TOR PI-3 kinase) that are adjacently aligned (Al-Bassam et al. 2007; Slep and Vale 2007). Each HEAT repeat is composed of two alpha helices connected by a loop. These intra-HEAT loops comprise the most conserved surface of the domain, and are most similar in composition and structure to the tubulin-binding intra-HEAT loops found in ch-TOG and CLASP protein family TOG domain structures (Al-Bassam and Chang 2011; Das et al. 2015). The *C.reinhardtii* TOG2 domain contained all these features including a beta-sheet hairpin, that is thought to promote domain stability, specific to TOG domains belonging to the Crescerin family (Figure 2B). In addition, the *C.reinhardtii* TOG2 domain contains conserved residues at amino acid positions for which mutation variants that lead to ciliopathies, such as JBS, have been identified (Figure 2B). These similarities reaffirm that the gene mutated in the *shf-A* strain is a bona fide Crescerin1 homolog. The facts that *C.reinhardtii* only has one Crescerin1 homolog

(compared to protists that contain multiple copies), and does not contain Crescerin2 (vertebrate-specific), creates an opportunity for studying the role of Crescerin1 in flagellar regeneration and length control .

To verify whether this genetic mutation was actually causing the *shf* phenotype, we began our complementation efforts by generating an SHF-A transgene. This transgene included the endogenous promoter, 5'UTR and 3'UTR, with a 3x-FLAG epitope tag positioned after aspartic acid 1169 to permit confirmation of transgene expression (Figure 3A). In an effort to minimize the impact of potential disruption to the secondary structure of the protein when introducing these epitopes, we introduced these epitopes with the following criteria 1. The region is predicted to be in an unstructured, disordered region between TOG3 and TOG4 and, 2. The regions flanking the epitope contain intrinsic flexible linkers (GGS or GGA) (Chen, Zaro, and Shen 2013). When *shf-B* mutants were transformed with this transgene, cells expressing the FLAG epitope, detected through immunoblots (Figure 3B), were found to rescue the flagellar length phenotype (Figure 3, C and D), thereby confirming that the Crescerin gene mutation was indeed responsible for the *shf* phenotype.

We noticed that the Crescerin gene that we identified was in the same region of the genetic map (Figure 4A) as a previously described gene, SHF1, mutations in which also cause a short flagella phenotype (Jarvik et al. 1984). *shf-1* had several curious features: its length distributions resembled those of W.T except that the means were only about half the means of W.T, its flagellar motility appeared normal and they displayed normal phototaxis. Jarvik and co-workers noted that in contrast to *shf-1*, other mutants that had been previously isolated and characterized to have *shf* phenotypes, also had paralyzed flagella. In addition to the thorough physiological characterization of *shf-1*, they also mapped the responsible gene to chromosome VI, approximately 5 map units

from the centromere. The SHF1 gene was not, however, cloned and its identity has remained unknown. We therefore hypothesized that SHF1, which was the first short flagella gene to be reported, was in fact the gene encoding Crescerin1. To test this, we ordered *shf-1-253*, *shf-1-277* and *shf-1-236* from the Chlamydomonas Resource Project and confirmed that they still had the *shf* phenotype (Supplementary Figure 2A). We performed one pooled whole-genome-sequencing experiment whereby a single library was created that contained different ratios of each genome: 65% *shf-1-277*, 30% *shf-1-253* and 5% *shf-1-236*. This was a biased approach since we planned to align all reads only to Cre06.g278219 and analyze the allele frequencies. Our results showed that chromosome 6, position 4,096,355 contained a T-A transversion at 74% frequency and chromosome 6, position 4,096,059 contained a base pair deletion that accounted for 28% of the aligned reads, both variants residing in Exon 10 of Cre06.g278219 and both leading directly or indirectly (frameshift mutation leading to an early stop codon), respectively, to a nonsense mutation (Figure 4B). We infer that the short flagella phenotype in *shf-1-277* is due to the T-A nonsense mutation, and in *shf-1-253* it is due to the single base deletion, since the approximate input of each genome in the sequenced pool, 65% and 30%, roughly parallels the observed allele frequency, 74% and 28%, respectively. The discrepancy in the ratios is due to the sensitivity and accuracy of the DNA concentration readings and possibly DNA degradation. Due to these issues and because the DNA input for *shf-1-236* was too low and within the range of noise, the sequence for this allele was not determined. Upon transformation with an SHF-C transgene (see Figure 3A for a description of each transgene), we found transformants that were capable of rescuing the mutant phenotype in *shf-1-277* (Figure 4C and Supplementary Figure 2B). This experiment allowed us to identify the causative alleles of *shf-1*. From here on, we will refer to this gene product as Crescerin/SHF1.

One interesting result reported for the *shf1* mutant (Kuchka and Jarvik 1987) was that *shf-1* regenerated their flagella after deflagellation with similar initial kinetics as W.T, but the final length plateaued at a shorter value. We replicated this experimental result using pH shock-induced deflagellation on W.T, *shf-B*, and the rescue strain (*shf-B:SHF-A*) (Figure 5A and Supplemental Figure 3A), as well as the original *shf-1* mutant allele, *shf-1-253* (Supplemental Figure 3B). This result demonstrates that Crescerin/SHF1 is not a prerequisite for initiation of regeneration, but becomes functionally necessary around half-length to complete the structure. Although assembly of precursor molecules, such as tubulin, is essential for completion, a major, concerted effort by the cell entailing synthesis of precursor molecules is also required for flagellar regeneration to full length. Genes encoding flagellar proteins are synchronously up-regulated and protein synthesis pathways are activated upon flagellar detachment (Keller et al. 1984; Lefebvre and Rosenbaum 1986; Stolc et al. 2005; Yuan et al. 2012). When new protein synthesis is blocked through the use of cycloheximide, flagella regenerate with initially normal kinetics, but reach a shorter final length (Rosenbaum, Moulder, and Ringo 1969; Lefebvre et al. 1978). Typically, the length point that flagella grows in cycloheximide is referred to as the “precursor pool size” and it can be interpreted as the amount of preexisting precursor molecules that the cell body has in storage at any given moment. Conversely, since this pool size (~6 μm) is approximately 50-60% of the average length of flagella (10-12 μm), the remaining amount of precursor molecules must be actively synthesized during regeneration to complete a full-length flagellum. For most mutations that alter flagellar length, the same trend is seen that the length regenerated in the absence of protein translation is roughly half the length prior to deflagellation. If the size of the flagellar precursor pool were proportionally reduced in *shf-1*, the a priori expectation is that cells would regenerate flagella to ~50-60% of its original length, ~ 3-3.5 μm , in cycloheximide drug treatment. Our results show that

shf-B is capable of growing back its flagella to ~92% of its original length (final average length in cycloheximide of 6.2 μm / pre-deflagellation average length of 6.7 μm), therefore, the precursor pool size as defined by these experiments is seemingly unaffected compared to W.T and the rescue strain as exhibited by their final average length of, 6.9 μm and 6.7 μm , respectively (Figure 5B and Supplemental Figure 3B). To corroborate this finding, we also tested the *shf1* allele, *shf1-253*, and found that it was also capable of growing back to ~90% of its original length (final average length in cycloheximide of 5.4 μm / pre-deflagellation average length of 6.0 μm) (Supplemental Figure 3C). Another short-flagella mutant, *ift56-2*, was reported to grow back to its original *shf* length in the presence of cycloheximide (Jiang 2017), which further argues that a fixed scaling factor, between the length of flagella prior to deflagellation and the precursor pool size, may not exist. Rather, we find it plausible that in our *shf* mutants, the transcription and protein synthesis pathways are upregulated normally due to the unaltered early regeneration rates which allows for replenishing of the precursor pool to the same extent as W.T cells. Supporting this hypothesis, Kannegarrd and colleagues reported that the flagellar transcriptional response ensued upon deflagellation was unaffected in the *shf1* allele, *shf1-253* (Kannegaard et al. 2014).

To better understand Crescerin/SHF1's role in flagellar growth and length maintenance, we decided to determine its localization in steady state versus during regeneration. Our initial attempt was to visualize Crescerin/SHF1 directly by integrating a modified transgene containing a fluorescent protein (mCherry and GFP) within the Crescerin/SHF1 protein (Figure 3A), however, we were unable to detect any signal despite successful integration and complementation (Supplementary Figure 1 A and B and Supplementary Figure 2B). Moving forward, we immunostained complemented HA-Crescerin/SHF1 strains against HA and α -tubulin, at steady-state and during regeneration- 30 minutes and 60 minutes post deflagellation. In each

condition, we found both diffuse and pronounced puncta of HA-Crescerin/SHF1 within the cell body, at the base of the flagella and within the flagella (Figure 6A and Supplementary Figure 5A). The puncta localization within the cell body strongly resembles IFT puncta detected through immunofluorescence of *Chlamydomonas reinhardtii*, which implies coupling of Crescerin/SHF1 to IFT (Wood et al. 2012; Ishikawa et al. 2014). In order to get a quantifiable understanding of the signal within the flagella, we determined the intensity values for each channel by taking linescans of flagella, performing background subtraction, then normalizing the flagellar intensity of HA-Crescerin/SHF1 to tubulin. We found that the mean intensity of HA-Crescerin/SHF1 (normalized to tubulin, HA:TUB) per unit length was positively correlated with flagellar length in steady-state (steady state, $R^2 = 0.77$) and late regeneration (60 minutes regenerating, $R^2 = 0.74$), but even more strongly correlated at mid-regeneration (30 minutes regenerating, $R^2 = 0.94$) (Figure 6B). This is in line with the idea that Crescerin/SHF1 acts as a positive regulator of flagellar length, particularly through regeneration. To better analyze the puncta within the flagella, previously reported in (Das et al. 2015), we performed puncta detection for flagella in all three conditions. We found that most puncta reside at the tip of the flagella in steady-state cells, and both at the tip or near tip for 30 minute-regenerating flagella (Figure 6C), but not for 60 minute-regenerating flagella, in line with previous accounts on Crescerin/SHF1 localization (Louka et al. 2018). Interestingly, puncta were detected very early on in short flagella during regeneration which decreases the likelihood that Crescerin/SHF1 import is regulated at a set length during regeneration. In all three conditions there was no particular flagellar length for which puncta was most enriched, suggesting that Crescerin/SHF1 is not exclusive to any particular length (Supplementary Figure 5B). The number of puncta per μm of flagella increased slightly during 30 minutes of regeneration compared to 60 minutes of regeneration and steady-state cells (Supplementary Figure 5C) which prompted us to

analyze the number of puncta per μm of flagella as a function of flagellar length. Overall, the trend follows that as flagella get longer during regeneration, the number of puncta per μm seems to decrease which is an observation that mirrors the frequency of IFT trains (Figure 6D) (Engel, Ludington, and Marshall 2009; Ludington et al. 2015)

The results thus far establish that Crescerin/SHF1 is necessary for achieving normal flagellar length in *Chlamydomonas reinhardtii*. Given that Crescerin/SHF1 contains several putative microtubule-binding TOG domains, and appears to be associated with both IFT trains and the flagellar tip (Louka et al. 2018; Das et al. 2015; Bacaj, Lu, and Shaham 2008), there are at least two potential ways that Crescerin/SHF1 may contribute to length regulation. In one model (Figure 7A), Crescerin/SHF1 acts as a microtubule polymerase at the flagellar tip, facilitating the incorporation of tubulin dimers onto the end of the growing outer doublet microtubules. An alternative model is that Crescerin/SHF1 may help to bind tubulin dimers in the cytoplasm and transport them into the flagellum (Figure 7B). Are both of these models equally able to explain the *shf1* phenotype? We implemented a computational model (see Methods) that represents the processes of tubulin import, flagellar microtubule turnover, and cytoplasmic microtubule dynamics. Using this model, we asked which of the two scenarios, microtubule polymerization or tubulin transport, can best explain the observed mutant phenotype, which we characterize in terms of three features: (A) a steady state flagellar length that is roughly half that of wild type cells, (B) no observable change in flagellar growth rate during the initial phase of growth up to several μm , and (C) during regeneration in the absence of protein synthesis, wild-type flagella grow back to roughly half their pre-shock length while mutant flagella grow back to approximately 80% of pre-shock length. Given the highly simplified nature of our model, we do not seek for precise

numerical matching of experimental data. Rather we ask whether the simplified model can or cannot replicate the three qualitative aspects of the phenotype.

As seen in Figure 8A, a model based on loss of an elongation factor at the tip does not account for the observed phenotypes. It can explain the reduced steady state length in the mutant, but in such a model, it is predicted that flagella regenerated in cycloheximide should be extremely short, or not regenerate at all. This is consistent with prior reports from (Kuchka and Jarvik 1987), but is not consistent with our observations (Figure 5B and Supplementary Figure 3C). In contrast, a model based on loss of high affinity tubulin binding domains from the IFT particle, corresponding to the TOG domains of Crescerin/SHF1, does recapitulate the observation that flagella regenerate to a length closer to pre-shock length in cycloheximide treated mutants than in cycloheximide treated wild type cells (Figure 8B, Figure 5B and Supplementary Figure 3C).

If we increase the quantity of Crescerin/SHF1 in the model, such as could be achieved by over-expression, we find that a longer steady-state length can be obtained (Figure 8C). However, we find that the relationship between Crescerin/SHF1 levels and steady state length is non-linear, such that even a ten-fold increase in Crescerin/SHF1 would produce less than a doubling of length. Thus, our model makes the prediction that Crescerin/SHF1 over-expression should lead to a measurable length increase, but even with a strongly expressing construct, less than an overall doubling of length.

Next, we wanted to look into how the absence of Crescerin/SHF1 would affect growth from flagella at longer lengths. In *C.reinhardtii*, incubation of cells with lithium chloride (LiCl) is used to induce flagellar growth from steady-state lengths (Nakamura, Takino, and Kojima 1987). Although the exact mechanism is not known, LiCl elongation is associated with increased IFT within the flagellum (Ludington et al. 2013) and is known to occur through the recruitment of

flagellar precursor proteins from the cell body pool (Wilson and Lefebvre 2004). Our expectation was that LiCl- induced elongation would be impaired in the *shf-B* mutant possibly due to decreased capacity for tubulin transportation. We found that upon 60 minutes of LiCl treatment, W.T and the rescue line increased their lengths by an average of 4 μm and 3.5 μm , respectively, whereas *shf-B* only increased its length by 1.6 μm (Figure 8A and Supplementary Figure 4A).

One prediction of the model is that increased levels of Crescerin/SHF1 would increase the steady-state flagellum length (Figure 8C). This result was first reported in hTERT-RPE1 cells where overexpression of Crescerin/SHF1 was shown to increase cilia length (Latour et al. 2020). To test this hypothesis, we introduced a Crescerin/SHF1 transgene in W.T cells. Cumulative frequency plots show that transformants overexpressing Crescerin/SHF1 had increased flagellum length distribution compared to unaltered W.T cells (Figure 8B and Supplementary Figure 4B and 4C). This suggests that one possible method for regulating the steady state length of the flagellum is to dial the levels of Crescerin/SHF1.

DISCUSSION

Our model generates testable, hypothesis-driven experiments

The above-mentioned, proposed model drove us to hypothesize that our *shf* mutants would have issues elongating at longer lengths. We tested this by treating both W.T and *shf-B* mutants in LiCl which induces elongation from their steady-state length and found that the *shf-B* mutant cells were in fact impaired in their ability to elongate (Figure 8A and Supplemental Figure 4A). Drawing from our experiment where we tested the size of the precursor pool with the use of cycloheximide (Figure 5B and Supplemental Figure 3B), we can rule out the possibility that in *shf-B*, LiCl-induced elongation is impaired due to a shortage in the precursor pool supply. Additionally, given that the early rapid phase of regeneration is primarily driven by IFT and the *shf-B* mutant is unaffected in this growth phase, it is improbable that IFT frequency rates are grossly affected in the *shf-B* mutant and thus the root cause for this decreased potential in LiCl-induced elongation. We find it more likely that in this *shf* mutant, tubulin incorporation onto the axoneme at the distal tip is decreased, although not abolished, due to the absence of the Crescerin/SHF1 protein. This result is in contrast to the actin mutant, *ida5*, which is completely incapable of flagellar elongation upon LiCl treatment possibly due to an impairment of actin-dependent IFT recruitment to the basal bodies and/or train size regulation (Avasthi et al. 2014).

The computational simulations we performed allowed us to distinguish between two possible models that describe Crescerin/SHF1's role in flagellar length control. The model best paralleling our results is the one where Crescerin/SHF1 increases tubulin loading by increasing the amount of tubulin bound to IFT through higher affinity of tubulin to IFT and increased tubulin binding sites on IFT. This simulation predicted that increased expression of Crescerin/SHF1 would lead to longer steady-state flagellar lengths which we tested and confirmed (Figure 9B and

Supplementary Figure 5C). Thus, modeling based on the results we obtained allowed us to paint a better picture that then allowed us to formulate possible scenarios that we could test.

Tubulin and Crescerin/SHF1 in flagella length control models

Since tubulin represents the most abundant, main structural unit of the axoneme, large quantities of tubulin need to move from the cell body to the tip of an assembling flagella. One question that has been largely explored is how to reconcile the observed kinetics of flagellar assembly with the rate at which tubulin reaches the flagellar tip (Bhogaraju et al. 2014). The primary driving factor for proposing these models is to account for flagellar growth rates by identifying mechanisms for increasing tubulin concentration at the distal tip given observations that demonstrate opposing mechanisms showing tubulin levels dropping significantly.

Bhogaraju and colleagues hypothesized that aside from the tubulin-cargo binding site they had discovered, several other tubulin-cargo binding sites in IFT proteins exist to offset multiple mechanisms that decrease tubulin amounts at the tip during assembly (Bhogaraju et al. 2014). While this may turn out to be true, our results suggest an alternative solution: increased binding sites by the tubulin binding, TOG-domains of Crescerin/SHF1. Our immunofluorescence experiments show Crescerin/SHF1 in puncta at the distal region and along the flagella from the commencement of regeneration, even though the flagellar regeneration curve indicates that Crescerin/SHF1 becomes functionally essential when the flagella reach a certain length. Our model suggests that a tubulin concentrating mechanism via Crescerin/SHF1 is in effect during early regeneration to allow for assembly when the frequency of IFT cargo deposits at the tip decreases later on in regeneration. Corroborating this model are previous findings showing that the Crescerin/SHF1 homologue in *C. elegans*, CHE-12, requires the IFT particle B to localize to the

flagella (Bacaj, Lu, and Shaham 2008). Furthermore, CHE-12 GFP puncta were detected showing anterograde and retrograde movement in the flagella (Das 2016).

During assembly, tubulin concentration at the tip is predicted to decrease in part due to IFT trains decreasing in size and injection rates decreasing as a function of ciliary length (W. F. Marshall and Rosenbaum 2001; Wallace F. Marshall et al. 2005; Engel, Ludington, and Marshall 2009; Ludington et al. 2013). Even though tubulin can reach the tip of an assembling flagella through diffusion, IFT is necessary to promote the proper concentration for assembly of tubules at the tip (Weghe et al. 2020). In fact, when a tubulin binding motif on the IFT cargo molecules is mutated, flagellar regeneration and length is impaired significantly (Bhogaraju, Engel, and Lorentzen 2013; Kubo et al. 2016). Our preferred model invoked two parameter variations that led to simulations that parallel our experimental results: increased affinity for binding of tubulin to IFT and increased binding sites through Crescerin/SHF1's TOG-domains. While the increased binding sites through IFT seems reasonable given the ability of TOG-domains to bind tubulin, the other parameter, increasing affinity of IFT to tubulin, is not very intuitive. This could reflect a regulatory point that would affect tubulin loading onto IFT as is the case with the structural protein DRC-4 (Wren et al. 2013). Proteomic data of *C. reinhardtii* cells has identified multiple phosphorylated and oxidized residues in the disordered regions between the TOG-domains and within TOG-3 (H. Wang et al. 2014; Ford et al. 2020). One intriguing possibility is that these residues get modified by kinases to dial the affinity of Crescerin/SHF1 to tubulin and IFT molecules. Within the realm of regulatory proteins, kinases represent the most well studied and many have been found to play a role in flagellar length control (Berman et al. 2003; Pan, Wang, and Snell 2004; Wilson and Lefebvre 2004; Bradley and Quarmby 2005; Tam, Wilson, and Lefebvre 2007; Luo et al. 2011; Tam, Ranum, and Lefebvre 2013).

Another important factor affecting the ability to form IFT-tubulin cargos is the soluble tubulin concentration at the base of the flagella which in turn depends on the cytoskeleton microtubule dynamics in the cell body. In *C.reinhardtii*, katanin, a cytoplasmic microtubule severing protein, and kinesin-13, a microtubule depolymerizer, have loss-of-function mutant phenotypes that lead to flagellar length abnormalities (Piao et al. 2009; Qasim Rasi et al. 2009; L. Wang et al. 2013; Kannegaard et al. 2014). These results suggest that the tubulin dynamics of the cell body affect flagellar length which underscores the need to better understand soluble tubulin concentrations both at the tip and at cargo assembly locations near the basal bodies since subtle changes in tubulin concentration can lead to major changes in the frequency of IFT-tubulin complex formation.

TOG domains have conserved tubulin-binding features that are in several well-studied protein families such as XMAP-215 and CLASP proteins (Slep and Vale 2007; Al-Bassam et al. 2010; Fox et al. 2014; Byrnes and Slep 2017). Structural analysis of a TOG domain in Crescerin/SHF1 has identified conserved key features such as the intra-HEAT loops that bind to tubulin in XMAP-215 and CLASP protein families (Das et al. 2015). We also found these features are conserved in the TOG domains of the *C.reinhardtii* homologue (Figure 2B). In-vitro polymerization assays with purified Crescerin/SHF1 TOG domains from the mammalian homolog of Crescerin/SHF1 has shown that each domain can increase tubulin polymerization and combinations of them can increase the effect on tubulin polymerization even more significantly than individual domains (Das et al. 2015). Moreover, point mutations that disrupt binding of the TOG-domains to tubulin phenocopies a Crescerin/SHF1 knock-out in its shorter flagellar length at steady-state suggesting that tubulin binding is paramount for its activity. Cumulatively, these results imply that Crescerin/SHF1 is binding to tubulin and increasing polymerization, however,

the latter has never been explored in-vivo. Our modeling simulations point more towards a mechanism whereby Crescerin/SHF1's tubulin binding ability acts as a recruiting factor for IFT particles as they enter the flagellum.

Crescerin/SHF1 in the context of Cep104/Fap256, a TOG-domain containing, microtubule associated protein (MAP)

Flagella axoneme structure varies based on organism, tissue types, and motility (Conkar and Firat-Karalar 2021). The common feature of the axoneme is the 9 doublet structure arranged in radial symmetry. The doublet refers to one full microtubule consisting of 13 protofilaments fused to a microtubule consisting of only 10 protofilaments, referred to as the A-tubule and B-tubule, respectively. In *Tetrahymena*, Cep104/Fap256, another TOG-domain containing protein, was localized near the A-tubule whereas Crescerin/SHF1 was found near the B-tubule, which led Louka and co-workers to suggest that each of these proteins helps assemble tubulin on each respective tubule (Louka *et al.*, 2018). Among flagella there is dramatic variation in the size and composition of the distal segment defined as a region at the tip consisting of only an A-tubule singlet due to a gap between the plus-ends of the longer A-tubule and shorter B-tubule.. In *C. reinhardtii* and *Trypanosoma brucei*, the distal segment was not observed through cryo-electron tomography reconstructions at steady-state (Höög *et al.* 2014). Furthermore, during assembly of flagella, *C. reinhardtii* flagella had approximately equal lengths of A and B tubules (Höög *et al.* 2014). Given that the early flagellar regeneration kinetics was nearly the same in W.T as in the *shf-1* mutant, we find it improbable that Crescerin/SHF1 is only important for B-tubule formation. We cannot, however, rule out the possibility that compensatory mechanisms have been co-opted by *shf* mutant cells to achieve equal assembly of both tubules and unimpaired regeneration kinetics.

Of the microtubule associated proteins implicated in flagellar dynamics, Cep104/Fap256 stands out because it has been extensively studied in many organisms and in particular, *C.reinhardtii* (Satish Tammana et al. 2013; Rezabkova et al. 2016; Al-Jassar et al. 2017). Like in the Crescerin/SHF1 mutant, the mutant Cep104/Fap256 knock-out, known as *roc22*, has shortened flagella, however, most cells (~70%) fail to regenerate flagella after pH-shock induced deflagellation (Satish Tammana et al. 2013). Unlike *shfl* mutant cells, which at a population level regenerate flagella to the same degree as W.T, this result suggests that Cep104/Fap256's function is crucial from the onset of regeneration. The mutant phenotypes of *roc22* and *shfl* cells indicate that these proteins have different temporal regulatory roles in flagellar assembly: Cep104/Fap256 is key for the start of assembly and Crescerin/SHF1 is crucial during the early stages to enrich for tubulin at the tip. Interestingly, in a recent study, Cep104/Fap256 and Crescerin/SHF1 were found as part of a larger protein complex in mammalian cell lines (Latour et al. 2020). Given the presence of one TOG domain in Cep104/Fap256 and three TOG domains in Crescerin/SHF1, we speculate that the two proteins in complex with each other and possibly with other MAPs can lead to altered on and off rates with tubulin compared to each individual component.

From these perspectives, it will be intriguing to uncover how these two proteins work together to regulate flagellar microtubule dynamics. In *C.reinhardtii* and *Tetrahymena* flagella, Cep104/Fap256 has been found exclusively at the tip during assembly and at steady-state (Satish Tammana et al. 2013; Louka et al. 2018). In contrast, Crescerin/SHF1 localizes in puncta at the tip and along the flagella. Perhaps Crescerin/SHF1's extra stretches of positive residues located C-terminal to its TOG domains, shown to be important in binding to the microtubule lattice in XMAP215 and CLASP (Al-Bassam et al. 2006; Brouhard et al. 2008; Al-Bassam et al. 2010), allow for attachment modules along the lattice of the microtubules which could increase tubule

stability during steady-state. Crescerin/SHF1 contains a similar TOG-domain architecture as the CLASP proteins. The family of CLASP proteins decrease microtubule catastrophe and promote microtubule rescue (Slep 2018). This added functionality could also explain the increased prevalence of Crescerin/SHF1 puncta at the tip in non-assembling flagella.

AUTHOR CONTRIBUTIONS

K.P., M.M., H.I., and W.M. contributed to the design of the research, analysis, and writing of the manuscript.

ACKNOWLEDGEMENTS

We thank the members of the Marshall Lab for insightful discussions. We are thankful for past members' contributions to the understanding of flagellar length control which drove the modeling performed in this study. We thank Carol Gross and Peter Walter for their direction and input throughout this project.

MATERIALS AND METHODS

Initial identification of strain carrying a candidate short flagella mutation

We originally set out to understand how the massive transcriptional response that is turned on during flagellar regeneration ties back to flagellar length control. A publication focusing on gene expression during the cell cycle highlighted the expression profiles of putative transcription factors that are upregulated following deflagellation. Assuming there could be a feedback loop that turns on these transcription factors during flagellar regeneration, we hypothesized that mutations in these upregulated transcription factors would result in flagellar length abnormalities. Therefore, we screened for changes in flagellar length in a set of insertional mutants predicted to disrupt genes encoding these putative transcription factors. Candidate genes were identified as annotated transcription factors in (Zones et al. 2015) (summarized in sheet 1 of Supplemental_Table_1). The mutants we screened for did not have any visible length abnormalities in steady state conditions with the exception of mutant LMJ.RY0402.093488_1, which was predicted to contain a genetic lesion in Cre01.g003376. This mutant had shorter flagella (*shf*) than wild-type (W.T). To test whether the transcription factor disruption was leading to this phenotype, we analyzed another mutant, LMJ.RY0402.230098, with a predicted insertion cassette (95% confidence) in the intron of the same gene, Cre01.g003376. This second mutant did not have a *shf* phenotype in steady-state conditions. Given these differences in phenotypes, we asked whether some other mutation besides the insertion at Cre01.g003376 was leading to this phenotype. Therefore, we back-crossed the mutant exhibiting the short-flagellar phenotype (LMJ.RY0402.093488_1) to W.T cells to see if the mutant phenotype co-segregated with the Paromomycin cassette. Through tetrad analysis, we found that there was one full Paromomycin cassette present (2:2 segregation), that the short-flagellar phenotype segregated 2:2 and was therefore presumably due to a single mutation, but that

Paromomycin resistance and the short flagella phenotype did not co-segregate . Furthermore, a PCR reaction designed to detect the junction site of the Cre01.g003376 locus (sheet 2 of Supplemental_Table_1) with the Paromomycin cassette showed that the Paromomycin resistance was indeed coming from the Cre01.g003376 locus disruption, eliminating the possibility that a full Paromomycin resistance cassette inserted elsewhere in the genome was causing the short-flagellar phenotype. Thus, it became increasingly clear that the short flagella phenotype was not actually due to the transcription factor gene lesion we had originally chosen to screen. The mutation apparently identifies a gene involved in flagellar length control, and we denoted it initially as SHF-A, to indicate the fact that we did not initially know whether it related to any previously described short flagella genes.

Strains and media

Chlamydomonas strains were obtained from the Chlamydomonas stock center. W.T strains include CC125 mt+ and CC- 5325 CW mt- (the latter is the background strain of the Chlamydomonas Library Project). The original un-backcrossed *shf-A* mutant is LMJ.RY0402.093488. *shf-A* was backcrossed three times to CC125 mt+. *shf-B* (LMJ.RY0402.172376) has a Paromomycin resistance cassette insertion at the same location where the 5 base pair deletion starts in *shf-B*. For the *shf-1* mutants, the following strains were used: cc2348 (*shf1-253*), cc2347 (*shf1-277*), and cc-2345 (*shf1-236*). For liquid cultures, cells were either grown in M1 media (Sager and Granick Medium 1) in a 14:10-h light/dark cycle and measured during the light part of the cycle or they were grown in Tris-Acetate Phosphate (TAP) media for about 2-3 days in constant light. Cells were maintained in 1.5% TAP agar plates, however, if a strain carried a Paromomycin resistance cassette, they were kept in media supplemented with 20 $\mu\text{g ml}^{-1}$ paromomycin. Strains containing

an Crescerin/SHF1 transgene construct were maintained in solid media containing 20 $\mu\text{g ml}^{-1}$ of Hygromycin.

For gamete formation, cells were re-streaked onto fresh TAP agar and incubated in low light. They were then transferred onto TAP- N medium for 4-5 days to induce gametogenesis. The gametes from each strain were then resuspended using 150–200 μl of TAP until a dark green resuspension was obtained. Sporulation and dissection was done as in (Perlaza et al. 2019).

Whole genome sequencing

Culture conditions for original mutant pooled spores:

The original mutant LMJ.RY0402.093488 was backcrossed twice to cc125 mt + [137c]. Spores from tetrads and octads were scored for short vs. W.T length flagella. 20 spores corresponding to each category, W.T or short, were grown as follows: 2ml cultures per well for each spore was grown on 24 well plates in alternating dark:light cycles (14:10) for 3 days. To make sure there was equal representation of each spores genomes, the cell density for each spore was checked to ensure equal input before pooling. 1 ml per spore was used for each phenotypic pool for a total of 20 ml per sample, W.T vs Mutant. The genomic DNA extraction was performed as described in the pooled genome sequencing method in (Perlaza et al. 2019).

The sequencing libraries were prepared with the aid of the KAPA hyperprep library kit by the Vincent J. Coates Genomics Sequencing Laboratory and Functional Genomics Laboratory at the University of California, Berkeley. One cycle of PCR was used to linearize the library molecules. Fragment analyzer traces and Qubit values were assessed for each sequencing library as quality control checks. Pooled 150PE NovaSeq S4 sequencing was performed at the UCSF Center for Advanced Technology Lab. 20 GB of data was requested per sample.

Culture conditions and genomic DNA preparation for shf1 mutants:

Strains cc2345 (*shf1-236*), cc2347 (*shf1-277*), cc2348 (*shf1-253*) were streaked out to singles to ensure an isogenic population of cells. The cultures conditions and genomic DNA extractions were done exactly as described in “culture conditions for the original mutant pooled spores”, with the exception that the starting volume of each strain was ~7ml. The concentrations of the DNA were determined by a nanodrop. The final genomic DNA sample that was sent to sequence was a pooled sample that combined ~65% of *shf1-277*, ~30% *shf1-253* and 5% *shf1-236* genomic DNA.

The genomic DNA pool was prepped for sequencing using the NEB Ultra II DNA library kit. Fragment analyzer traces and Qubit values were assessed for each sequencing library as quality control checks. Novaseq 6000 sequencing was performed by Novogene with 15 GB of data requested.

Processing of sequence data:

Unless otherwise noted, the following steps were used for analyzing data from both the W.T vs mutant pooled experiment samples, and the varying ratios of *shf-1* alleles pool sample.

The raw sequences were processed using FastQC version 0.11.8 (Andrews and Others 2017) (<https://www.bioinformatics.babraham.ac.uk/projects/fastqc/>). Trimmomatic was used for quality filtering of the reads and to remove sequences that match the adapter (Lohse *et al.*, 2012). These reads were then aligned to version 5.0 of the *C.reinhardtii* genome DOE Joint Genome Institute (JGI), reference strain CC503, mt+ (Merchant et al. 2007) using the Burrows-Wheeler Aligner (BWA) (H. Li and Durbin 2009). Conversion of SAM files to BAM files was done using SAMtools (H. Li et al. 2009). Deduplication was done using Picard (<http://broadinstitute.github.io/picard>).

Further processing of the W.T vs mutant pooled experiment samples:

The following steps are exclusive for the sequence processing of the W.T vs mutant pooled experiment. At this point, we attempted two parallel approaches to call variants. Given that there was not any indication as to the nature of the mutation (SNP, long vs short insertion, deletion, duplication), we decided to use both the Genome Analysis Toolkit (GATK) variant caller (DePristo et al. 2011) and Pindel (Ye et al. 2009).

GATK:

GATK base recalibration was performed using The Supplemental VCF file including SNVs and small InDels from Gallaher 2015 was used for the BQSR step. GATK Haplotype Caller followed by GATK GenotypeGVCF commands were performed to get a file with SNPs and Indels. These were then separated to generate a file with SNPS and another with Indels. Using the bcftools isec (-c all) command option, the two sample pools (W.T vs MUT) were compared to one another to get variants unique to each sample. The variants unique to the mutant pool were further filtered by only including variants with $GQ \geq 20$ and $AF \geq 0.9$. Common SNPs and Indels found in laboratory strains were removed using the <http://stormo.wustl.edu/SNPlibrary/index.html> database. Next, using the variant effect predictor, snpEff (Cingolani et al. 2012), only alleles with a High and Moderate effect were included.

Pindel:

The deduplicated BAM files for each sample, W.T and mutant, were inputted into the Pindel software which gave separate files for different types of genetic lesions as the output. The short

insertions and deletions files were filtered to only include alleles whereby the genotype was 1/1 in one pool and 0/0 in the other.

The final filtered SNP file from the GATK pipeline contained 2 variants. The final filtered indel file from the GATK pipeline contained 10 variants. The Pindel file containing deletion variants contained 8 different variants. We used the Integrated Genomics Viewer (IGV) (Thorvaldsdottir, Robinson, and Mesirov 2013) to directly compare the pool alignments to each other and the reference genome focusing on the regions of interest provided by the final filtered variant files. We found that most of the unique variants called in the mutant sample were in fact common between the two samples or common to known variants listed in Phytozome. The 5 base pair (bp) deletion called in Chromosome 6, position 4,097,271 was interesting because it was the only variant called both in the filtered Pindel deletion file and in the final, filtered GATK variant file. In addition, the aligned reads very clearly demonstrated that the deletion could only be seen in the mutant pool and not in the W.T pool. Interestingly, one of the two SNPs from the final filtered SNP variant file produced by GATK, chromosome_6 position 3344626, C to A, was only found in the mutant pool when aligned reads were viewed through IGV. This genotype has been reported previously since it was present in the Phytozome variation list for the gene *Cre06.g277500*. Therefore, we did not believe it was the mutation leading to the short flagellar phenotype. We do believe that this is worth noting since it is located relatively close to the 5 bp deletion indicating that these mutations are linked.

Further processing of the varying genomic ratios of shf1 alleles pool sample

Given that the *shf1* allele was previously mapped to linkage group VI near the centromere, we had a strong suspicion that the gene affected in this mutant was Crescerin/CHE12. Therefore, we took

a biased, but quick approach to looking for the causative mutation by only focusing on the Crescerin/CHE12 gene. The BAM file generated SAMtools conversion was used to view the reads in IGV. Scrolling through the gene, there were two notable variants. In chromosome 6, position 4,096,059 there was a single base change from T to A with a frequency of 74% A and 26% T. In chromosome 6, position 4,096,059 there was a bp deletion that accounted for 28% of the aligned reads. The T to A nonsense mutation leads to an early stop codon and the bp deletion leads to a frameshift in the open reading frame that leads to an early stop codon. We infer that the short flagella phenotype in *shfl-277* is due to the T to A nonsense mutation, and in *shfl-253* it is due to the single base deletion, since the approximate input of each genome in the sequenced pool (65% and 30%), roughly parallels the observed allele frequency, 74% and 28%, respectively. We were not able to obtain a predicted allele for *shfl-236*, presumably because 5% of the pool was under the limit of sensitivity.

Crescerin/SHF1 gene cloning (pKPL_1- SHF-A)

A hybrid approach of stitching together gDNA and cDNA was used to generate the template Crescerin/SHF1 transgene plasmid (pKPL_1) which was then used to generate pKPL_2 and pKPL_3. Given the high GC content and the size of the gene (~10.4kb including a 500bp promoter region, 5'UTR-exon1-exon14-3'UTR), the final transgene was a result of piecewise stitching via In-fusion by way of intermediate plasmids. This approach was used because the original approach, a one-shot In-fusion reaction with several DNA pieces, failed to give any colonies. Two intermediate plasmids were generated through In-Fusion in a sequential manner that then led to one of the final transgene plasmids (pKPL_1) used for transformation of cells. Supplemental_Table_2 has a thorough description of all the gene regions amplified. Phusion Hotstart II polymerase (Thermofisher) was used to generate all the inserts. In the following steps

each amplicon generated either by PCR amplification or vector digestion was isolated and extracted from a 1% agarose gel through the NucleoSpin Gel (Macherey-Nagel) and PCR Clean-Up Kit (Takara) then In-Fusion (Takara) was used to combine these homologous inserts and linearized vectors. In brief, the first intermediate plasmid was generated by fusing 3 inserts with homologous overhangs and a linearized vector that contains a Hygromycin resistance gene for selection. This first intermediate plasmid was linearized via EcoRV (New England Biolabs-NEB) digestion and 2 inserts were added to it by In-Fusion to generate the second intermediate plasmid. The final plasmid (pKPL_1) was generated by linearizing the second intermediate plasmid with EcoRV digestion and adding 2 more inserts. One of these two final inserts included a 3x-FLAG tag inserted in-frame after Glycine 1289. Sanger sequencing was used to verify the sequence of pKPL_1.

Additional Crescerin/SHF1 gene tagging (pKPL_2 (SHF-B))

To generate a construct with an mCherry + 3x-HA tag at the same location as the tag in pKPL_1 (Glycine 1289), the pKPL_1 plasmid was used as PCR template and linearized vector while the pBR9-mCherry plasmid was used to amplify the mCherry coding region (Rasala et al. 2013). Supplemental_Table_2, has a thorough description of all the gene regions amplified. In brief, the pKPL_1 plasmid was linearized with EcoNI (NEB) and SapI (NEB) to generate a 11,989 bp region with most of the Crescerin gene. Three inserts generated by PCRs were added to this linearized vector in one In-Fusion reaction. The final plasmid, pKPL_2 is essentially the same as pKPL_1 with the exception that after Glycine 1289, there is an mCherry + 3x-HA tag rather than a 3x-FLAG. Sanger sequencing was used to verify the sequence of pKPL_2.

Additional Crescerin gene tagging (pKPL_1-CrGFP (SHF-C))

For the pKPL_1-CrGFP plasmid, the codon-optimized Chlamydomonas GFP tag was amplified by PCR from the plasmid pBR9 GFP (Rasala *et al.*, 2013) with primers (CrCHE12-CrGFP:IFS-2 and CrGFP-CrCHE12:IFR-2) and inserted into a unique StuI site in the pKPL_1 plasmid. Supplemental_Table_2, has a thorough description of the primer sequences. The GFP PCR insert was added to the StuI linearized vector in one In-Fusion reaction. The final plasmid, pKPL_1-CrGFP is essentially the same as pKPL_1 with the exception that in addition to the 3x-FLAG after Glycine 1289 there is a GFP tagged after Phenylalanine 9.

Sequence alignment and phylogenetic tree

Crescerin/SHF1 homologues from different organisms were identified using BLASTP (Altschul *et al.* 1990). NCBI accession numbers of these homologues which were used for the phylogenetic tree analysis are listed in sheet 3 of Supplemental_Table_1. The phylogenetic analysis was done using the algorithms of MEGAX (Kumar *et al.* 2018). The evolutionary tree was inferred by using the Maximum Likelihood method and JTT matrix-based model (Jones, Taylor, and Thornton 1992). The sequence alignment between the *M. musculus* and *C. reinhardtii* proteins was done using T-coffee, <http://tcoffee.crg.cat/apps/tcoffee/index.html>, (Notredame, Higgins, and Heringa 2000). Secondary structure prediction was done using the PSIPRED servers (Buchan *et al.* 2013; McGuffin, Bryson, and Jones 2000).

Transgene nuclear transformation

The Crescerin/SHF1 transgene was integrated into the nuclear genome using the NEPA21 electroporator (Nepagene) using the settings found to be most effective in (Yamano, Iguchi, and Fukuzawa 2013) and the protocol described in (Perlaza *et al.* 2019). Briefly, 5-8 μ l of non-linearized, plasmid DNA at a concentration of 1-2 mg ml⁻¹ was mixed with 5 μ l of Salmon Sperm

DNA (10mg ml⁻¹) (Thermofisher Scientific) prior to electroporation. *Chlamydomonas* cells in the logarithmic stage were spun down and resuspended in TAP media and placed in a cuvette in a final volume of 50 µl. Electroporation parameters are thoroughly described in (Perlaza et al. 2019). Transformants were isolated on TAP agar containing 20 µg ml⁻¹ hygromycin.

Screening of transformants grown in Hygromycin plates

Typically, any *shf* mutant transformed with a Crescerin/SHF1 plasmid was screened by selecting about 10-20 colonies from the hygromycin plates, isolating them onto fresh Hygromycin TAP plates (20 µg ml⁻¹) and then looking at their flagella using the Deltavision. This first pass allowed us to narrow down the samples needed for epitope immunoblot verification. Every transformant that we selected as having W.T-like flagella also expressed Crescerin/SHF1. For the W.T background transformations with the Crescerin/SHF1 plasmids, we did not pre-screen through the transformants because we did not know what to expect. Instead, we selected about 10-20 colonies and directly analyzed them through epitope immunoblots.

Immunofluorescence microscopy

Immunofluorescence experiments on *Chlamydomonas* strains were done essentially as described previously (Wood et al. 2012). with several deviations described below. Cells were allowed to adhere onto the poly-lysine coated coverslips for a maximum of 3 minutes since flagella begin to curl if left for longer. Both primary and secondary antibodies were diluted in 20% of the blocking buffer (in phosphate buffered saline). The cells were incubated in a mixture of primary antibodies, anti- alpha tubulin rabbit polyclonal- Abcam 18251 (1:1000) and anti-HA tag mouse monoclonal antibody ([HA.C5] Abcam ab18181) (1:400), for one hour at room temperature. The fluorophore-conjugated secondary antibodies, Thermofisher Alexa Fluor Plus 488 goat anti-mouse (1:1000) and Thermofisher Alexa Fluor 546 goat anti-rabbit (1:1000), were diluted in 20% blocking buffer

and subsequently used to coat over the cells. Laser scanning confocal microscopy was performed using a Nikon Ti inverted fluorescence microscope with CSU-22 spinning disk confocal.

Image Processing and Analysis

Image Processing

Multichannel z-stacks were imported in FIJI (Schindelin et al. 2012) as 32-bit TIFFs, and Sum Slices z-projection was performed on composite images. Single cells were cropped for analysis if they had at least 1 intact flagellum, at least 1.5 μm long, which did not overlap with any other fluorescent structure. Flagellar intensity linescans were taken from base to tip of each flagellum for tubulin and crescerin-HA channels using the Segmented Line tool and Plot Profile function in FIJI. Measurements were saved as separate .csv files for each channel. Background fluorescence for each channel was taken as the Mean Intensity of a circular area of 1-2 μm diameter near the cell using the Measurement tool. Background measurements were saved as one .csv file containing measurements for all flagella in the dataset. Image metadata including z-sizes of stacks were extracted in Python and saved in a separate file.

Analysis

Data formatting, processing, statistical analysis, and plotting were performed in Python and Microsoft Excel. Intensity and position values from each flagellum preprocessed in the following steps: 1) positions normalized to total flagellar length (“normalized x”), 2) Sum Slices intensities divided by z-size for Average Slices intensity, 3) Background subtraction of Sum Slices and Average Slices intensities, 4) HA normalized to tubulin at each point for Average Slices intensities (HA:TUB), in order to control for artefacts such as flagellar curling at the tip (resulting in locally increased tubulin and HA-crescerin intensity) and 3) moving average smoothing of HA:TUB.

Based on HA:TUB intensity, mean and standard deviation of flagellar intensities, as well as flagellar length, were pooled into a common file.

For analysis of HA:TUB puncta in flagella, puncta detection was performed as follows. Binary thresholding (average + 1.4 standard deviations) of smoothed HA:TUB intensity for each flagellum was performed. All intensities below the threshold were averaged for the mean baseline intensity. A new threshold of $1+1.25$ std of the baseline intensity was applied to the smoothed HA:TUB data. Consecutive regions above the threshold were recorded as a series of puncta start and end positions. Puncta consisting of only 1 point were removed. Within the boundaries of each punctum, the mean, standard deviation, max, and sum intensity were calculated based on unsmoothed HA:TUB intensity. Puncta size, mid-point position, max position, and mean & max intensity enrichment (normalized to mean baseline intensity), and number of puncta per flagellum were calculated. Lastly, presence of puncta at the flagellar tip was scored if the final point was inside of a punctum (final point of thresholded binary equal to 1).

Note: Five flagella from steady-state were not plotted in Figure 6B because their lengths were shorter than 5 μm which could mean that they correspond to cells actively regenerating flagella due to mechanical shearing or they may have been cut off during fixation.

Modeling

In order to model potential roles of for Crescerin/SHF1 in flagellar length control, we started with a computational model we previously developed for studying the effect of katanin on flagellar length control, in which the length of flagellar microtubules is represented by a differential equation for flagellar length combined with a stochastic model for cytoplasmic microtubule dynamics (Kannegaard et al. 2014). Our model is identical to the previously described model except that we modified it to explicitly model soluble tubulin within the flagellar compartment. At

each time step, the current concentration of soluble tubulin in the cell body is used to calculate the fraction of IFT particles entering the flagella that have tubulin bound. This calculation assumes saturable binding with a dissociation constant that is a parameter of the model. A second parameter of the model is the number of tubulin binding sites per IFT particle. IFT particles are then modeled as entering the flagellum at a rate proportional to $1/L$, based on previous observations (Engel, Ludington, and Marshall 2009; Ludington et al. 2013). As IFT particles enter the flagellum, they release their tubulin cargo. The concentration of tubulin is described by a differential equation that takes into account the rate at which new tubulin is delivered by IFT and the rate at which tubulin is assembled onto the growing axoneme. The net flagellar growth rate is calculated as the difference between an assembly and disassembly term. The disassembly term is a length-independent constant, consistent with previous observations (W. F. Marshall and Rosenbaum 2001). Based on the assumption that tubulin removed from the axoneme via disassembly is in the GDP bound form and hence incapable of re-assembly, the tubulin produced by disassembly is added back to the cytoplasmic pool. The assembly rate is a linear function of the tubulin concentration in the flagellum, with the slope and intercept being two adjustable parameters of the model. Flagellar length is updated using an Euler method with a timestep of 0.05 seconds. At each time point, after the tubulin concentration and flagellar lengths are updated, a stochastic simulation is carried out to determine how the lengths of a set of 10 cytoplasmic microtubules may have changed during the time step. This simulation is based on a previously described simplified model of tubulin dynamics (Gregoretta et al. 2006) augmented to include the action of a microtubule depolymerizing kinesin at the tip and a microtubule-severing protein along the length, as previously described (Kannegaard et al. 2014). This last step updates the free tubulin concentration that will then be used to calculate import at the next time step.

Simulations start with an initial condition of length equal to 0.1 μm (we avoid 0 to prevent division by zero), and the simulation is allowed to run for a specified number of iterations, sufficient to reach a visible steady state. This first part of the simulation provides a prediction for the steady state flagellar length. Next, the flagellar length is reset to 0.1 and the total quantity of available tubulin is reduced by a quantity equivalent to that stored in the two flagella. The flagella are now simulated regrowing in the presence of this reduced pool, in order to simulate the experiments in which regeneration is done in the absence of protein synthesis. This second phase is allowed to run to steady state, allowing us to calculate the predicted flagellar length after regeneration in cycloheximide.

We modeled two different possible effects of the Crescerin/SHF1 mutation. In the first scenario, we make the assumption that Crescerin/SHF1 is acting as a microtubule polymerase to catalyze microtubule assembly at the flagellar tip. To represent the effect of a Crescerin/SHF1 mutation, we reduced the slope of the elongation versus tubulin concentration function in the assembly term of the flagellar length rate equation. In the second scenario, we make the assumption that Crescerin/SHF1 is acting primarily as a tubulin recruiting factor for IFT particles as they enter the flagellum. To represent the effect of a Crescerin/SHF1 mutation in this scenario, we reduced the number of tubulin binding sites in the model and also increased the dissociation constant for tubulin binding, to represent the idea that Crescerin/SHF1 can bind tubulin more tightly than the built-in tubulin binding sites on the IFT particles (Bhogaraju et al. 2013)).

Denaturing protein extract and immunoblot assay

Cell cultures were grown to mid-log phase and subsequently spun down at 3000 g for 8 min. The pellets were resuspended in 150 μl of TAP. An equal volume of 0.2M NaOH was added to the pellets, vortexed at RT for 5 min and pelleted at 15,000g for 5 min. The supernatant was removed,

the pellet was resuspended in ~200 μ l of SDS samples buffer (0.06 M Tris-HCl pH 6.8, 5% glycerol, 2% SDS, 4% 2-Mercaptoethanol, 0.0025% bromophenol blue), boiled for 5 min and then pelleted again. Proteins were separated by SDS-PAGE using Criterion Precast Gels (Bio-Rad) and transferred onto nitrocellulose membrane, 0.2 μ m pore. Non-specific signal was blocked with PBS-T supplemented with 5% instant nonfat dry milk for 1 hour at RT or overnight at 4°C. All primary and secondary antibodies were diluted in this blocking buffer. The following antibodies (at the indicated dilution) were used for this publication: monoclonal mouse anti-Flag (1:2,000) (M2, Sigma F1804), and monoclonal mouse anti- α -tubulin (1:5,000) (Sigma #T6074). To detect the primary antibodies, HRP-conjugated anti-rabbit and anti-mouse secondary antibodies (Promega) were used at dilution 1:10,000 in PBS-T supplemented with 5% instant nonfat dry milk for 1 hour at RT. In between the incubation with primary and secondary antibody and after the incubation with the secondary antibody, three washes of about 10 min each time, at RT, were performed using PBS-T in 5% instant nonfat dry milk. Chemiluminescence (ECL) method was applied to develop the signal. For most immunoblot analysis, the SuperSignal West Dura Extended Duration Substrate kit (Thermofisher Scientific) was used according to manufacturer's directions. The ECL signal was detected with the LI-COR Odyssey imaging system.

Flagellar regeneration

pH shock was used to induce flagellar regeneration. For 1 ml of culture, 50ul of 0.5N acetic acid culture was used to de-flagellate the cells. After 1 minute, 55ul of 0.5N KOH was added. Immediately after this, the cells were spun down for about 3 minutes at 500g and resuspended in the same starting volume of TAP or M1 media. For time point experiments, cells were fixed in a final concentration of 1.5% glutaraldehyde. Flagella was imaged using DIC microscopy

(Deltavision) at 100x magnification. Then, flagellar lengths were measured using the line segment tracing tool on the ImageJ software.

LiCl elongation and cycloheximide regeneration experiments

For the LiCl experiments, strains were grown in TAP media to $\sim 2-4 \times 10^6$ cells/ml. A stock solution of 7.5 M LiCl in water was diluted in TAP medium to a final concentration of 50 mM of LiCl. The cell culture was then diluted two-fold by mixing in an equal volume of 50 mM LiCl medium. In experiments using cycloheximide, cells were grown in TAP media to $\sim 6 \times 10^6$ cells/ml and then cycloheximide was added to a final concentration of 12.5 $\mu\text{g/ml}$ from a stock solution of 10 mg/ml in water. The drug was added to the cells 15 minutes before pH shock. Immediately after pH shock, cells were spun down for 3 minutes at 500g and resuspended in TAP media containing 12.5 $\mu\text{g/ml}$ of cycloheximide. For both the LiCl and cycloheximide experiments an equal volume of water was added as a control for drug addition.

REFERENCES

1. Al-Bassam, Jawdat, Mark van Breugel, Stephen C. Harrison, and Anthony Hyman. 2006. “Stu2p Binds Tubulin and Undergoes an Open-to-Closed Conformational Change.” *The Journal of Cell Biology* 172 (7): 1009–22.
2. Al-Bassam, Jawdat, and Fred Chang. 2011. “Regulation of Microtubule Dynamics by TOG-Domain Proteins XMAP215/Dis1 and CLASP.” *Trends in Cell Biology* 21 (10): 604–14.
3. Al-Bassam, Jawdat, Hwajin Kim, Gary Brouhard, Antoine van Oijen, Stephen C. Harrison, and Fred Chang. 2010. “CLASP Promotes Microtubule Rescue by Recruiting Tubulin Dimers to the Microtubule.” *Developmental Cell* 19 (2): 245–58.
4. Al-Bassam, Jawdat, Nicholas A. Larsen, Anthony A. Hyman, and Stephen C. Harrison. 2007. “Crystal Structure of a TOG Domain: Conserved Features of XMAP215/Dis1-Family TOG Domains and Implications for Tubulin Binding.” *Structure* 15 (3): 355–62.
5. Al-Jassar, Caesar, Antonina Andreeva, Deepak D. Barnabas, Stephen H. McLaughlin, Christopher M. Johnson, Minmin Yu, and Mark van Breugel. 2017. “The Ciliopathy-Associated Cep104 Protein Interacts with Tubulin and Nek1 Kinase.” *Structure* 25 (1): 146–56.
6. Altschul, S. F., W. Gish, W. Miller, E. W. Myers, and D. J. Lipman. 1990. “Basic Local Alignment Search Tool.” *Journal of Molecular Biology* 215 (3): 403–10.
7. Andrews, Simon, and Others. 2017. “FastQC: A Quality Control Tool for High Throughput Sequence Data. 2010.”
8. Asleson, C. M., and P. A. Lefebvre. 1998. “Genetic Analysis of Flagellar Length Control in *Chlamydomonas Reinhardtii*: A New Long-Flagella Locus and Extragenic Suppressor Mutations.” *Genetics* 148 (2): 693–702.

9. Avasthi, Prachee, Masayuki Onishi, Joel Karpiak, Ryosuke Yamamoto, Luke Mackinder, Martin C. Jonikas, Winfield S. Sale, Brian Shoichet, John R. Pringle, and Wallace F. Marshall. 2014. "Actin Is Required for IFT Regulation in *Chlamydomonas Reinhardtii*." *Current Biology: CB* 24 (17): 2025–32.
10. Bacaj, Taulant, Yun Lu, and Shai Shaham. 2008. "The Conserved Proteins CHE-12 and DYF-11 Are Required for Sensory Cilium Function in *Caenorhabditis Elegans*." *Genetics* 178 (2): 989–1002.
11. Barsel, S. E., D. E. Wexler, and P. A. Lefebvre. 1988. "Genetic Analysis of Long-Flagella Mutants of *Chlamydomonas Reinhardtii*." *Genetics* 118 (4): 637–48.
12. Berman, Steven A., Nedra F. Wilson, Nancy A. Haas, and Paul A. Lefebvre. 2003. "A Novel MAP Kinase Regulates Flagellar Length in *Chlamydomonas*." *Current Biology: CB* 13 (13): 1145–49.
13. Bhogaraju, Sagar, Lukas Cajanek, Cécile Fort, Thierry Blisnick, Kristina Weber, Michael Taschner, Naoko Mizuno, et al. 2013. "Molecular Basis of Tubulin Transport within the Cilium by IFT74 and IFT81." *Science* 341 (6149): 1009–12.
14. Bhogaraju, Sagar, Benjamin D. Engel, and Esben Lorentzen. 2013. "Intraflagellar Transport Complex Structure and Cargo Interactions." *Cilia* 2 (1): 10.
15. Bhogaraju, Sagar, Kristina Weber, Benjamin D. Engel, Karl-Ferdinand Lechtreck, and Esben Lorentzen. 2014. "Getting Tubulin to the Tip of the Cilium: One IFT Train, Many Different Tubulin Cargo-Binding Sites?" *BioEssays: News and Reviews in Molecular, Cellular and Developmental Biology* 36 (5): 463–67.

16. Bradley, Brian A., and Lynne M. Quarmby. 2005. "A NIMA-Related Kinase, Cnk2p, Regulates Both Flagellar Length and Cell Size in *Chlamydomonas*." *Journal of Cell Science* 118 (Pt 15): 3317–26.
17. Brouhard, Gary J., Jeffrey H. Stear, Tim L. Noetzel, Jawdat Al-Bassam, Kazuhisa Kinoshita, Stephen C. Harrison, Jonathon Howard, and Anthony A. Hyman. 2008. "XMAP215 Is a Processive Microtubule Polymerase." *Cell* 132 (1): 79–88.
18. Buchan, Daniel W. A., Federico Minneci, Tim C. O. Nugent, Kevin Bryson, and David T. Jones. 2013. "Scalable Web Services for the PSIPRED Protein Analysis Workbench." *Nucleic Acids Research* 41 (Web Server issue): W349–57.
19. Byrnes, Amy E., and Kevin C. Slep. 2017. "TOG-Tubulin Binding Specificity Promotes Microtubule Dynamics and Mitotic Spindle Formation." *The Journal of Cell Biology* 216 (6): 1641–57.
20. Chan, Yee-Hung M., and Wallace F. Marshall. 2012. "How Cells Know the Size of Their Organelles." *Science* 337 (6099): 1186–89.
21. Chen, Xiaoying, Jennica L. Zaro, and Wei-Chiang Shen. 2013. "Fusion Protein Linkers: Property, Design and Functionality." *Advanced Drug Delivery Reviews* 65 (10): 1357–69.
22. Cingolani, Pablo, Adrian Platts, Le Lily Wang, Melissa Coon, Tung Nguyen, Luan Wang, Susan J. Land, Xiangyi Lu, and Douglas M. Ruden. 2012. "A Program for Annotating and Predicting the Effects of Single Nucleotide Polymorphisms, SnpEff: SNPs in the Genome of *Drosophila Melanogaster* Strain w1118; Iso-2; Iso-3." *Fly* 6 (2): 80–92.
23. Conkar, Deniz, and Elif Nur Firat-Karalar. 2021. "Microtubule-Associated Proteins and Emerging Links to Primary Cilium Structure, Assembly, Maintenance, and Disassembly." *The FEBS Journal* 288 (3): 786–98.

24. Craft, Julie M., J. Aaron Harris, Sebastian Hyman, Peter Kner, and Karl F. Lehtreck. 2015. "Tubulin Transport by IFT Is Upregulated during Ciliary Growth by a Cilium-Autonomous Mechanism." *The Journal of Cell Biology* 208 (2): 223–37.
25. Czarnecki, Peter G., and Jagesh V. Shah. 2012. "The Ciliary Transition Zone: From Morphology and Molecules to Medicine." *Trends in Cell Biology* 22 (4): 201–10.
26. Das, Alakananda. 2016. "THE CRESCERIN PROTEIN FAMILY USES ARRAYED TOG DOMAINS TO REGULATE MICROTUBULES IN CILIA." Edited by Neher, Saskia Slep, Kevin Anton, Eva Kuhlman, Brian Redinbo, Matthew R. Doctor of Philosophy, University of North Carolina at Chapel Hill Graduate School.
27. Das, Alakananda, Daniel J. Dickinson, Cameron C. Wood, Bob Goldstein, and Kevin C. Slep. 2015. "Crescerin Uses a TOG Domain Array to Regulate Microtubules in the Primary Cilium." *Molecular Biology of the Cell* 26 (23): 4248–64.
28. DePristo, Mark A., Eric Banks, Ryan Poplin, Kiran V. Garimella, Jared R. Maguire, Christopher Hartl, Anthony A. Philippakis, et al. 2011. "A Framework for Variation Discovery and Genotyping Using next-Generation DNA Sequencing Data." *Nature Genetics* 43 (5): 491–98.
29. Dutcher, Susan K., Linya Li, Huawen Lin, Leslie Meyer, Thomas H. Giddings Jr, Alan L. Kwan, and Brian L. Lewis. 2012. "Whole-Genome Sequencing to Identify Mutants and Polymorphisms in *Chlamydomonas Reinhardtii*." *G3* 2 (1): 15–22.
30. Engel, Benjamin D., Hiroaki Ishikawa, Kimberly A. Wemmer, Stefan Geimer, Ken-Ichi Wakabayashi, Masafumi Hirono, Branch Craige, et al. 2012. "The Role of Retrograde Intraflagellar Transport in Flagellar Assembly, Maintenance, and Function." *The Journal of Cell Biology* 199 (1): 151–67.

31. Engel, Benjamin D., William B. Ludington, and Wallace F. Marshall. 2009. "Intraflagellar Transport Particle Size Scales Inversely with Flagellar Length: Revisiting the Balance-Point Length Control Model." *The Journal of Cell Biology* 187 (1): 81–89.
32. Ford, Megan M., Sheldon R. Lawrence 2nd, Emily G. Werth, Evan W. McConnell, and Leslie M. Hicks. 2020. "Label-Free Quantitative Phosphoproteomics for Algae." *Methods in Molecular Biology* 2139: 197–211.
33. Fox, Jaime C., Amy E. Howard, Joshua D. Currie, Stephen L. Rogers, and Kevin C. Slep. 2014. "The XMAP215 Family Drives Microtubule Polymerization Using a Structurally Diverse TOG Array." *Molecular Biology of the Cell* 25 (16): 2375–92.
34. Gregoret, Ivan V., Gennady Margolin, Mark S. Alber, and Holly V. Goodson. 2006. "Insights into Cytoskeletal Behavior from Computational Modeling of Dynamic Microtubules in a Cell-like Environment." *Journal of Cell Science* 119 (Pt 22): 4781–88.
35. Hao, Limin, Melanie Thein, Ingrid Brust-Mascher, Gul Civelekoglu-Scholey, Yun Lu, Seyda Acar, Bram Prevo, Shai Shaham, and Jonathan M. Scholey. 2011. "Intraflagellar Transport Delivers Tubulin Isoforms to Sensory Cilium Middle and Distal Segments." *Nature Cell Biology* 13 (7): 790–98.
36. Hooper, J. K. 1989. "The Chlamydomonas Sourcebook. A Comprehensive Guide to Biology and Laboratory Use. Elizabeth H. Harris. Academic Press, San Diego, CA, 1989. Xiv, 780 Pp., Illus. \$145." *Science* 246 (4936): 1503–4.
37. Höög, Johanna L., Sylvain Lacombe, Eileen T. O'Toole, Andreas Hoenger, J. Richard McIntosh, and Keith Gull. 2014. "Modes of Flagellar Assembly in *Chlamydomonas Reinhardtii* and *Trypanosoma Brucei*." *eLife* 3 (January): e01479.

38. Iomini, C., V. Babaev-Khaimov, M. Sassaroli, and G. Piperno. 2001. "Protein Particles in Chlamydomonas Flagella Undergo a Transport Cycle Consisting of Four Phases." *The Journal of Cell Biology* 153 (1): 13–24.
39. Ishikawa, Hiroaki, Takahiro Ide, Toshiki Yagi, Xue Jiang, Masafumi Hirono, Hiroyuki Sasaki, Haruaki Yanagisawa, et al. 2014. "TTC26/DYF13 Is an Intraflagellar Transport Protein Required for Transport of Motility-Related Proteins into Flagella." *eLife* 3 (January): e01566.
40. Jarvik, Jonathan W., Frederick D. Reinhart, Michael R. Kuchka, and Sally A. Adler. 1984. "Altered Flagellar Size-Control Inshf-1 Short-Flagella Mutants of Chlamydomonas Reinhardtii." *The Journal of Protozoology* 31 (2): 199–204.
41. Jiang, Xue. 2017. "EUKARYOTIC FLAGELLAR ASSEMBLY: INSIGHTS LEARNED FROM INTRAFLAGELLAR TRANSPORT (IFT) AND SMALL GTPASE ARL3." Edited by Hongmin Qin. Microbiology, Texas A&M University. <https://oaktrust.library.tamu.edu/bitstream/handle/1969.1/161580/JIANG-DISSERTATION-2017.pdf?sequence=1&isAllowed=y>.
42. Johnson, K. A., and J. L. Rosenbaum. 1992. "Polarity of Flagellar Assembly in Chlamydomonas." *The Journal of Cell Biology* 119 (6): 1605–11.
43. Jones, D. T., W. R. Taylor, and J. M. Thornton. 1992. "The Rapid Generation of Mutation Data Matrices from Protein Sequences." *Computer Applications in the Biosciences: CABIOS* 8 (3): 275–82.
44. Kannegaard, Elisa, E. Hesper Rego, Sebastian Schuck, Jessica L. Feldman, and Wallace F. Marshall. 2014. "Quantitative Analysis and Modeling of Katanin Function in Flagellar Length Control." *Molecular Biology of the Cell* 25 (22): 3686–98.

45. Kathir, Pushpa, Matthew LaVoie, William J. Brazelton, Nancy A. Haas, Paul A. Lefebvre, and Carolyn D. Silflow. 2003. "Molecular Map of the Chlamydomonas Reinhardtii Nuclear Genome." *Eukaryotic Cell* 2 (2): 362–79.
46. Keller, L. R., J. A. Schloss, C. D. Silflow, and J. L. Rosenbaum. 1984. "Transcription of Alpha- and Beta-Tubulin Genes in Vitro in Isolated Chlamydomonas Reinhardtii Nuclei." *The Journal of Cell Biology* 98 (3): 1138–43.
47. Kozminski, K. G., K. A. Johnson, P. Forscher, and J. L. Rosenbaum. 1993. "A Motility in the Eukaryotic Flagellum Unrelated to Flagellar Beating." *Proceedings of the National Academy of Sciences of the United States of America* 90 (12): 5519–23.
48. Kubo, Tomohiro, Jason M. Brown, Karl Bellve, Branch Craige, Julie M. Craft, Kevin Fogarty, Karl F. Lehtreck, and George B. Witman. 2016. "Together, the IFT81 and IFT74 N-Termini Form the Main Module for Intraflagellar Transport of Tubulin." *Journal of Cell Science* 129 (10): 2106–19.
49. Kuchka, M. R., and J. W. Jarvik. 1987. "Short-Flagella Mutants of Chlamydomonas Reinhardtii." *Genetics* 115 (4): 685–91.
50. Kumar, Sudhir, Glen Stecher, Michael Li, Christina Knyaz, and Koichiro Tamura. 2018. "MEGA X: Molecular Evolutionary Genetics Analysis across Computing Platforms." *Molecular Biology and Evolution* 35 (6): 1547–49.
51. Latour, Brooke L., Julie C. Van De Weghe, Tamara Ds Rusterholz, Stef Jf Letteboer, Arianna Gomez, Ranad Shaheen, Matthias Gesemann, et al. 2020. "Dysfunction of the Ciliary ARMC9/TOGARAM1 Protein Module Causes Joubert Syndrome." *The Journal of Clinical Investigation* 130 (8): 4423–39.

52. Lefebvre, P. A., S. A. Nordstrom, J. E. Moulder, and J. L. Rosenbaum. 1978. "Flagellar Elongation and Shortening in Chlamydomonas. IV. Effects of Flagellar Detachment, Regeneration, and Resorption on the Induction of Flagellar Protein Synthesis." *The Journal of Cell Biology* 78 (1): 8–27.
53. Lefebvre, P. A., and J. L. Rosenbaum. 1986. "Regulation of the Synthesis and Assembly of Ciliary and Flagellar Proteins during Regeneration." *Annual Review of Cell Biology* 2: 517–46.
54. Li, Heng, and Richard Durbin. 2009. "Fast and Accurate Short Read Alignment with Burrows–Wheeler Transform." *Bioinformatics* 25 (14): 1754–60.
55. Li, Heng, Bob Handsaker, Alec Wysoker, Tim Fennell, Jue Ruan, Nils Homer, Gabor Marth, Goncalo Abecasis, Richard Durbin, and 1000 Genome Project Data Processing Subgroup. 2009. "The Sequence Alignment/Map Format and SAMtools." *Bioinformatics* 25 (16): 2078–79.
56. Lin, Huawen, Nicholas P. Nauman, Alison J. Albee, Silas Hsu, and Susan K. Dutcher. 2013. "New Mutations in Flagellar Motors Identified by Whole Genome Sequencing in Chlamydomonas." *Cilia* 2 (1): 14.
57. Li, Xiaobo, Weronika Patena, Friedrich Fauser, Robert E. Jinkerson, Shai Saroussi, Moritz T. Meyer, Nina Ivanova, et al. 2019. "A Genome-Wide Algal Mutant Library and Functional Screen Identifies Genes Required for Eukaryotic Photosynthesis." *Nature Genetics* 51 (4): 627–35.
58. Li, Xiaobo, Ru Zhang, Weronika Patena, Spencer S. Gang, Sean R. Blum, Nina Ivanova, Rebecca Yue, et al. 2016. "An Indexed, Mapped Mutant Library Enables Reverse Genetics

- Studies of Biological Processes in *Chlamydomonas Reinhardtii*.” *The Plant Cell* 28 (2): 367–87.
59. Louka, Panagiota, Krishna Kumar Vasudevan, Mayukh Guha, Ewa Joachimiak, Dorota Wloga, Raphaël F-X Tomasi, Charles N. Baroud, et al. 2018. “Proteins That Control the Geometry of Microtubules at the Ends of Cilia.” *The Journal of Cell Biology* 217 (12): 4298–4313.
60. Lucker, Ben F., Mark S. Miller, Slawomir A. Dziejczak, Philip T. Blackmarr, and Douglas G. Cole. 2010. “Direct Interactions of Intraflagellar Transport Complex B Proteins IFT88, IFT52, and IFT46.” *The Journal of Biological Chemistry* 285 (28): 21508–18.
61. Ludington, William B., Hiroaki Ishikawa, Yevgeniy V. Serebrenik, Alex Ritter, Rogelio A. Hernandez-Lopez, Julia Gunzenhauser, Elisa Kannegaard, and Wallace F. Marshall. 2015. “A Systematic Comparison of Mathematical Models for Inherent Measurement of Ciliary Length: How a Cell Can Measure Length and Volume.” *Biophysical Journal* 108 (6): 1361–79.
62. Ludington, William B., Kimberly A. Wemmer, Karl F. Lehtreck, George B. Witman, and Wallace F. Marshall. 2013. “Avalanche-like Behavior in Ciliary Import.” *Proceedings of the National Academy of Sciences of the United States of America* 110 (10): 3925–30.
63. Luo, Minna, Muqing Cao, Yinan Kan, Guihua Li, William Snell, and Junmin Pan. 2011. “The Phosphorylation State of an Aurora-like Kinase Marks the Length of Growing Flagella in *Chlamydomonas*.” *Current Biology: CB* 21 (7): 586–91.
64. Marshall, Wallace F., Hongmin Qin, Mónica Rodrigo Brenni, and Joel L. Rosenbaum. 2005. “Flagellar Length Control System: Testing a Simple Model Based on Intraflagellar Transport and Turnover.” *Molecular Biology of the Cell* 16 (1): 270–78.

65. Marshall, W. F., and J. L. Rosenbaum. 2001. "Intraflagellar Transport Balances Continuous Turnover of Outer Doublet Microtubules: Implications for Flagellar Length Control." *The Journal of Cell Biology* 155 (3): 405–14.
66. Matsuura, Kumi, Paul A. Lefebvre, Ritsu Kamiya, and Masafumi Hirono. 2002. "Kinesin-II Is Not Essential for Mitosis and Cell Growth in *Chlamydomonas*." *Cell Motility and the Cytoskeleton* 52 (4): 195–201.
67. McGuffin, L. J., K. Bryson, and D. T. Jones. 2000. "The PSIPRED Protein Structure Prediction Server." *Bioinformatics* 16 (4): 404–5.
68. McVittie, A. 1972. "Flagellum Mutants of *Chlamydomonas Reinhardtii*." *Journal of General Microbiology* 71 (3): 525–40.
69. Merchant, Sabeeha S., Simon E. Prochnik, Olivier Vallon, Elizabeth H. Harris, Steven J. Karpowicz, George B. Witman, Astrid Terry, et al. 2007. "The *Chlamydomonas* Genome Reveals the Evolution of Key Animal and Plant Functions." *Science* 318 (5848): 245–50.
70. Morbidoni, Valeria, Emanuele Agolini, Kevin C. Slep, Luca Pannone, Daniela Zuccarello, Matteo Cassina, Enrico Grosso, et al. 2020. "Biallelic Mutations in the TOGARAM1 Gene Cause a Novel Primary Ciliopathy." *Journal of Medical Genetics*, August. <https://doi.org/10.1136/jmedgenet-2020-106833>.
71. Nakamura, Shogo, Hiroyoshi Takino, and Manabu K. Kojima. 1987. "Effect of Lithium on Flagellar Length in *Chlamydomonas Reinhardtii*." *Cell Structure and Function*. <https://doi.org/10.1247/csf.12.369>.
72. Notredame, C., D. G. Higgins, and J. Heringa. 2000. "T-Coffee: A Novel Method for Fast and Accurate Multiple Sequence Alignment." *Journal of Molecular Biology* 302 (1): 205–17.

73. Pan, Junmin, Qian Wang, and William J. Snell. 2004. "An Aurora Kinase Is Essential for Flagellar Disassembly in *Chlamydomonas*." *Developmental Cell* 6 (3): 445–51.
74. Pazour, G. J., C. G. Wilkerson, and G. B. Witman. 1998. "A Dynein Light Chain Is Essential for the Retrograde Particle Movement of Intraflagellar Transport (IFT)." *The Journal of Cell Biology* 141 (4): 979–92.
75. Pazour, Gregory J., Nathan Agrin, John Leszyk, and George B. Witman. 2005. "Proteomic Analysis of a Eukaryotic Cilium." *The Journal of Cell Biology* 170 (1): 103–13.
76. Perlaza, Karina, Hannah Toutkoushian, Morgane Boone, Mable Lam, Masakazu Iwai, Martin C. Jonikas, Peter Walter, and Silvia Ramundo. 2019. "The Mars1 Kinase Confers Photoprotection through Signaling in the Chloroplast Unfolded Protein Response." *eLife* 8 (October). <https://doi.org/10.7554/eLife.49577>.
77. Piao, Tian, Minna Luo, Liang Wang, Yan Guo, De Li, Peng Li, William J. Snell, and Junmin Pan. 2009. "A Microtubule Depolymerizing Kinesin Functions during Both Flagellar Disassembly and Flagellar Assembly in *Chlamydomonas*." *Proceedings of the National Academy of Sciences of the United States of America* 106 (12): 4713–18.
78. Qasim Rasi, M., Jeremy D. K. Parker, Jessica L. Feldman, Wallace F. Marshall, and Lynne M. Quarmby. 2009. "Katanin Knockdown Supports a Role for Microtubule Severing in Release of Basal Bodies before Mitosis in." *Vol.* 20: 379–88.
79. Rasala, Beth A., Daniel J. Barrera, Jenny Ng, Thomas M. Plucinak, Julian N. Rosenberg, Donald P. Weeks, George A. Oyler, Todd C. Peterson, Farzad Haerizadeh, and Stephen P. Mayfield. 2013. "Expanding the Spectral Palette of Fluorescent Proteins for the Green Microalga *Chlamydomonas Reinhardtii*." *The Plant Journal: For Cell and Molecular Biology* 74 (4): 545–56.

80. Rezabkova, Lenka, Sebastian H. W. Kraatz, Anna Akhmanova, Michel O. Steinmetz, and Richard A. Kammerer. 2016. "Biophysical and Structural Characterization of the Centriolar Protein Cep104 Interaction Network." *The Journal of Biological Chemistry* 291 (35): 18496–504.
81. Rosenbaum, J. L., and F. M. Child. 1967. "Flagellar Regeneration in Protozoan Flagellates." *The Journal of Cell Biology* 34 (1): 345–64.
82. Rosenbaum, J. L., J. E. Moulder, and D. L. Ringo. 1969. "Flagellar Elongation and Shortening in Chlamydomonas. The Use of Cycloheximide and Colchicine to Study the Synthesis and Assembly of Flagellar Proteins." *The Journal of Cell Biology* 41 (2): 600–619.
83. Satish Tammana, Trinadh V., Damayanti Tammana, Dennis R. Diener, and Joel Rosenbaum. 2013. "Centrosomal Protein CEP104 (Chlamydomonas FAP256) Moves to the Ciliary Tip during Ciliary Assembly." *Journal of Cell Science* 126 (Pt 21): 5018–29.
84. Schierenbeck, Lisa, David Ries, Kristin Rogge, Sabrina Grewe, Bernd Weisshaar, and Olaf Kruse. 2015. "Fast Forward Genetics to Identify Mutations Causing a High Light Tolerant Phenotype in Chlamydomonas Reinhardtii by Whole-Genome-Sequencing." *BMC Genomics* 16 (February): 57.
85. Schindelin, Johannes, Ignacio Arganda-Carreras, Erwin Frise, Verena Kaynig, Mark Longair, Tobias Pietzsch, Stephan Preibisch, et al. 2012. "Fiji: An Open-Source Platform for Biological-Image Analysis." *Nature Methods* 9 (7): 676–82.
86. Slep, Kevin C. 2018. "A Cytoskeletal Symphony: Owed to TOG." *Developmental Cell*.
87. Slep, Kevin C., and Ronald D. Vale. 2007. "Structural Basis of Microtubule plus End Tracking by XMAP215, CLIP-170, and EB1." *Molecular Cell* 27 (6): 976–91.

88. Song, L., and W. L. Dentler. 2001. "Flagellar Protein Dynamics in Chlamydomonas." *The Journal of Biological Chemistry* 276 (32): 29754–63.
89. Stolc, Viktor, Manoj Pratim Samanta, Waraporn Tongprasit, and Wallace F. Marshall. 2005. "Genome-Wide Transcriptional Analysis of Flagellar Regeneration in Chlamydomonas Reinhardtii Identifies Orthologs of Ciliary Disease Genes." *Proceedings of the National Academy of Sciences of the United States of America* 102 (10): 3703–7.
90. Tam, Lai-Wa, William L. Dentler, and Paul A. Lefebvre. 2003. "Defective Flagellar Assembly and Length Regulation in LF3 Null Mutants in Chlamydomonas." *The Journal of Cell Biology* 163 (3): 597–607.
91. Tam, Lai-Wa, Paul T. Ranum, and Paul A. Lefebvre. 2013. "CDKL5 Regulates Flagellar Length and Localizes to the Base of the Flagella in Chlamydomonas." *Molecular Biology of the Cell* 24 (5): 588–600.
92. Tam, Lai-Wa, Nedra F. Wilson, and Paul A. Lefebvre. 2007. "A CDK-Related Kinase Regulates the Length and Assembly of Flagella in Chlamydomonas." *The Journal of Cell Biology* 176 (6): 819–29.
93. Taschner, Michael, Kristina Weber, André Mourão, Melanie Vetter, Mayanka Awasthi, Marc Stiegler, Sagar Bhogaraju, and Esben Lorentzen. 2016. "Intraflagellar Transport Proteins 172, 80, 57, 54, 38, and 20 Form a Stable Tubulin-Binding IFT-B2 Complex." *The EMBO Journal* 35 (7): 773–90.
94. Thorvaldsdottir, H., J. T. Robinson, and J. P. Mesirov. 2013. "Integrative Genomics Viewer (IGV): High-Performance Genomics Data Visualization and Exploration." *Briefings in Bioinformatics*. <https://doi.org/10.1093/bib/bbs017>.

95. Wang, Hongxia, Brian Gau, William O. Slade, Matthew Juergens, Ping Li, and Leslie M. Hicks. 2014. "The Global Phosphoproteome of *Chlamydomonas Reinhardtii* Reveals Complex Organellar Phosphorylation in the Flagella and Thylakoid Membrane." *Molecular & Cellular Proteomics: MCP* 13 (9): 2337–53.
96. Wang, Liang, Tian Piao, Muqing Cao, Tao Qin, Lei Huang, Haiteng Deng, Tonglin Mao, and Junmin Pan. 2013. "Flagellar Regeneration Requires Cytoplasmic Microtubule Depolymerization and Kinesin-13." *Journal of Cell Science* 126 (Pt 6): 1531–40.
97. Weghe, Julie Craft Van De, Julie Craft Van De Weghe, J. Aaron Harris, Tomohiro Kubo, George B. Witman, and Karl F. Lehtreck. 2020. "Diffusion rather than IFT Likely Provides Most of the Tubulin Required for Axonemal Assembly." *Journal of Cell Science*. <https://doi.org/10.1242/jcs.249805>.
98. Wemmer, Kimberly A., and Wallace F. Marshall. 2007. "Flagellar Length Control in *Chlamydomonas*--Paradigm for Organelle Size Regulation." *International Review of Cytology* 260: 175–212.
99. Wemmer, Kimberly, William Ludington, and Wallace F. Marshall. 2020. "Testing the Role of Intraflagellar Transport in Flagellar Length Control Using Length-Altering Mutants of *Chlamydomonas*." *Philosophical Transactions of the Royal Society of London. Series B, Biological Sciences* 375 (1792): 20190159.
100. Wilson, Nedra F., and Paul A. Lefebvre. 2004. "Regulation of Flagellar Assembly by Glycogen Synthase Kinase 3 in *Chlamydomonas Reinhardtii*." *Eukaryotic Cell* 3 (5): 1307–19.
101. Witman, G. B. 1975. "The Site of in Vivo Assembly of Flagellar Microtubules." *Annals of the New York Academy of Sciences* 253 (June): 178–91.

102. Wood, Christopher R., Zhaohui Wang, Dennis Diener, James Matt Zones, Joel Rosenbaum, and James G. Umen. 2012. "IFT Proteins Accumulate during Cell Division and Localize to the Cleavage Furrow in *Chlamydomonas*." *PloS One* 7 (2): e30729.
103. Wren, Kathryne N., Julie M. Craft, Douglas Tritschler, Alexandria Schauer, Deep K. Patel, Elizabeth F. Smith, Mary E. Porter, Peter Kner, and Karl F. Lehtreck. 2013. "A Differential Cargo-Loading Model of Ciliary Length Regulation by IFT." *Current Biology: CB* 23 (24): 2463–71.
104. Yamano, Takashi, Hiro Iguchi, and Hideya Fukuzawa. 2013. "Rapid Transformation of *Chlamydomonas Reinhardtii* without Cell-Wall Removal." *Journal of Bioscience and Bioengineering* 115 (6): 691–94.
105. Ye, Kai, Marcel H. Schulz, Quan Long, Rolf Apweiler, and Zemin Ning. 2009. "Pindel: A Pattern Growth Approach to Detect Break Points of Large Deletions and Medium Sized Insertions from Paired-End Short Reads." *Bioinformatics* 25 (21): 2865–71.
106. Yuan, Shialou, Jade Li, Dennis R. Diener, Michael A. Choma, Joel L. Rosenbaum, and Zhaoxia Sun. 2012. "Target-of-Rapamycin Complex 1 (Torc1) Signaling Modulates Cilia Size and Function through Protein Synthesis Regulation." *Proceedings of the National Academy of Sciences of the United States of America* 109 (6): 2021–26.
107. Zones, James Matt, Ian K. Blaby, Sabeeha S. Merchant, and James G. Umen. 2015. "High-Resolution Profiling of a Synchronized Diurnal Transcriptome from *Chlamydomonas Reinhardtii* Reveals Continuous Cell and Metabolic Differentiation." *The Plant Cell* 27 (10): 2743–69.

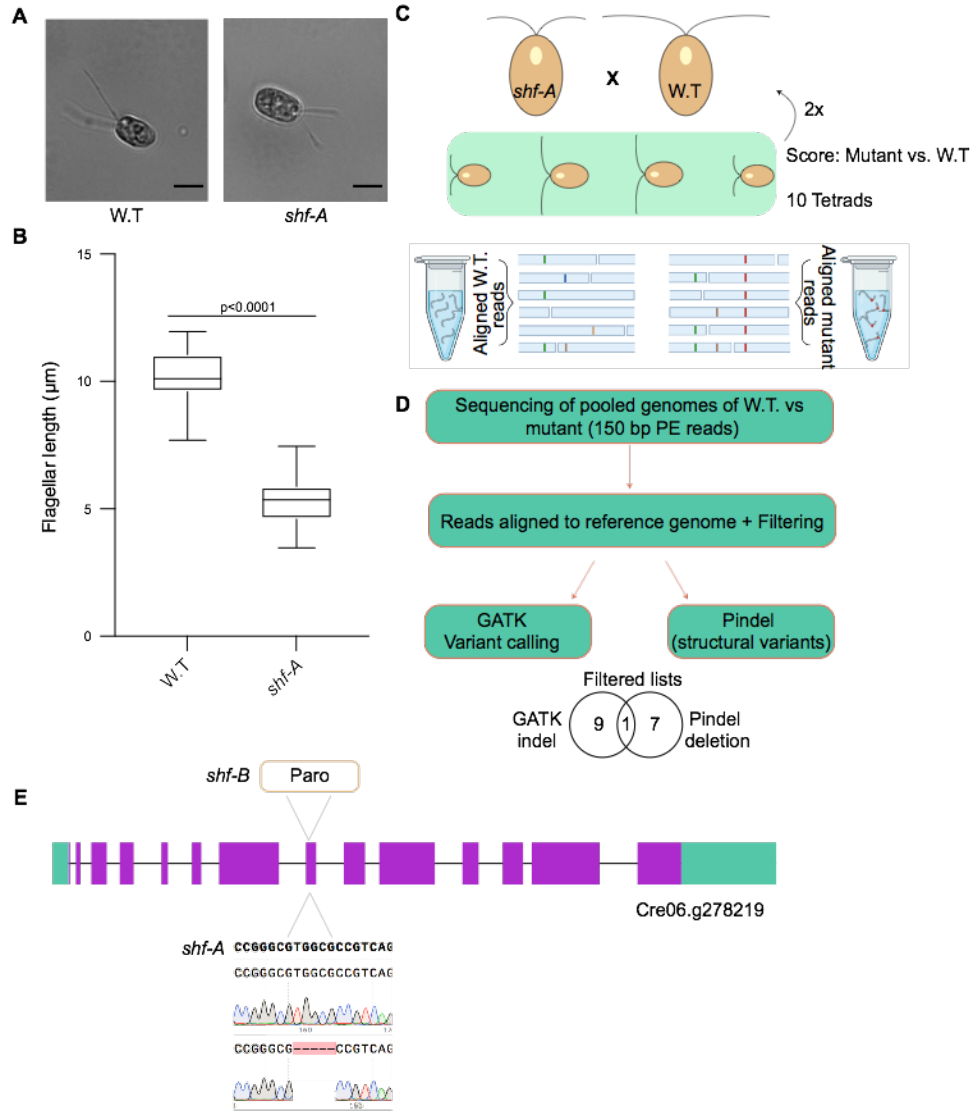


Figure 2-1. Discovery of gene lesion resulting in short-flagellar phenotype.

(A) Representative DIC images of Wild-type (W.T: cc125) and *shf-A* Chlamydomonas cells. Scale bar: 5 μ m. (B) A box and whisker plot displaying flagellar length data for W.T (n=48) and *shf-A* (n=54) fixed cells. An unpaired *t*-test was conducted to determine the *P*-value ($p < 0.0001$). (C) A schematic showing our approach to discover the genetic lesion underpinning the short-flagellar phenotype. *shf-A* (mt -) was backcrossed to cc125 (mt +), then an *shf*- exhibiting offspring spore from this first cross was used to backcross once more to cc125. The spores from tetrads and octads were scored for *shf* vs W.T flagella lengths and separated into two different genomic DNA pools to enrich for the allele of interest. (D) Schematic describing the bioinformatic workflow for the mutational analysis. PE: Paired end, GATK: Genome Analysis Toolkit. (E) The diagram depicts the Cre06.g278219 gene with the green outermost boxes representing the 5' untranslated region (5'UTR) and the 3' untranslated region (3'UTR) from left to right, respectively. The purple boxes represent the exons and the connecting black lines are the introns. The 5 base pair deletion site for *shf-a* is shown through the Sanger Sequencing chromatogram whereas the insertion site of the mutagenic cassette (PARO) is indicated for the *shf-B* allele.

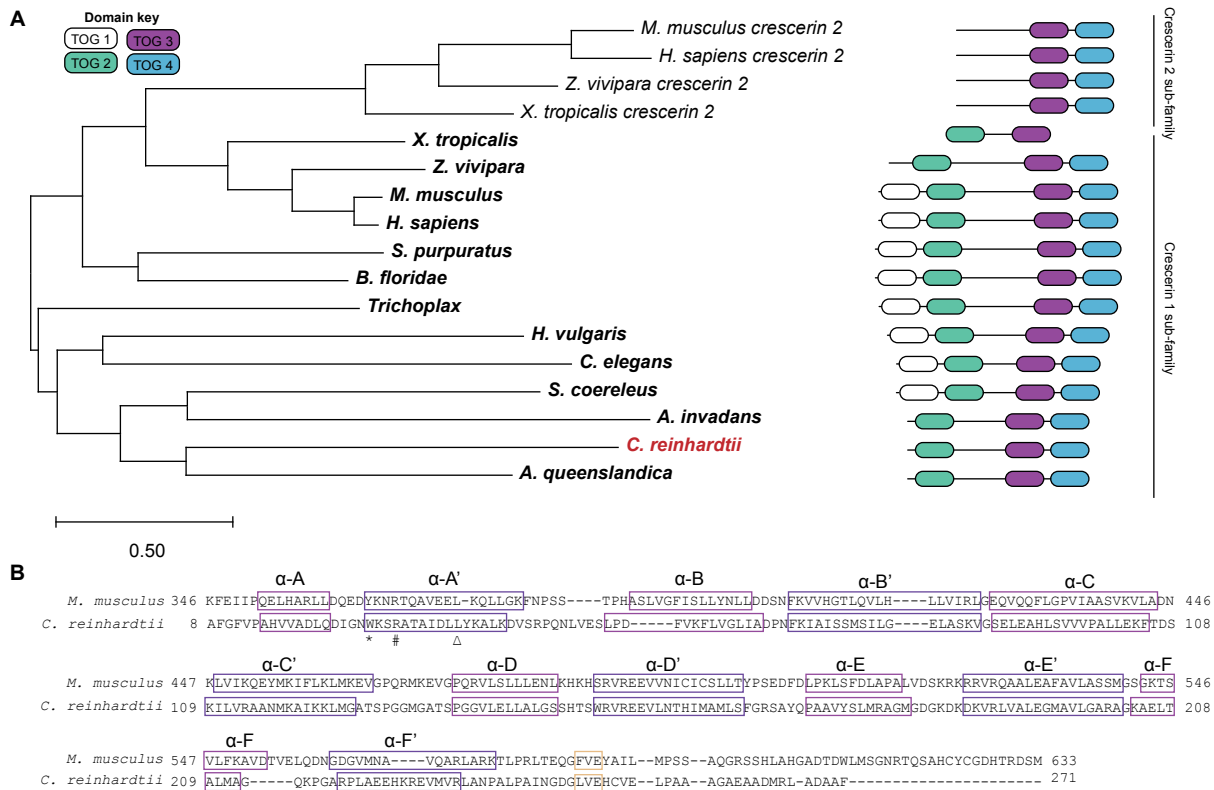


Figure 2-2. Cre06.g278219 encodes a conserved TOG-domain array protein.

(A) The left side shows a cladogram depicting the relationships between Crescerin subfamilies. The tree is drawn to scale, with branch lengths measured in the number of substitutions per site. The right side are the corresponding domain architectures for each organism. Each of the organisms' predicted domain structure and architecture are compared to the human TOG domains with all TOG domains and unstructured regions scaled to the human TOG domain array-containing protein. TOG domains 1 through 4 are color coded as shown in the top left-side corner under the domain key. Supplemental Table 1, sheet 3 contains the NCBI sequence identifiers for the Crescerin homologues used in this tree. (B) An amino acid sequence alignment of the Crescerin 1 TOG2 domain of *M.musculus* and *C.reinhardtii* shows the archetypical structure of the TOG domain with six HEAT repeats (A-F) each containing a highly conserved alpha helical fold. The *m. musculus* crystal structure from Das et al., 2015 was used to demarcate the alpha helices in purple outlined rectangles whereas a structural prediction program, PSIPRED, was used for the *C.reinhardtii* sequence. The yellow box highlights part of a unique feature of the Crescerin protein that differentiates it from other TOG-domain proteins. It is a stretch of amino acids that is important for forming a Beta- hairpin, a structure that helps promote domain stability (Das et al. 2015). The residue number for each Crescerin sequence is shown to the left of the residues. The following are descriptions of variants found to be crucial for the protein's function and highlighted to point out that the *C.reinhardtii* homologue contains all of these conserved features. An asterisk (*) underneath the sequence alignment indicates a conserved residue critical for binding to tubulin in both Crescerin (Das et al. 2015) and in other TOG-domain array proteins like CLASP and XMAP215 (Al-Bassam and Chang 2011). The pound sign (#) underneath the sequence alignment indicates a residue which was found to be mutated in ciliopathies (Latour et al. 2020; Morbidoni et al. 2020). Lastly, the triangle (Δ) underneath the sequence alignment highlights a residue found mutated in Joubert syndrome ciliopathy patients.

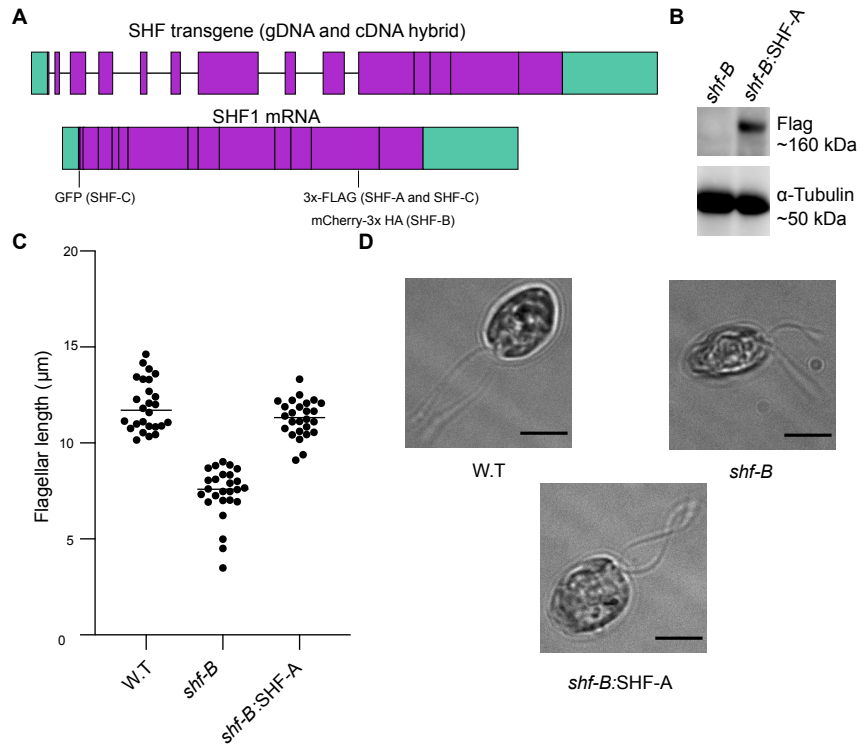


Figure 2-3. Expression of Crescerin transgene leads to rescue of short-flagellar phenotype.

(A) The top panel shows the SHF transgene, a genomic DNA (gDNA) and complementary DNA (cDNA) hybrid, engineered for complementation efforts. The left green outermost rectangle depicts the 5' untranslated region (UTR) whereas the right green outermost rectangle is the 3' UTR. The first part of the transgene contains exons and introns 1 through 9 and the rest of the transgene is strictly exonic regions 10 through 16. In both the top and bottom panel, the horizontal lines demarcate the exon boundaries. The bottom panel shows the SHF coding region and the different variety of transgenes used in this study: SHF-A, SHF-B, and SHF-C. The positions of the epitopes and/or fluorescent proteins for the different transgene constructs are shown. The 3x-flag epitope in SHF-A and SHF-C, mCherry-3xHA in SHF-B and the GFP in SHF-C. (B) An immunoblot analysis of samples prepared from strains *shf-B* and *shf-B:SHF-A*, a transformant selected for its W.T-like length. Detection was done with antibodies against Flag (SHF-A), and alpha-Tubulin (loading control). (C) Flagellar lengths were measured for each strain (n=26) grown in TAP media. The horizontal line represents the median length of each strain. (D) Representative D.I.C images of the following strains: W.T, *shf-B*, and *shf-B:SHF-A*. Scale bar: 5 μm .

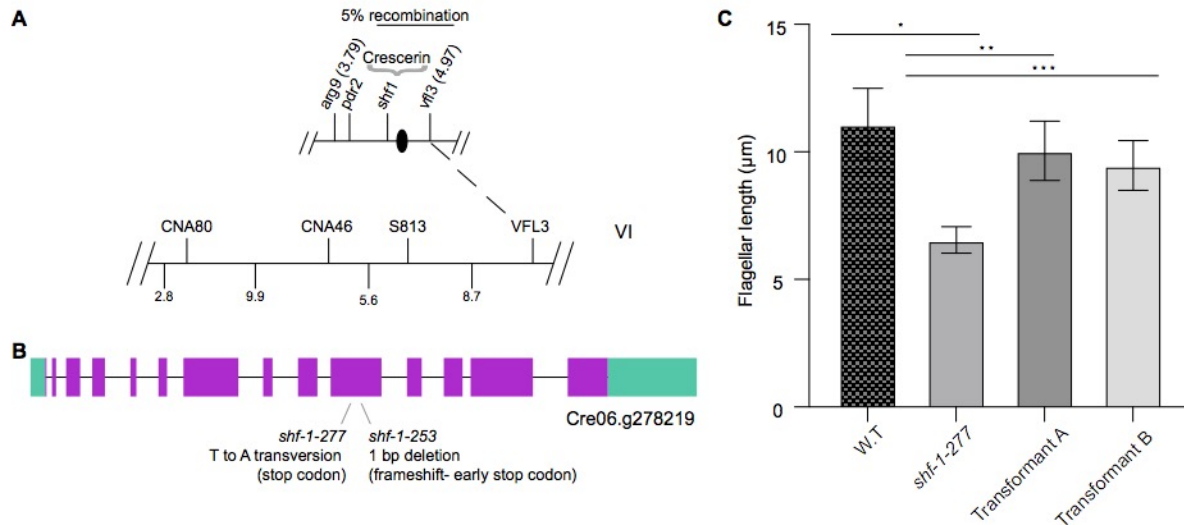


Figure 2-4. The previously identified SHF1 gene is encoded by Crescerin/Cre06.g278219.

(A) Genetic map position of the SHF1 gene. The genetic map of linkage group VI (redrawn from (Hooper 1989; Kathir et al. 2003). is shown on the top with the centromere represented by the black oval. The scale bar showing the percentage of recombination is above the genetic map. The starting base pair position (million) for genetic markers *arg9* and *vfl3* is indicated in parenthesis. The predicted relative location of the Crescerin gene is indicated. For reference, the Crescerin gene begins at position 4.08 (million) of Chromosome 6. The molecular map is shown on the bottom with the vertical lines indicating centimorgans; it is estimated that 1 centimorgan is equivalent to ~100,000 base pairs. The dashed line connecting the genetic and molecular map indicates a molecular marker corresponding directly to a previously mapped phenotypic marker. (B) The full Cre06.g278219 gene with exons in rectangles and introns as the connecting lines. Both the *shf-1-277* and *shf-1-253* alleles are indicated. (C) The mean flagellar lengths of W.T, *shf-1-277*, and two strains (Transformant A and Transformant B) selected for their W.T-like length after transformation with the SHF-C genetic construct. An unpaired T-test was conducted for the following pairs, * *shf-1-277* and W.T $p < 0.0001$, ** *shf-1-277* and Transformant A, *** *shf-1-277* and Transformant B $p < 0.0001$.

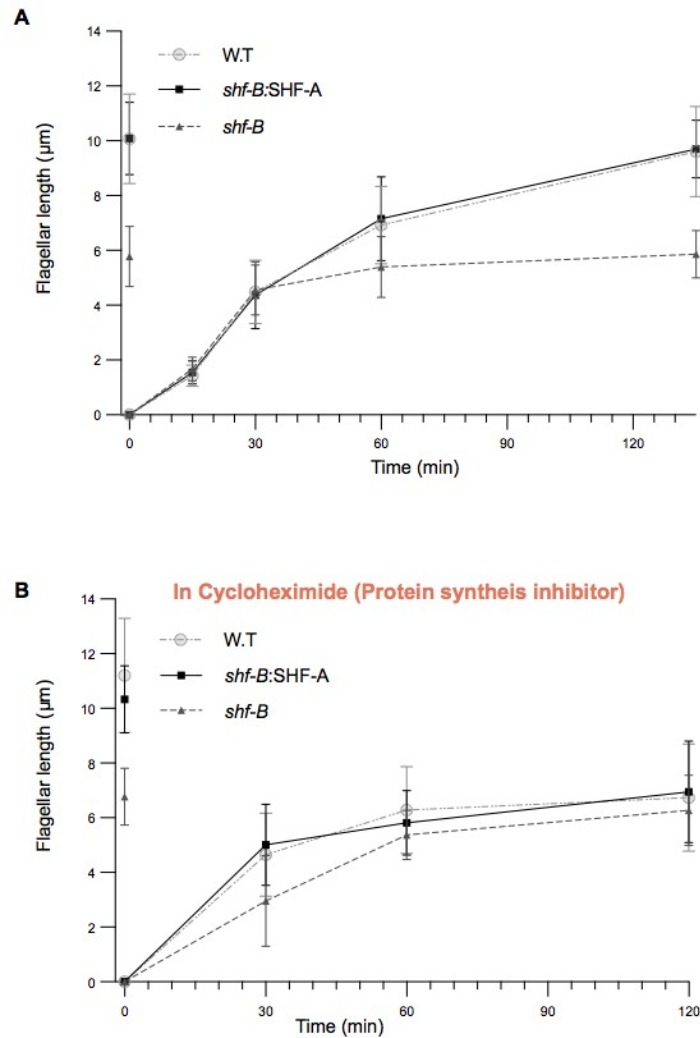


Figure 2-5. The *shf-B* mutant regenerates with similar early kinetics as W.T and has a precursor pool size similar to W.T.

(A) A pH shock-induced flagellar length regeneration curve for cells grown in TAP media and in (B) the presence of cycloheximide is shown for W.T, *shf-B*, and *shf-B:SHF-A* strains. Pre-deflagellation lengths are shown before the 0 minute time mark. The mean and error bars depicting the standard deviation are plotted with an $n \geq 49$ for each time point, strain, and treatment.

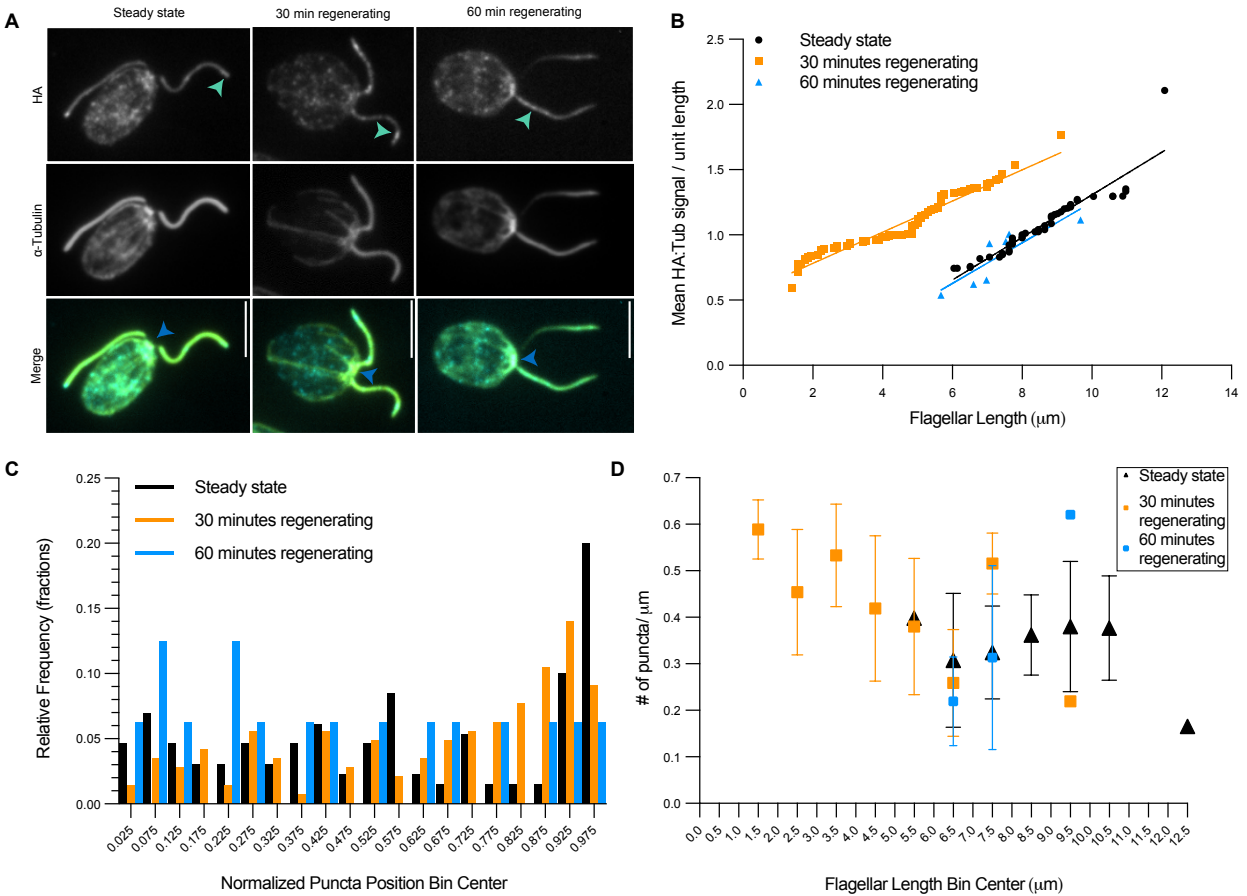


Figure 2-6. Localization of HA-Crescerin/SHF1 and tubulin within flagella during regeneration.

(A) Mutant strains complemented with HA-Crescerin/SHF1 were fixed at steady state (pre-deflagellation) or during regeneration at 30 or 60-minutes post-pH shock, immunostained against HA-Crescerin/SHF1 and α -tubulin, and displayed as a sum-slices z-projection. The light green arrowheads show examples of puncta within the flagella whereas the blue arrowheads show accumulation of HA-Crescerin/SHF1 at the base of the flagella. (B-E) Intensity line scans for each channel were taken from flagellar base to tip. Puncta were identified by thresholds described in Materials & Methods. B) Scatter Plot of mean HA:TUB intensity per unit length vs. length of each flagellum (1 data point is 1 flagellum). Steady-state: 47 flagella, 30 minutes regenerating: 78 flagella, 60 minutes regenerating: 7 flagella. C) A relative frequency distribution plot of the location of all puncta within the flagella that were identified in steady state flagella and flagella regenerating for 30 and 60 minutes. Puncta location is normalized to the measured flagellar length. Steady state: 130 puncta, 30 minutes regenerating: 143 puncta, 60 minutes regenerating: 16 puncta. The bin size is 0.05. D) The mean and standard deviation of the number (#) of puncta per μm of flagella was plotted against the measured flagellar length for steady state flagella and flagella regenerating for 30 and 60 minutes. The bin size is 1 μm .

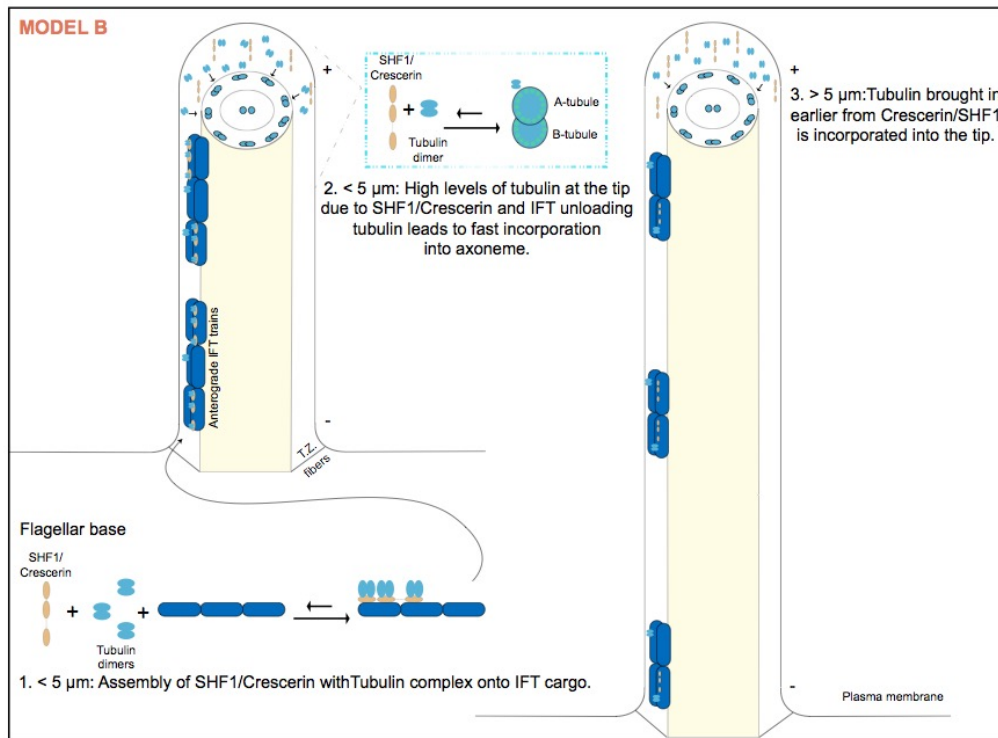
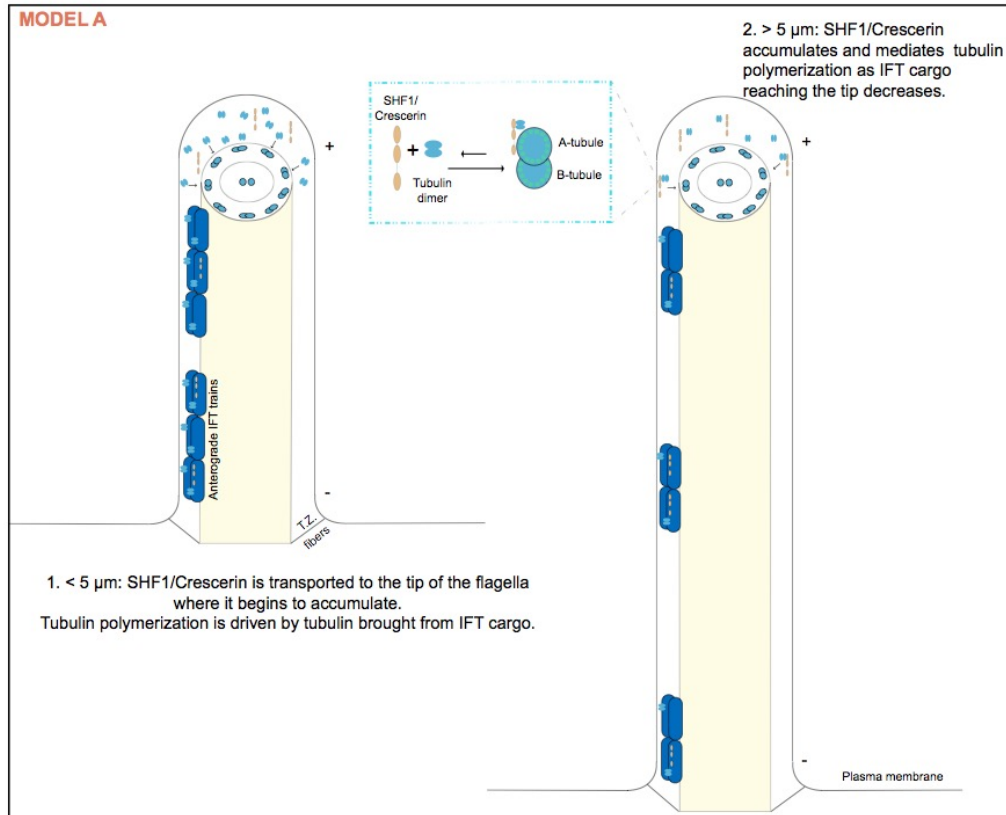


Figure 2-7. Two hypothesized mechanisms for how Crescerin/SHF1 could regulate flagellar length.

(A) Model A. In the early stages of regeneration, flagella have anterograde IFT trains that are large in size and that frequently reach the tip. This would lead to a readily available tubulin pool at the tip of the

flagella. As flagellar regeneration continues, IFT train size decreases as does the frequency of trains reaching the plus ends. If the tubulin concentration dips below the critical concentration for self-polymerization, Crescerin/SHF1 would become crucial for accelerating polymerization and decreasing the effective tubulin concentration necessary for polymerization. (B) Model B. In the early stages of regeneration, the TOG domains of Crescerin/SHF1 bind to tubulin and load onto the IFT trains. This Crescerin/SHF1 + tubulin cargo would increase the amount of tubulin at the tip compared to if IFT molecules were the exclusive partner of tubulin. During these early stages, the axonemal growth rate is at its maximum because the amount of tubulin reaching the tip is in excess. In this model, Crescerin/SHF1 acts preemptively by substantially increasing the concentration of tubulin at the tip to allow for growth at later stages when IFT trains reaching the tip start to decline.

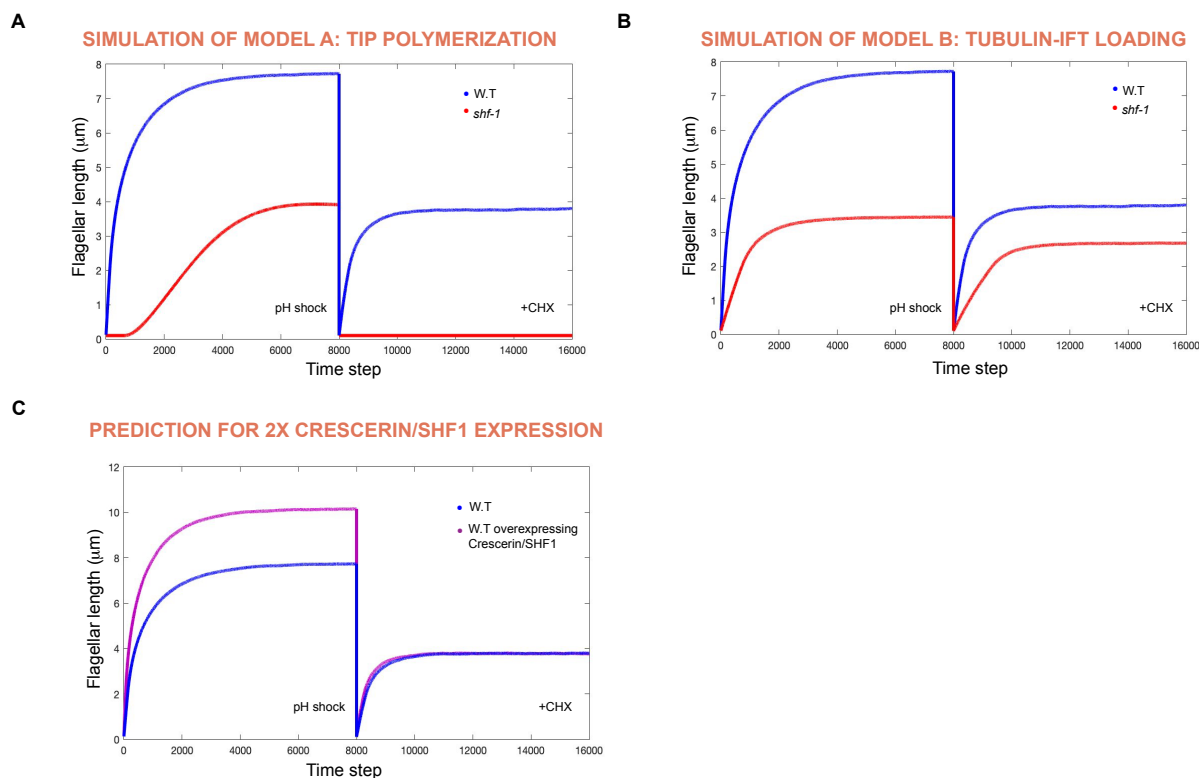


Figure 2-8. The modeling simulations of regeneration kinetics in W.T and the *shf-1* mutant fit best with Model B: Tubulin-IFT loading.

(A-B) The model simulations represents a case where the flagellum is allowed to grow out from zero length until it reaches steady state (left on the graph) and then the flagellum is removed once more and allowed to regrow (right on the graph). The right side is analogous to the cycloheximide experiment (+CHX) because it uses the pool of unassembled components in the cell-body that remained after the recent flagellar assembly. (A) The sole parameter that changed between W.T and *shf-1* is the elongation rate of the microtubule as a function of tubulin concentration inside the flagella. In this scenario, the flagellum length of the *shf-1* mutant reflects the ~2-fold decrease compared to W.T experimental values (left side), however, it is incapable of re-growing in the +CHX simulation (right side). (B) Two parameters were altered to allow for the differences between W.T and the *shf-1* mutant. First, the dissociation constant of the IFT particles for capturing tubulin was increased two-fold in the mutant. Second, the constant describing the number of IFT particles and effective cargo-carrying capacity was decreased two-fold in the mutant. In this scenario, the flagellum length difference between W.T and *shf-1* mutant reflects the experimental values (left side) and the +CHX simulation shows that the *shf-1* mutant is capable of regenerating to ~78% of its pre-deflagellation length (right side) which is similar to the experimental results shown in Figure 5B and Supplementary Figure 3C. (C) This model simulates the regeneration curve of W.T and a strain that has two-fold overexpression of Crescerin/SHF1. In this simulation, the constant describing the number of IFT particles and effective cargo-carrying capacity was increased two-fold relative to W.T.

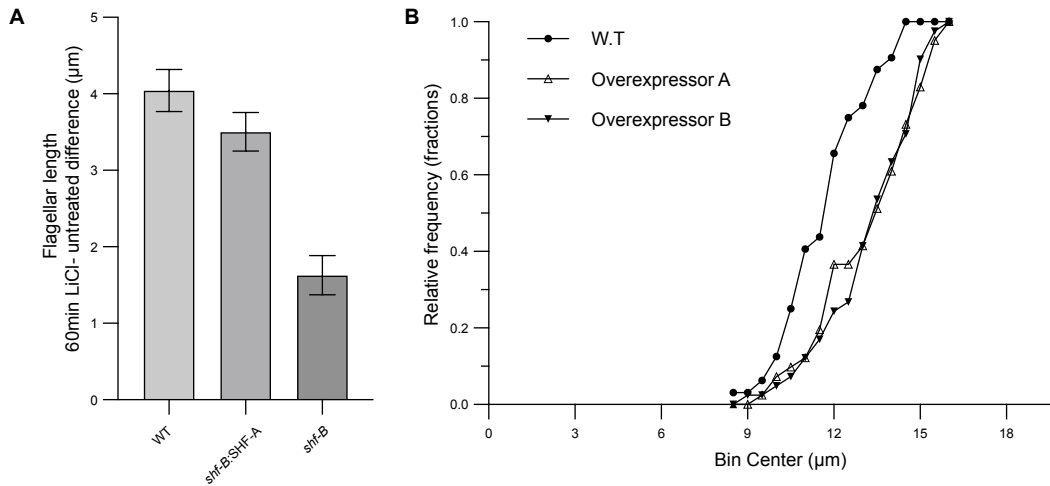


Figure 2-9. Crescerin/SHF1 is important for growth from longer lengths.

(A) The flagellar length mean difference between cells grown for 60 minutes in the presence of LiCl and untreated cells is shown for W.T, *shf-B:SHF-A*, and *shf-B*. The error bars are the standard error for the difference between the two means. (B) Steady-state flagella of W.T (cc5325) cells (n=32), and W.T cells expressing the SHF-B construct, Overexpressor A (n=41) and Overexpressor B (n=41), were measured and plotted as a cumulative frequency graph. A Kolmogorov- Smirnov test was performed between the following pairs: W.T and Overexpressor A ($p=0.0055$); W.T and Overexpressor B ($p=0.0005$).

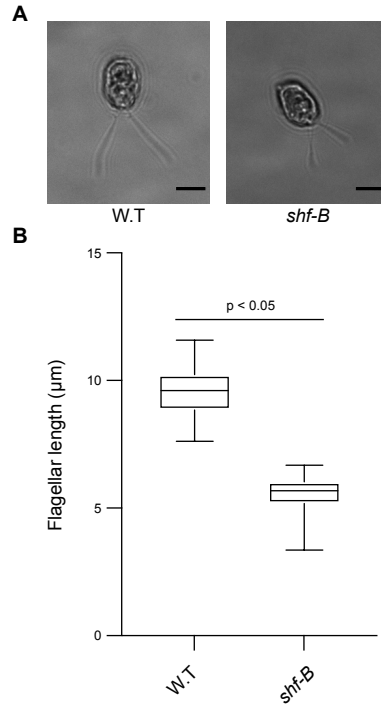


Figure 2-1S1. Discovery of gene lesion resulting in short-flagellar phenotype (related to Figure (1)).

(A) Representative DIC images of Wild-type (W.T: cc5325) and *shf-B* Chlamydomonas cells. Scale bar: 5 µm. (B) A box and whisker plot displaying flagellar length data for W.T (n=119) and *shf-B* (n=107) fixed cells. An unpaired *t*-test was conducted to determine the *P*-value ($p < 0.05$).

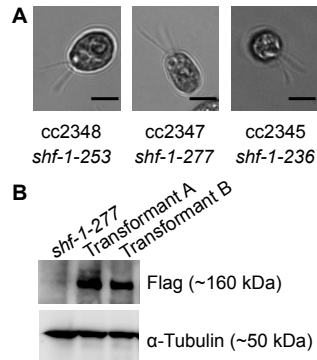


Figure 2-4S1. The previously identified SHF1 gene is encoded by Crescerin/Cre06.g278219 (related to Figure (4)).

(A) DIC images of the SHF1 mutants, *shf-1-253*, *shf-1-277* and *shf-1-236*, first described in Jarvik *et al.*, 1984; Kuchka and Jarvik., 1987. (B) An immunoblot analysis of samples prepared from strains *shf-1-277* and two transformants, Transformant A and Transformant B, in the *shf-1-277* background expressing the SHF-C construct. Detection was done with antibodies against Flag (SHF-C), and alpha-Tubulin (loading control).

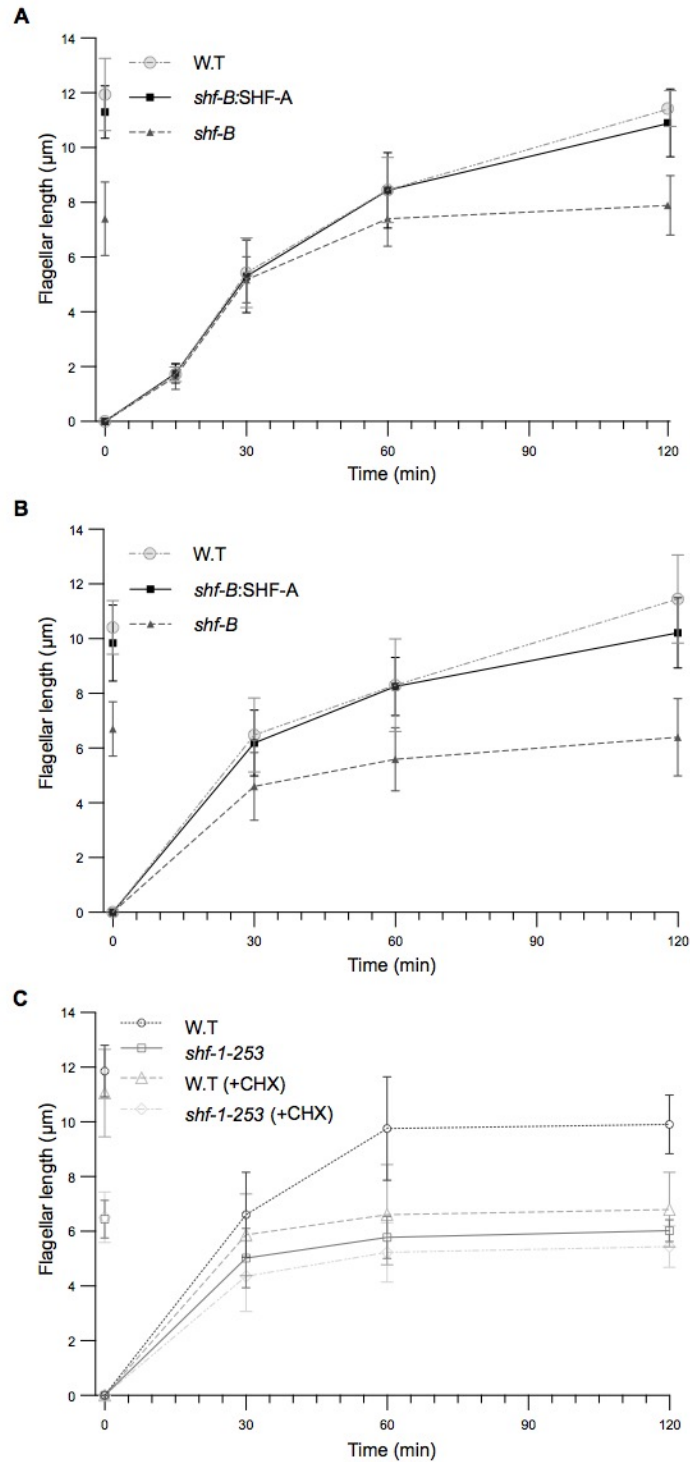


Figure 2-5S1 The *shf-B* and *shf-1* mutant regenerate with similar early kinetics as W.T and have precursor pool sizes similar to W.T (related to Figure (5)).

(A) pH shock-induced flagellar regeneration curves for a separate (independent from the main figure experiment) experiment for cells grown in TAP media is shown for W.T, *shf-B*, and *shf-B*:SHF-A strains. The mean and error bars depicting the standard deviation are plotted with an $n \geq 25$ for each time point, strain, and treatment. Pre-deflagellation lengths are shown before the 0 minute time mark (B) pH

shock-induced flagellar regeneration curves for the same cultures as in Figure 5B with the exception that cycloheximide treatment was not used, only vehicle control, water. Pre-deflagellation lengths are shown before the 0 minute time mark. The mean and error bars depicting the standard deviation are plotted with an $n \geq 19$ for each time point, strain, and treatment. (C) A different set of alleles, W.T and *shf-1-253*, were tested to validate the pool size result seen in the *shf-B* background. pH shock-induced flagellar regeneration curves for these two stains in the presence and absence of cycloheximide (CHX) is shown. Pre-deflagellation lengths are shown before the 0 minute time mark. The mean and error bars depicting the standard deviation are plotted with an $n \geq 19$ for each time point and strain for the vehicle control samples and an $n \geq 25$ for each time point and strain for the cycloheximide treated samples.

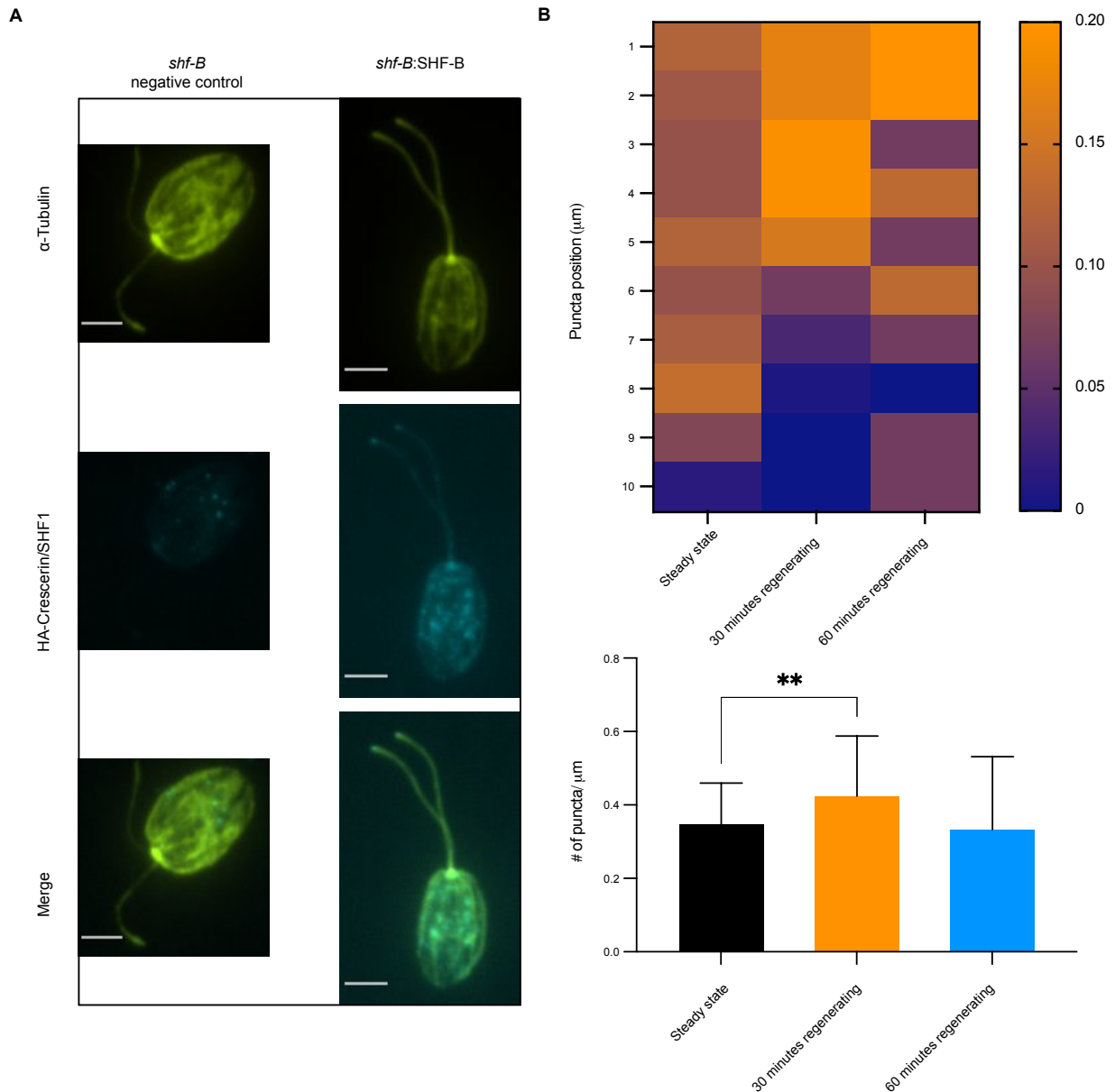


Figure 2-6S1. Localization of HA-Crescerin/SHF1 and tubulin within flagella during regeneration (related to Figure (6)).

(A) Steady state *shf-B* and *shf-B:SHF-B* cells were immunostained against HA-Crescerin/SHF1 and α -tubulin, and displayed as an average intensity z-stack projection. The *shf-B* acted as a negative control. Scale bar: 3 μ m. (B) A heatmap showing the relative frequency of the location of the puncta within the flagella of steady state and regenerating (30 minutes and 60 minutes) cells. (C) The mean puncta per μ m of flagella and standard deviation for all three conditions. ** highlights an unpaired *t*-test comparing 30 minutes regenerating and steady-state flagella was conducted to determine the *P*-value ($p=0.0068$). None of the other pair-wise comparisons were statically significant.

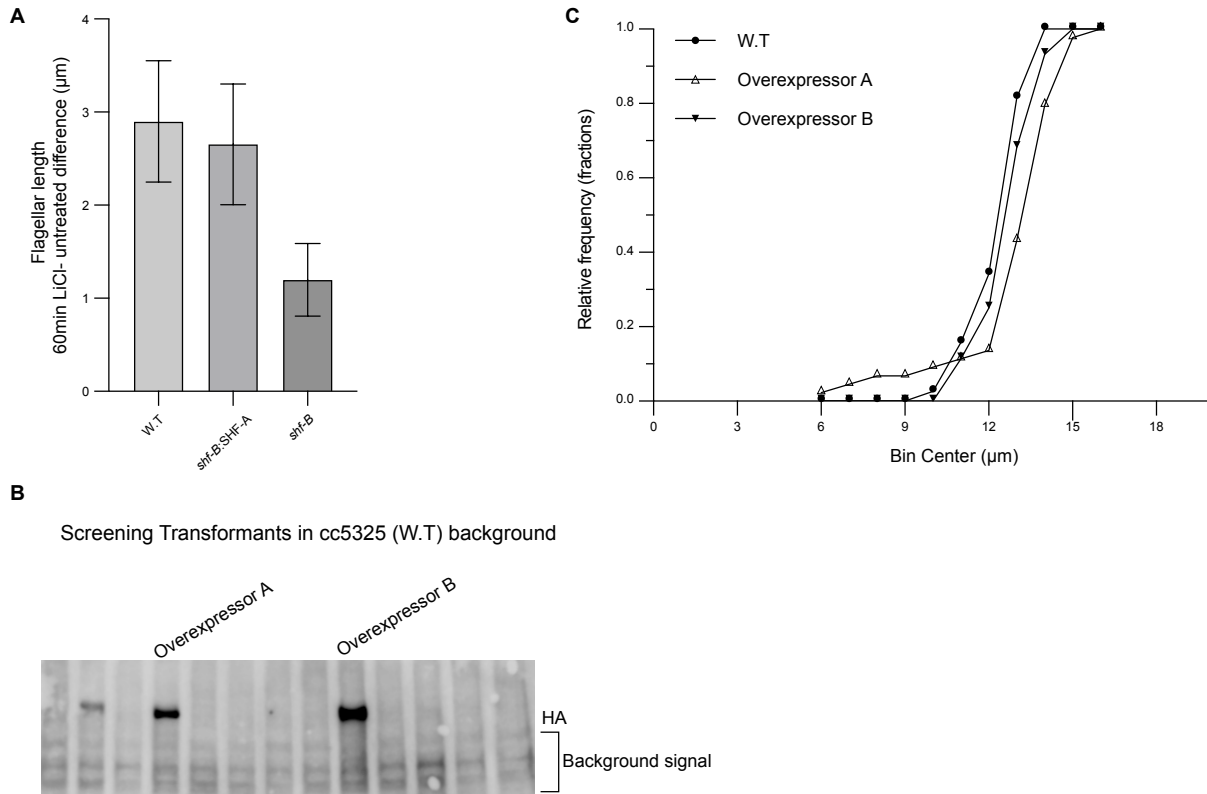


Figure 2-9S1. Crescerin/SHF1 is important for growth from longer lengths (related to Figure (9)).

(A) A separate (independent from the main figure experiment) experiment showing the flagellar length mean difference between cells grown for 60 minutes in the presence of LiCl and untreated cells was done on W.T, *shf-B:SHF-A*, and *shf-B*. The error bars are the standard error for the difference between the two means. Following transformation with the SHF-B construct in the W.T (*cc5325*) background, random Hygromycin resistant spores were screened for by checking HA expression through immunoblot analysis. Two transformants, Overexpressor A and Overexpressor B, were selected for further analysis. (B) Following transformation with the SHF-B construct in the W.T (*cc5325*) background, random Hygromycin resistant spores were screened for by checking HA expression through immunoblot analysis. Two transformants, Overexpressor A and Overexpressor B, were selected for further analysis. (C) A separate (independent from the main figure experiment) experiment was done on W.T (*cc5325*) cells ($n=38$), and W.T cells expressing the SHF-B construct, Overexpressor A ($n=44$) and Overexpressor B ($n=44$), to measure the steady-state flagella length to produce the cumulative frequency graph. A Kolmogorov-Smirnov test was performed between the following pairs: W.T and Overexpressor A ($p=0.0008$); W.T and Overexpressor B ($p=0.2594$).

Publishing Agreement

It is the policy of the University to encourage open access and broad distribution of all theses, dissertations, and manuscripts. The Graduate Division will facilitate the distribution of UCSF theses, dissertations, and manuscripts to the UCSF Library for open access and distribution. UCSF will make such theses, dissertations, and manuscripts accessible to the public and will take reasonable steps to preserve these works in perpetuity.

I hereby grant the non-exclusive, perpetual right to The Regents of the University of California to reproduce, publicly display, distribute, preserve, and publish copies of my thesis, dissertation, or manuscript in any form or media, now existing or later derived, including access online for teaching, research, and public service purposes.

DocuSigned by:

Karina Perlaza

7B871FDDACA04D0...

Author Signature

8/19/2021

Date